



Pacific Northwest
NATIONAL LABORATORY

Proudly Operated by Battelle Since 1965

Geochemical, Microbial, and Physical Characterization of 200-DV-1 Operable Unit B-Complex Cores from Boreholes C9552, C9487, and C9488 on the Hanford Site Central Plateau

September 2018

JE Szecsody
MJ Truex
BD Lee
CE Strickland
JJ Moran
MM Snyder
CT Resch
AR Lawter
L Zhong
BN Gartman

DL Saunders
SR Baum
II Leavy
JA Horner
BD Williams
BB Christiansen
EM McElroy
MK Nims
RE Clayton
D Appriou

DISCLAIMER

This report was prepared as an account of work sponsored by an agency of the United States Government. Neither the United States Government nor any agency thereof, nor Battelle Memorial Institute, nor any of their employees, makes **any warranty, express or implied, or assumes any legal liability or responsibility for the accuracy, completeness, or usefulness of any information, apparatus, product, or process disclosed, or represents that its use would not infringe privately owned rights.** Reference herein to any specific commercial product, process, or service by trade name, trademark, manufacturer, or otherwise does not necessarily constitute or imply its endorsement, recommendation, or favoring by the United States Government or any agency thereof, or Battelle Memorial Institute. The views and opinions of authors expressed herein do not necessarily state or reflect those of the United States Government or any agency thereof.

PACIFIC NORTHWEST NATIONAL LABORATORY
operated by
BATTELLE
for the
UNITED STATES DEPARTMENT OF ENERGY
under Contract DE-AC05-76RL01830

Printed in the United States of America

Available to DOE and DOE contractors from the
Office of Scientific and Technical Information,
P.O. Box 62, Oak Ridge, TN 37831-0062;
ph: (865) 576-8401
fax: (865) 576-5728
email: reports@adonis.osti.gov

Available to the public from the National Technical Information Service
5301 Shawnee Rd., Alexandria, VA 22312
ph: (800) 553-NTIS (6847)
email: orders@ntis.gov <<http://www.ntis.gov/about/form.aspx>>
Online ordering: <http://www.ntis.gov>



This document was printed on recycled paper.

(8/2010)

Geochemical, Microbial, and Physical Characterization of 200-DV-1 Operable Unit B-Complex Cores from Boreholes C9552, C9487, and C9488 on the Hanford Site Central Plateau

JE Szecsody
MJ Truex
BD Lee
CE Strickland
JJ Moran
MM Snyder
CT Resch
AR Lawter
L Zhong
BN Gartman

DL Saunders
SR Baum
II Leavy
JA Horner
BD Williams
BB Christiansen
EM McElroy
MK Nims
RE Clayton
D Appriou

September 2018

Prepared for
the U.S. Department of Energy
under Contract DE-AC05-76RL01830

Pacific Northwest National Laboratory
Richland, Washington 99352

Executive Summary

The 200-DV-1 Operable Unit (OU) is in the process of characterizing the vadose zone to support a remedial investigation and feasibility study. Contaminants disposed of at the land surface must migrate through the vadose zone before entering groundwater. Quantifying contaminant attenuation and contaminant transport processes in the vadose zone, in support of the conceptual site model (CSM) and fate and transport modeling, are important for assessing the needs for, and types of, remediation in the vadose zone and groundwater. The framework to characterize attenuation and transport processes provided in U.S. Environmental Protection Agency (EPA)¹ guidance documents was used to guide the laboratory effort with the following objectives:

- Quantify contaminant distribution and geochemical, microbial, and physical setting
- Identify attenuation processes and mechanisms (abiotic and biotic)
- Quantify the mobility of contaminants and transport parameters needed to evaluate remedies

These objectives are elements of the framework identified in EPA guidance for evaluating monitored natural attenuation (MNA) of inorganic contaminants, and they directly support updating the CSM for these waste sites (and generally for the Hanford Central Plateau). Through a data quality objectives process, specific 200-DV-1 waste sites were selected for evaluation of attenuation and transport processes for mobile uranium, technetium-99 (Tc-99), iodine-129 (I-129), chromium, cyanide, nitrate, and other co-contaminants. The information in this report supports defining suitable contaminant transport parameters that are needed to evaluate transport of contaminants through the vadose zone and to the groundwater and the feasibility of remedies for the 200-DV-1 OU.

This report describes geochemical, microbial, and physical characterization of Hanford vadose zone cores from boreholes in three B-Complex waste sites: BY Cribs (borehole C9552), B-7AB (C9487), and B-8 (C9488) (Table ES.1). Sediment characterization included determining contaminant concentrations (and oxidation state for some contaminants), concentrations of important geochemical constituents, microbial ecology relevant to contaminant attenuation, physical properties and pore-water oxygen and hydrogen isotopes. Additional information to help assess attenuation processes included sequentially applying increasingly harsh extraction solutions to the sediment and measuring contaminants and geochemical constituents in the extractions (sequential-extraction analysis). This technique helps interpret the distribution of contaminants among mobile, partially mobile, and functionally immobile phases in the sediments. The character of iron and manganese phases in the sediments was also determined in relation to their role in redox reactions. Several types of methods were applied to evaluate transport characteristics and develop transport parameters for contaminants, including (a) short- (a few hours) and long-term (1000-hour) reaction of groundwater with sediment, (b) sediment column leaching, and (c) addition of iodate and uranium to sediment columns to evaluate contaminant reduction rate. Stable isotopes ($\delta^2\text{H}$ [deuterium] and $\delta^{18}\text{O}$ [18-oxygen]) were measured in the pore water to evaluate natural and anthropogenic water sources at different locations. Information in this summary is presented in terms of contaminants of concern, then by waste sites.

¹ EPA. 2015. *Use of Monitored Natural Attenuation for Inorganic Contaminants in Groundwater at Superfund Sites*. OSWER Directive 9283.1-36, U.S. Environmental Protection Agency, Office of Solid Waste and Emergency Response, Washington, D.C.

Table ES.1. Location of B-Complex cores.

Waste Site	Borehole	Depth (ft)	Core	Geologic Unit
BY Cribs	C9552	102 - 105	13A – 13C	Hanford Formation (H2)
BY Cribs	C9552	132 - 135	19A – 19C	Hanford Formation (H2)
BY Cribs	C9552	192 - 195	30A – 30C	Cold Creek Unit (CCU _g)
B7-AB	C9487	58 - 60	2D, 2E, Opt 11C	Hanford Formation (H2)
B7-AB	C9487	132 - 135	17A – 17C	Hanford Formation (H2)
B7-AB	C9487	227 - 231	Opt. 12C, 12E, 13D	Cold Creek Unit (CCU _z)
B-8	C9488	218 - 223	36B, 36C, 37A	Cold Creek Unit (CCU _z)

• Uranium

- Uranium concentrations ranged in samples from low to moderate (0.3 to 58 µg/g), where the lowest uranium concentrations are likely natural background concentrations.
- The dominant form of uranium mobilized was U(VI) as aqueous calcium-uranyl-carbonate complexes.
- A small fraction of the uranium was present as highly mobile aqueous or adsorbed uranium, with larger fractions present in partially soluble carbonates and other solid phases with less mobility. Sediments with high uranium had a higher fraction of mobile aqueous and adsorbed uranium.
- Because uranium is present in multiple surface phases, leaching sediments with groundwater showed the aqueous and adsorbed mass, then a portion of the carbonate-associated uranium was mobilized from the sediment.
- The uranium release rate from sediment decreased over time, and correlated well with initial rapid release of aqueous and adsorbed uranium, followed by slower uranium release from carbonates. The uranium release rate was well correlated with the uranium concentration in sediments.
- Adsorbed uranium (as calcium-uranyl-carbonate complexes) in contact with sediment for greater times (i.e., decades) forms precipitates, as indicated by the observed uranium incorporated into carbonates, with higher carbonate sediments retaining more uranium.

• Iodine

- I-129 concentrations were non-detect for all samples. Total iodine (I-127) was measured in samples because the same chemical species form as iodide and iodate, which are suitable for evaluating adsorption and reduction processes of I-129.
- Total iodine (I-127) was present in B-complex sediments in low concentrations (0.014 to 0.054 µg/g). The aqueous and adsorbed iodine fraction was below detection limits. There was 60 to 75% of the iodine-127 associated with carbonates and 25 to 40% associated with Fe/Mn oxides.
- Leaching sediments with groundwater showed the initial rapid release of I-127 as iodide in most sediments, followed by the release of I-127 as iodate. This behavior is consistent with low reported adsorption of iodide and moderate sorption of iodate. The leached mass in most sediments was dominated by iodide, although two sediment samples were dominated by iodate. A portion of the carbonate-associated iodine was released during the leaching tests.

- The iodine release rate from sediments decreased over time and was correlated to the iodine mass in the sediment, similar to the trend observed with uranium.
- Reduction of iodate to iodide was observed in most sediments to which iodate was added. Iodate reduction was also observed in some sediments with no iodate addition. Reduction may occur due to reduced Fe/Mn phases present or may be microbially-induced.
- **Tc-99**
 - Low concentrations of Tc-99 were detected in some B-Complex sediments ($< 0.013 \mu\text{g/g}$).
 - The Tc-99 was present in sediments as aqueous or adsorbed species (pertechnetate), which was easily mobilized during leaching. There was no detectable Tc-99 present in sediments after leaching.
 - The Tc-99 release rate from sediments decreased over time and showed a small correlation with Tc-99 mass in the sediment.
- **Chromium**
 - Cr(VI) was not detected in B-Complex sediments. The total chromium measured in acid extractions (in detectable concentrations) was likely from naturally occurring minerals.
- **Cyanide**
 - Low concentrations of cyanide were detected in two B-complex sediments ($< 0.042 \mu\text{g/g}$).
- **Cations**
 - Cations in B-Complex sediments were present in concentrations one to three orders of magnitude higher than the natural background in pore water. Cation concentrations varied significantly between boreholes and with depth in the same borehole.
 - Cations were dominated by sodium, then calcium, then potassium.
 - Leaching showed that cation concentrations required significant flushing (i.e., tens of pore volumes of water) to reach background concentrations. This was due to high adsorption by ion exchange for divalent (calcium, magnesium) and less for monovalent (sodium, potassium) cations.
- **Nitrate and Other Anions**
 - Anions in B-Complex sediments are present in concentrations one to three orders of magnitude higher than the natural background in pore water. Anion concentrations varied significantly between boreholes and with depth in the same borehole.
 - Most cores showed anions dominated by nitrate, then sulfate, then carbonate, then chloride. Some cores showed anions dominated by carbonate then sulfate. Low concentrations of nitrite and phosphate were present in some cores.
 - Leaching showed that anion concentrations reached background concentrations rapidly (i.e., within 10 pore volumes of water). This was due to low adsorption of most anions.

The following conclusions were developed for the specific boreholes/waste sites analyzed in this study.

- **BY Cribs (Borehole C9552)**

- Cation concentrations are dominated by sodium (104 and 134' in Hanford formation H2 unit), then calcium (194' in Cold Creek CCU_g) two to three orders of magnitude higher than natural concentrations. Anions are dominated by nitrate, then sulfate two to three orders of magnitude higher (104'), and carbonate an order of magnitude higher than natural concentrations. Lower sulfate concentrations are measured in deeper (134', 194') cores.
- Uranium concentrations were relatively uniform with depth with a similar surface phase distribution (aqueous, adsorbed, carbonate associated, oxide/silicate associated). Iodine (I-127) is present in similar concentrations at 104, 134, and 194' depth. Tc-99 concentration decreases with depth. Low concentrations of cyanide were measured at 104' and 134' depths.
- Because a high fraction of uranium and iodine (I-127) is precipitated in carbonates, leaching rapidly removes only the aqueous and adsorbed fractions of uranium and iodine, and then there is slow uranium and iodine release from carbonates due to partial dissolution. Some abiotic and/or microbial reduction was observed in the laboratory with iodate added to these sediments reducing to iodide over hundreds of hours. Leaching samples were dominated by iodide, with a smaller fraction of iodate.

- **B7-AB (Borehole C9487)**

- Pore water was elevated in sodium and potassium at the 58' depth, in contrast to elevated sodium at 134 and 230' depths. Anions were dominated by carbonate, then nitrate (58') or sulfate (134 and 230').
- While there was no measureable Tc-99 or cyanide in water extractions of these cores, low concentration of Tc-99 leached from the 230' depth core, as leaching had lower detection limits.
- The uranium concentration was high at 58' depth (in Hanford formation H2 unit) and moderate at 134' (in Hanford formation H2 unit) and 230' (in Cold Creek Unit CCU_z). The iodine concentration was moderate at 58' and low at 134' and at 230'.
- Iodate reduction to iodide was observed, but there was also increased iodate concentration (presumed to be from carbonate dissolution) over hundreds of hours in the 58' depth core. Iodate dominated the iodine speciation at the 58' and 230' depths, but iodide dominated the iodine speciation at the 134' depth.
- Leaching resulted in rapid removal of aqueous and adsorbed uranium and iodine (initially iodide, then iodate) within the first 5 pore volumes, followed by slow uranium and iodine release from carbonates due to partial dissolution.

- **B-8 (Borehole C9488)**

- The Cold Creek Unit (CCU_z) core at 218' depth of fine silty sand had cation and anion concentrations an order of magnitude greater than natural pore water. The pore water was dominated by sodium, potassium, carbonate, and sulfate, with lower concentrations of nitrate, nitrite, and phosphate.

- The total uranium concentration was moderate with a low aqueous and adsorbed fraction. The iodine concentration was low, which was mainly precipitated in carbonates. The Tc-99 concentration was low.
- Leaching mobilized the aqueous, adsorbed, and part of the carbonate-associated uranium, 40% of the iodine associated with carbonates, and all of the Tc-99. Leaching behavior showed rapid mobilization of Tc-99 (i.e., all of the mass was mobilized within 10 pore volumes), and rapid mobilization of half of the uranium and iodine (I-127) within 10 pore volumes followed by slow release of uranium and iodine from carbonate dissolution. Equal concentrations of iodate and iodide were present in leach samples, although the slow carbonate dissolution should release iodate from the carbonate.

This study provides a set of data that addressed the study objectives and can support future evaluation of remedies, including MNA, and the associated fate and transport assessments that are needed as a basis for remedy evaluations. The first objective was to jointly evaluate contaminant concentrations and the biogeochemical and hydrologic setting for these data. This information provides a baseline for interpreting attenuation and transport processes. As noted, while there was significant variations in physical transport parameter values (i.e., permeability), sediment geochemical characteristics of these B-complex cores did not vary significantly (e.g., carbonate content, ferrous iron phase distribution, organic carbon content). Differences in observed contaminant leaching were likely mainly due to different concentrations of waste constituents in the samples.

Another objective of the study was to identify attenuation processes that appear to be active in these samples and which will affect contaminant transport through the vadose zone. Sorption processes are important for uranium and iodate, and to a lesser extent for iodide, chromate, and Tc-99. Carbonate content appeared to be important for uranium and iodate adsorption and accumulation of iodate and uranium in carbonate precipitates. Slow release of uranium and total iodine was evident in leaching experiments. Iodate reduction to iodide was observed in all of these B-complex cores at different rates. The BY crib borehole C9552 had the slowest iodate reduction rates, which corresponded to lower populations of nitrate- and iron-reducing bacteria. There was little difference in reduced iron phases between different boreholes, which implies (but does not prove) iodate reduction may have been microbial.

A key objective of the study was to quantify attenuation and transport parameters to support parameterization of fate and transport assessments. This type of assessment will be needed to evaluate transport of contaminants through the vadose zone, the coupled vadose zone-groundwater system, and to assess the need for, magnitude of, and/or design of remediation. The contaminant- and sample specific release rates from stop-flow portions of soil-column experiments and batch leaching provide a set of information that can be directly used to develop transport parameters. A key finding is that K_d (adsorption) values for uranium, iodine species, and Tc-99 (as pertechnetate) are coupled to the co-contaminant ions present in the water. These contaminants exhibited less adsorption during initial leaching with high ions present, and significant flushing was needed to decrease ion concentrations to near natural pore water concentrations, where contaminant adsorption is somewhat higher.

Collectively, the information from this laboratory study can be considered in terms of updating the CSM for contaminants in the vadose zone. It can also provide input to describing the coupled vadose zone-groundwater system that needs to be considered for remedy determinations. CSM elements from

this laboratory study are listed below. These elements will need to be incorporated with other data collected during the 200-DV-1 OU remedial investigation as part of updating the CSMs for the 200-DV-1 OU component waste sites.

- Sequential extraction experiments (and more coarsely indicated by comparison of water- and acid-extraction contaminant data) show that only a small fraction of the uranium and iodine mass in samples is in a mobile form that would transport under equilibrium-partitioning conditions. Leaching experiment results confirmed the initial rapid release of a portion of iodine and uranium mass (from aqueous and adsorbed phases) followed by the slow release due to partial dissolution of uranium- and iodate-containing carbonates. The relative amount of uranium and iodine mass in the mobile versus functionally immobile phases affects the potential for future mass discharge from the vadose zone to the groundwater. In contrast, Tc-99, present only in aqueous and adsorbed phases (for these B-Complex sediments), leached rapidly and could likely be modeled by equilibrium partitioning. It should be noted that in a previous study of sediments from BC Cribs and Trenches, some Tc-99 was associated with carbonates, and exhibited both rapid and slow release.
- Laboratory data suggest that formation and dissolution of uranium- and iodate-carbonate precipitates is a potential attenuation mechanism affecting the relative mobile and immobile mass fractions and the transport characteristics of uranium and iodine.
- For the waste sites included in this study, the effect of waste constituent concentrations (e.g., ionic strength, specific ions present), influenced contaminant sorption.
- There was some evidence of slow iodate reduction in all samples and rates of iodate reduction correlated with nitrate- and iron-reducing microbial biomass.

This laboratory study extended the characterization of the 200-DV-1 OU to include identification and quantification of contaminant attenuation processes and parameters that will be needed to evaluate transport of contaminants through the vadose zone into the groundwater. The data generated in this laboratory study enable the site CSMs and transport analyses to be updated to reflect the observed contaminant behavior. In addition, the laboratory study was structured to address the information requirements for considering MNA as all or part of a remedy (i.e., EPA's guidance document *Use of Monitored Natural Attenuation for Inorganic Contaminants in Groundwater at Superfund Sites*¹) and can be used as part of the technical defensibility for identifying attenuated transport through the vadose zone within the remedial investigation and feasibility study for the 200-DV-1 OU.

¹ EPA. 2015. *Use of Monitored Natural Attenuation for Inorganic Contaminants in Groundwater at Superfund Sites*. OSWER Directive 9283.1-36, U.S. Environmental Protection Agency, Office of Solid Waste and Emergency Response, Washington, D.C.

Acronyms and Abbreviations

1-D	one-dimensional
CHPRC	CH2M Hill Plateau Remediation Company
CSM	conceptual site model
EPA	U.S. Environmental Protection Agency
ESL	Environmental Sciences Laboratory
HASQARD	Hanford Analytical Services Quality Assurance Requirements Document
MNA	monitored natural attenuation
MPN	most probable number
OU	operable unit
PNNL	Pacific Northwest National Laboratory
QA	quality assurance

Contents

Executive Summary	iii
Acronyms and Abbreviations	ix
1.0 Introduction	1
2.0 Objectives	3
3.0 Experimental Methods.....	4
3.1 Sediment Selection and Analysis Objectives	4
3.2 Objective 1: Physical Characterization	6
3.3 Objective 2: Microbial Ecology	6
3.4 Geochemical Conditions	7
3.4.1 Objective 3: Contaminant Concentration, Distribution, and, Where Appropriate, the Oxidation-Reduction State	7
3.4.2 Objective 4: Geochemical Conditions.....	7
3.4.3 Objective 5: Contaminant Release Rate from Sediment and Mobility	8
3.4.4 Water and Acid Extraction of Contaminants from Sediments	9
3.4.5 Sequential Extractions and 1000-hour Carbonate Extraction	10
3.4.6 Iron and Manganese Extractions	11
3.4.7 Batch Leach Experiment	11
3.4.8 1-D Column Leach Experiment	12
3.4.9 1-D No-Flow Contaminant Reduction Rate Experiment	13
3.5 Objective 6: Oxygen and Hydrogen Isotopic Signature of the Pore Water	13
4.0 Results	15
4.1 Contaminant Distribution.....	16
4.1.1 Contaminants and Geochemical Constituents	16
4.1.2 Microbial Ecology.....	18
4.1.3 Iron and Manganese Characterization	21
4.1.4 Oxygen and Hydrogen Isotopes	23
4.1.5 Sediment Physical Characterization	30
4.2 Observation of Attenuation Processes.....	31
4.2.1 Sequential Liquid Extraction of Contaminants in Sediments.....	31
4.2.2 Sequential Extractions for Major Cations/Metals	38
4.2.3 U(VI) and Iodate Reduction Rate Experiments.....	42
4.3 Contaminant Mobility	45
4.3.1 Long-Term Contaminant Leaching in Batch Experiments	45
4.3.2 Long-Term Leaching of Contaminants from Sediments in 1-D Columns	48
4.3.3 1-D Water Leach of Co-Contaminant Ions	61
5.0 Conclusions and Implications for Field Transport of Contaminants	64
6.0 Quality Assurance.....	67

7.0 References	68
Appendix A Grain Size Distributions	A.1
Appendix B Extractable Contaminants and Ions	B.1

Figures

Figure 1.1. Factors (top row) that define the attenuation mechanisms (bottom row) affecting migration of inorganic contaminants through the vadose zone (Truex et al. 2015).....	1
Figure 3.1. Schematic of analysis on specific core intervals.	4
Figure 3.2. Images of (a) batch water leach experiments, (b) 1-D column water leaching experiments with continuous flow, and (c) no-flow column reduction rate and capacity experiments.	12
Figure 3.3. Pictures of the water extraction line system. The insert shows a single cell on the line where a sample is placed in the large tube on the right and water is cryogenically trapped in the smaller tube on the left. The backdrop shows the larger system setup, whereby a series of these cells are connected and share access to a common vacuum manifold (the stainless steel line behind the extraction cells).	14
Figure 4.1. Abundance of bacterial phyla based on DNA sequencing of bacteria extracted from sediments.	20
Figure 4.2. Iron (a) and manganese (b) surface phase distributions in sediments, based on liquid extractions.	22
Figure 4.3. Isotope data for vadose zone sediment and perched water analyses. (A) Data resulting from the full data set. (B) Data refined by a Modified Thompson Tau test to remove outlier points (continued on next page). Depiction of winter precipitation is after DePaolo et al. (2004) with a nominal value of $\delta^{18}\text{O}$ of $\sim -18\text{‰}$ and $\delta^2\text{H}$ of $\sim -138\text{‰}$	27
Figure 4.4. $\delta^{18}\text{O}$ relating to sample depth, average local winter precipitation, and local shallow groundwater within the Hanford Site. (A) Sample data from the T and S Complex. (B) Sample data from the B-Complex.	28
Figure 4.5. Correlation of isotopic ($\delta^2\text{H}$ and $\delta^{18}\text{O}$) analysis and measured nitrate concentration from T and S Complex samples.	29
Figure 4.6. Core images in borehole C9552 of: a) and b) Hanford formation, and c) Cold Creek Unit.	31
Figure 4.7. U-238 extractions: (a) and (b) sequential extractions pre-leach, (c) 1000-hour extraction pre-leach, (d) and (e) sequential extractions post-leach.	35
Figure 4.8. Iodine-127 sequential extractions conducted: (a) pre-leach, (b) post-leach, and (c) 1000-hour extraction conducted on pre-leach sediments.	36
Figure 4.9. Tc-99 sequential extractions conducted: (a) pre-leach, (b) post leach, and (c) 1000-hour extraction conducted on pre-leach sediments.	37
Figure 4.10. Chromium sequential extractions conducted: (a) pre-leach with total Cr analysis, and (b) post-leach with Cr(VI) analysis.	38
Figure 4.11. Cations/metals distribution measured in sequential extraction solutions. Cations are not reported for extraction solutions that contain that cation (i.e., Mg for extractions 2 and 3, Na for extractions 3 and 4, and Ca for extraction 4).	40
Figure 4.12. Major and trace cations/metals measured in sequential extractions: (a) Ca, (b) Mg, (c) Sr, (d) Na, (e) K, (f) Ba, (g) Fe, (h) Mn, (i) Si, (j) Al, and (k) Si/Al ratio. Sediments are:	

C9552 13C (E1), C9552 19C (E2), C9552 30C (E3), C9487 17C (E4), C9487 13D (E5 and E6), C9487 2D (E7), and C9488 36C (E8).....	41
Figure 4.13. Iodate reduction experiments with the addition of 100 µg/L iodate into no-flow sediment columns.	43
Figure 4.14. Rate of uranium removal from aqueous solution in no-flow 1-D columns after injection of 20 pore volumes of artificial groundwater containing 100 µg/L U (as Ca-uranyl-carbonate aqueous complexes) and 100 µg/L iodate.	44
Figure 4.15. Long-term leaching of contaminants from sediments in batch systems showing: (a) Cr(VI) release, (b) Tc-99 release, (c) U-238 for six sediments, and (d) U-238 for C9487 58'.	46
Figure 4.16. Long-term leaching of contaminants from sediments in batch systems showing (a) total I-127, and (b) iodine speciation for C9487 58'. Iodine speciation for most experiments was below analytical detection limits, with the exception of C9487 58' and single points in three experiments, which showed 62% iodide (C9552 104' at 103 hours), 55% iodide (C9488 219' at 103 hours), and 83% iodide (C9488 219' at 9.6 hours).	47
Figure 4.17. Added tracer (bromide) breakthrough in 1-D column experiments.	49
Figure 4.18. Chromate breakthrough in 1-D column leaching experiments.	50
Figure 4.19. Tc-99 breakthrough in 1-D column leaching experiments. Effluent Tc-99 (black triangles) and cumulative Tc-99 mass (purple triangles) are shown.	51
Figure 4.20. Tc-99 release rates calculated from stop-flow events in 1-D column leach experiments showing (a) Tc-99 release rate change with pore volumes, and (b) Tc-99 release rate and mass leached.	52
Figure 4.21. U-238 breakthrough in 1-D column leaching experiments. Effluent U-238 (black triangles) and cumulative U-238 mass (green triangles) are shown.	54
Figure 4.22. U-238 release rates calculated from stop-flow events in 1-D column leach experiments showing (a) U-238 release rate change with pore volumes, and (b) U-238 release rate and mass leached.	55
Figure 4.23. I-127 breakthrough in 1-D column leaching experiments. Effluent I-127 (black triangles) and cumulative I-127 mass (blue triangles) are shown.	57
Figure 4.24. Iodine speciation breakthrough in 1-D column leaching experiments for selected samples with speciation analysis. Iodine speciation on C9487 134' was below detection limits.	58
Figure 4.25. Cumulative iodine speciation breakthrough in 1-D column leaching experiments for selected samples with speciation analysis. Iodine speciation on C9487 134' was below detection limits.	59
Figure 4.26. I-127 release rates calculated from stop-flow events in 1-D column leach experiments showing (a) I-127 release rate change with pore volumes, and (b) I-127 release rate and mass leached.	60
Figure 4.27. Change in major cations leaching from sediments in 1-D column leach experiments.	62
Figure 4.28. Change in major anions leaching from sediments in 1-D column leach experiments.	63

Tables

Table 3.1. Depth intervals used for characterization of DV-1 cores.....	5
Table 3.2. Physical sediment analysis methods.	6
Table 3.3. Microbiological and molecular methods.....	7
Table 3.4. Geochemical extraction and characterization of sediment.....	8
Table 3.5. Geochemical analysis methods.	9
Table 4.1. Geochemical characterization of sediment pore water by water/sediment (1:1) extraction.	17
Table 4.2. Water and acid extractable concentration of contaminants in sediments.....	17
Table 4.3. Nitrate-, iron-, or sulfate-reducing microbial biomass by MPN.	18
Table 4.4. Ferrous and ferric iron phases in sediments based on liquid extractions.....	21
Table 4.5. Manganese phases in sediments based on liquid extractions.....	21
Table 4.6. Summary of Hanford mineralogy (Xue et al. 2003).	23
Table 4.7. Sediment samples selected for analyses and isotope data values (outliers removed).	24
Table 4.8. Physical characterization of sediments.	30
Table 4.9. Description of sediment grain size distribution.	30
Table 4.10. Physical characterization of sediments used in 1-D column experiments.	31
Table 4.11. Sequential extraction of contaminants from sediment samples.	32
Table 4.12. Contaminant distribution in sequential liquid extracted sediments and 1000-hour carbonate extraction for U-238, I-127, Tc-99, and Cr.	33
Table 4.13. Calculated release rates of I-127 and U-238 in long-term batch experiments.	48

1.0 Introduction

The purpose of this geochemical, microbial, and physical characterization work is to identify and evaluate attenuation processes and other factors that affect transport of contaminants of concern present in vadose zone sediment samples from the Hanford Site. The samples are from specific depth intervals in boreholes C9552, C9487, and C9488, located in the BY Crib, B-7AB, and B-8 waste sites, respectively. Samples were selected for analysis in coordination with CH2M Hill Plateau Remediation Company (CHPRC), who is conducting characterization of the 200-DV-1 operable unit (OU). These analyses described in this report are based on the characterization approaches described for evaluating monitored natural attenuation (MNA) of inorganic contaminants (EPA 2007a,b, 2010, 2015). The analyses were selected to provide data to support interpretation of contaminant behavior in the vadose zone, and will be used in conjunction with additional information produced by CHPRC as part of their related characterization efforts at these and other vadose zone boreholes. The analyses were also selected to complement other research being conducted as part of the Deep Vadose Zone Applied Field Research Initiative.

To reach groundwater, contaminants disposed in aqueous solution at the ground surface must traverse through the vadose zone. Contaminant migration through the vadose zone is affected by a range of attenuation processes, which results in a temporal profile of contaminant discharge into underlying groundwater that differs from the temporal profile of waste disposal. It is the temporal profile of contaminant discharge into underlying groundwater that defines the contaminant source characteristics with respect to groundwater plume development. Thus, quantifying contaminant attenuation and transport processes in the vadose zone, and the resulting temporal profile of contaminant discharge to the underlying groundwater, is important for assessing the need for, and type of, remediation in the vadose zone and groundwater. Contaminant transport through the vadose zone beneath aqueous waste disposal sites is affected by two types of attenuation processes: (1) attenuation caused by advective and dispersive factors related to unsaturated water flow (i.e., fluid and porous media properties) and (2) attenuation caused by biogeochemical reactions and/or physical/chemical interaction with sediments (e.g., phenomena such as sorption, precipitation/dissolution, and decay/degradation, which slow contaminant movement relative to water movement). Figure 1.1 summarizes the types of attenuation mechanisms that may affect contaminant transport in the vadose zone (e.g., Szecsody et al. 2013; Truex et al. 2014).

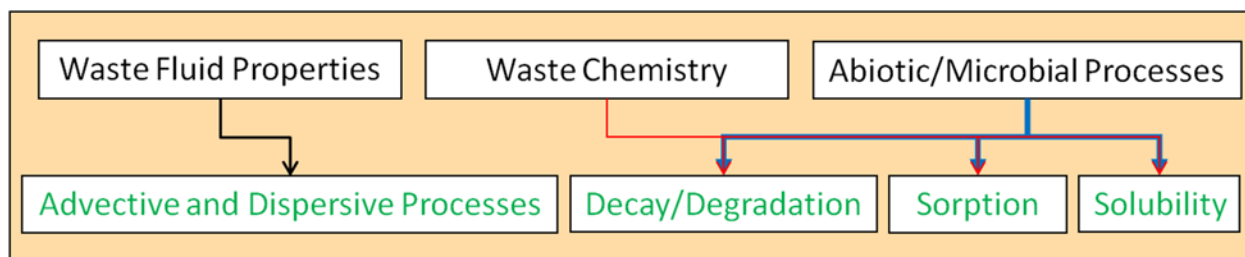


Figure 1.1. Factors (top row) that define the attenuation mechanisms (bottom row) affecting migration of inorganic contaminants through the vadose zone (Truex et al. 2015).

A framework to characterize these attenuation and transport processes is provided by the U.S. Environmental Protection Agency (EPA) guidance document *Use of Monitored Natural Attenuation for Inorganic Contaminants in Groundwater at Superfund Sites* (EPA 2015). Additional information for vadose zone attenuation processes reported by Truex and Carroll (2013) and Truex et al. (2015) is also relevant for characterization of the vadose zone. These documents point to approaches that can be applied to identify and describe transport parameters for a vadose zone site such as characterizing processes that influence attenuation and measurement of contaminant transport/leaching.

The 200-DV-1 OU is in the process of characterizing the vadose zone to support a remedial investigation and feasibility study. Through a data quality objectives process, specific 200-DV-1 waste sites were selected to evaluate attenuation and transport processes for uranium, technetium-99 (Tc-99), iodine-129 (I-129), chromium, and nitrate. Waste sites were selected based on the following factors:

- Waste stream inventory (i.e., significant radiological and/or chemical component)
- Waste stream differentiation (i.e., mainly acidic, significant volume)
- Disposal type (crib, trench, French drain, reverse well, etc.)
- Potential to obtain parameters from significant (site-specific) geologic units to fill transport data gaps

The data quality objectives process also identified that the characterization of attenuation and transport processes needed to include the following tasks:

- Evaluate contaminant and geochemical constituents in the samples
- Identify interactions of contaminants with sediments
- Quantify contaminant mobility
- Evaluate factors controlling contaminant mobility

The information from characterization of attenuation and transport processes will be used to refine conceptual site models by enhancing the understanding of controlling features and processes for transport of contaminants through the vadose zone to the groundwater. The characterization approach was developed based on EPA (2015) guidance, identifying specific objectives (Section 2.0) and types of laboratory analyses (Section 3.0) to conduct on sediment samples. This report provides results and interpretation of these laboratory on samples collected in fiscal year 2016 (Section 4.0), as well as recommendations for future analyses on these and other samples (Section 5.0).

2.0 Objectives

The specific types of data identified for inclusion in the laboratory study reported herein will provide data and associated interpretation to support the following three objectives. These objectives are elements of the framework identified in the EPA (2015) guidance for evaluating MNA of inorganic contaminants, which directly supports development of suitable contaminant transport parameters.

- Define the contaminant distribution in the hydrologic and biogeochemical setting
- Identify the relevant attenuation processes that influence the contaminant distribution
- Quantify attenuation and transport parameters for use in evaluating remedies

These overall objectives lead to a series of laboratory analyses designed to provide suitable data and information. A phased approach is used for this effort to progressively gather more detailed information based on initial results. This progressive/tiered approach is consistent with EPA MNA guidance (EPA 2015).

The information from these analyses will be used as input to evaluate the feasibility of MNA and other remedies for the 200-DV-1 OU because the information provides an understanding of the controlling features and processes for transport of contaminants through the vadose zone to the groundwater. The information from these analyses will also be used as input to refine the conceptual site model for the targeted vadose zone sites.

The objectives described above are accomplished by measuring the following:

- Concentration and mass of contaminants (uranium, technetium, iodine species, chromate, cyanide, other co-contaminants) associated with aqueous, adsorbed, and various solid phases by batch extractions
- Concentration and mass of contaminants that leach from sediments over time in low sediment/water ratio, long-term, batch studies
- Concentration and mass of contaminants that leach from sediments over time in high sediment-water ratio 1-D column studies
- Characterization of Fe- and Mn-oxide surface phases, including reduced phases that can potentially cause abiotic reduction of some contaminants and oxic phases that are available for microbial reduction
- Characterization of microbial biomass, and ability of the natural sediment consortium to reduce contaminants of concern (i.e., uranium as Ca-uranyl(VI)-carbonate aqueous species, pertechnetate, chromate, iodate, and nitrate)
- Characterization of the potential for uranium and iodate reduction in high sediment/water ratio stop-flow columns (i.e., reduction capacity and rate)
- Determination of the oxygen and hydrogen isotopic signature of the pore water for use in comparing to existing data that may enable the source of the pore water within the sample to be evaluated

3.0 Experimental Methods

3.1 Sediment Selection and Analysis Objectives

Pacific Northwest National Laboratory (PNNL) and CHPRC jointly selected samples for testing. Nominally, the selected samples will include three samples from boring C9552, three samples from boring C9487, and one sample from boring C9488 (SGW-58569). These samples are in 12-inch-long liners within a 5-ft-long sonic core. The cores will be shipped from the drilling site to the PNNL 331 Building, where they will be inspected and the chain of custodies completed. A liner disposition plan within a 5-ft core sample is shown in Figure 3.1. Target 5-ft cores selected for testing will divide liners for specific types of tests according to this plan.

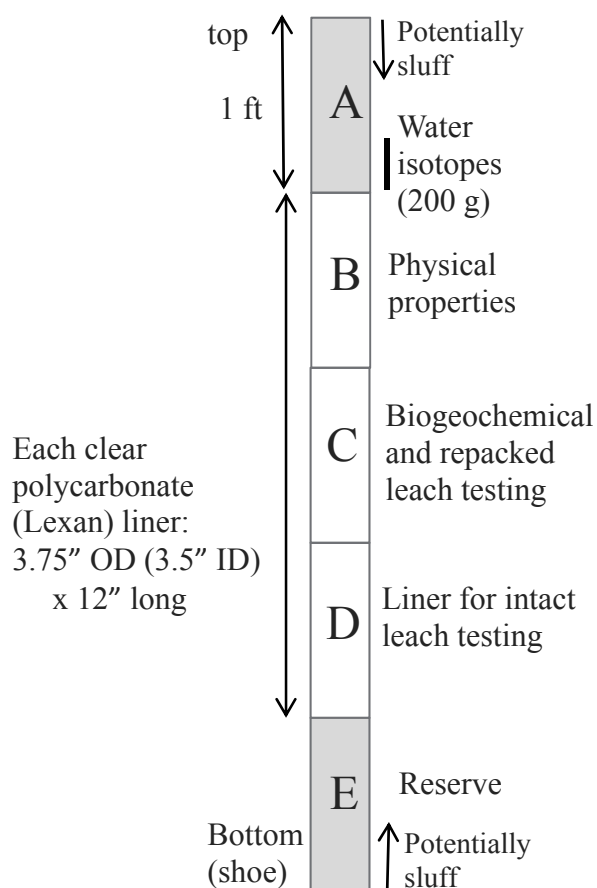


Figure 3.1. Schematic of analysis on specific core intervals.

The actual depth intervals analyzed for physical, microbial, and geochemical characterization, modified from the schematic shown in Figure 3.1, were based on the geology and recovery in each core liner (Table 3.1).

Table 3.1. Depth intervals used for characterization of DV-1 cores.

Borehole	Depth (ft)	Location	Sample #	Analysis Type
C9552	102.2 – 103.2	13A	B341B1	Pore water isotopes ($^2\text{H}/^1\text{H}$, $^{18}\text{O}/^{16}\text{O}$)
	103.2 – 104.2	13B	B34H36	Physical, geology characterization
	104.2 – 105.2	13C	B34H37	Microbial, geochemical characterization
C9552	127.3 - 128.3	18A	B341C1	Pore water isotopes ($^2\text{H}/^1\text{H}$, $^{18}\text{O}/^{16}\text{O}$)
C9552	132.1 – 133.1	19A	B341C3	Pore water isotopes ($^2\text{H}/^1\text{H}$, $^{18}\text{O}/^{16}\text{O}$)
	133.1 – 134.1	19B	B34H53	Physical, geology characterization
	134.1 – 135.1	19C	B34H55	Microbial, geochemical characterization
C9552	192.2 – 193.2	30A	B34H74	Pore water isotopes ($^2\text{H}/^1\text{H}$, $^{18}\text{O}/^{16}\text{O}$)
	193.2 – 194.2	30B	B34H77	Physical, geology characterization
	194.2 – 195.2	30C	B34H79	Microbial, geochemical characterization
C9487	58.2 - 59.2	2D	B34W66	Microbial, geochemical characterization
	59.5 – 60.0	Opt. 11C	B34WN7	Physical, geology characterization
C9487	132.1 – 133.1	17A	B34WB1	Pore water isotopes ($^2\text{H}/^1\text{H}$, $^{18}\text{O}/^{16}\text{O}$)
	133.1 – 134.1	17B	B34WB2	Physical, geology characterization
	134.1 – 135.1	17C	B34WB3	Microbial, geochemical characterization
C9487	220.0 - 221.0	35D	B34WH8	Pore water isotopes ($^2\text{H}/^1\text{H}$, $^{18}\text{O}/^{16}\text{O}$)
C9487	227.2 – 227.7	Opt. 12C	B354L1	Pore water isotopes ($^2\text{H}/^1\text{H}$, $^{18}\text{O}/^{16}\text{O}$)
	228.7 – 229.7	Opt. 12E	B354L3	Physical, geology characterization
	230.0 – 231.0	Opt. 13D	B354L8	Microbial, geochemical characterization
C9487	232.0 - 233.0	Opt. 14C	B354M3	Pore water isotopes ($^2\text{H}/^1\text{H}$, $^{18}\text{O}/^{16}\text{O}$)
C9488	218.3 – 219.3	36B	B355L2	Physical, geology characterization
	219.3 – 220.3	36C	B355L3	Microbial, geochemical characterization
	222.5 – 223.5	37B	B355L8	Pore water isotopes ($^2\text{H}/^1\text{H}$, $^{18}\text{O}/^{16}\text{O}$)

The laboratory experimental effort was organized using the following specific analysis objectives, which are related to the overall objectives described in Section 2.0. The subsequent sections describe the laboratory methods applied for each of the analysis objectives.

Analysis Objectives

1. Characterize the physical aspects of the sample(s) that are used to evaluate pore water flow and that provide the sediment information needed to interpret and scale biogeochemical analysis results.
2. Characterize the microbial ecology in the samples, focusing on identification of the microbial phenotypes that are present. This information will be used to interpret (1) microbial processes that can directly affect the chemical form of the contaminant, (2) the microbial community's relation to geochemical processes affecting sediment surface phases and contaminant chemical form, and (3) microbial processes related to sequestration or accumulation of contaminants.
3. Characterize the contaminant concentration, distribution, and, where appropriate, the oxidation-reduction state and chemical form in the pore water and on sediment surfaces. This information allows interpretation of contaminant mobility in the context of the biogeochemical system data.

4. Characterize the geochemical conditions in the pore water and on sediment surfaces to facilitate interpretation of attenuation and transport processes. Information about elements and compounds in the samples enables evaluation of biogeochemical processes related to the contaminant chemical form and mobility.
5. Characterize the contaminant mobility using tests that impose specific conditions, and collect temporal data for interpreting the mobility of the contaminant (e.g., by quantifying the rate of contaminant transfer to the aqueous phase).
6. Determine the oxygen and hydrogen isotopic signature of the pore water for use in comparing to existing data that may enable the source of the pore water within the sample to be evaluated.

3.2 Objective 1: Physical Characterization

Standard physical sediment analysis methods shown in Table 3.2 will be applied to meet physical characterization objectives. Additional detail on these analyses is provided in test instructions and procedures.

Table 3.2. Physical sediment analysis methods.

Required Data	Analytical Methods
Moisture content	ASTM D2216-10
Intact core dry bulk density, particle density, and porosity	ASTM D7263-09, D854-14
Intact core air permeability	ASTM D6539-13
Core particle size by sieve (4, 2, 1, 0.5 mm sieve)	ASTM D6913-04
Core particle size by laser diffraction (< 0.5 mm)	ASTM D4464-15
Lithology, texture, petrologic composition (sand, gravel, basalt, quartz) and photos	Geologist inspection of borehole samples

3.3 Objective 2: Microbial Ecology

Microbiological and molecular analyses performed on the soil samples are listed in Table 3.3. Two categories of analyses will be applied to evaluate the microbial ecology of the samples. The first category is based on applying an extract of the sample to different types of microbial culturing media. Microbial growth for these culturing media is measured and used to interpret the phenotypes of microbes present in the sample. The second category is based on extracting genetic material from the sample, identifying the genetic sequences present, and comparing these sequences to established databases to identify the microbes present at the genus or species level. Genetic material will also be probed for specific functional genes that are important in driving biogeochemical processes. This identification can be used to interpret the types of microbes present, and provide information on the types of biogeochemical reactions these microbes may catalyze. Additional, specific detail is provided in test instructions and procedures.

Methods for enumeration of total microbial numbers, bacterial density, and total heterotrophs are based on methods contained in the *Standard Methods for the Examination of Water and Wastewater*,

22nd Edition (APHA, AWWA, WEF 2012). Modifications for methods include verification of electron acceptor utilization using methods from the literature. Tests to quantify functional genes are based on gene amplification using a kit available from Bio- Rad Laboratories. Specific primers used to target functional genes are based on methods obtained from the peer-reviewed literature. The quality approach used for gene quantification is based on a guidance document from the EPA (2004).

Table 3.3. Microbiological and molecular methods.

Required Data	Method Basis
Total microbial numbers	TI-DVZ-AFRI-0009, Section 1.4 (APHA SM 9216A)
Total heterotrophs	TI-DVZ-AFRI-0009, Section 1.5 (APHA SM 9221C, modified)
	Nitrate (Callos et al. 1999)
	Iron (Gould et al. 2003)
	Manganese (Grebel et al. 2016)
Bacterial density	TI-DVZ-AFRI-0009, Section 1.6 (APHA SM 9215A, modified)
Total heterotrophs	
Anaerobic heterotrophs	
Nitrate-reducing bacteria	
Iron-reducing bacteria	
Manganese-reducing bacteria	
Overall phylogenetic diversity	Argonne National Lab Next Generation Sequencing Core Facility
Gene sequence information	Quality Assurance Policy
Bacterial identification	Benson et al. 2015; Rehm et al. 2013; O’Leary et al. 2015; Cole et al. 2013
APHA - American Public Health Association	

3.4 Geochemical Conditions

To meet analysis objectives 3, 4, and 5, specific types of geochemical characterization, contaminant characterization, or contaminant mobility characterization are conducted.

3.4.1 Objective 3: Contaminant Concentration, Distribution, and, Where Appropriate, the Oxidation-Reduction State

Contaminant conditions are interpreted based on the elements and compounds present in the sample pore water or on sediment surfaces. The type of extraction and the concentration of the contaminant are both needed to interpret the contaminant conditions. Extractions applied to evaluate the contaminant conditions include (a) water extraction, (b) acid extraction, (c) sequential extractions, and (d) carbonate extraction (see Table 3.4), with analysis of contaminants of concern. In addition, alkaline extraction is conducted on sediment samples by EPA Method 3060A to provide material for analysis of chromium. The analysis for the specific extractions is described in Table 3.5.

3.4.2 Objective 4: Geochemical Conditions

General geochemical conditions are interpreted based on the elements and compounds present in the sample pore water or on sediment surfaces. Some of the same extractions used for contaminants are also used to characterize geochemical conditions, and include (a) water extraction, (b) acid extraction, and

(c) sequential extractions (see Table 3.4), with analysis of cations, anions, and other geochemical parameters (pH, specific conductance). In addition, iron/manganese extractions are conducted on sediments (Table 3.4). The analysis for the specific extractions is described in Table 3.5.

3.4.3 Objective 5: Contaminant Release Rate from Sediment and Mobility

Contaminant mobility was evaluated for sediments by batch and soil column leaching approaches that impose specific conditions and collect temporal data. These tests expose contaminated sediment to an aqueous solution (simulated groundwater) and measure changes in contaminant concentration over time in quiescent (5.1 batch water leach in Table 3.4) or flowing conditions (6.1 column water leach in Table 3.4). For the column tests, sequential extractions for contaminants were also conducted on the post-test sediments from the column for comparison with the pre-leaching results obtained on the sediments. To evaluate the potential reduction of U(VI) and iodate in sediments, high sediment/water ratio no-flow reduction rate experiments were conducted (7.1 column no-flow experiments in Table 3.4) with the injection of 100 µg/L Ca-uranyl carbonate and 100 µg/L i iodate in artificial groundwater. Note that I-129 concentrations were non-detect for all samples. Total iodine (I-127) was measured in samples because the same chemical species form (iodide, iodate), suitable for evaluating adsorption and reduction processes of I-129.

Details of extractions and batch and column experiments are provided in the following sections.

Table 3.4. Geochemical extraction and characterization of sediment.

Required Data	Analysis (see Table 3.5)	Method
1.1. Water extraction (1:1 sediment: H ₂ O)	10.1, 10.2, 10.3, 10.4, 10.5, 10.7, 10.9, 10.10, 10.11, 10.12	Um et al. 2009 Zachara et al. 2007
1.2. Acid extraction (1:3 sediment: H ₂ O, 8M HNO ₃)	10.1, 10.2, 10.3, 10.4, 10.5, 10.7	Um et al. 2009 Zachara et al. 2007
2. Sequential extractions	10.1, 10.2, 10.3, 10.5	Gleyzes et al. 2002
2.1. Artificial groundwater		Beckett 1989
2.2. Ion exchangeable		Larner et al. 2006
2.3. pH 5.0 acetate		Sutherland and Tack 2002
2.4. pH 2.3 acetic acid		Massop and Davison 2003
2.5. Oxalate, oxalic acid		
2.6. 8M HNO ₃ , 95°C		
2.7. 1000-h carbonate extraction	10.2, 10.3, 10.5	Zachara et al. 2007 Kohler et al. 2004
3. Iron/Mn phase extractions:	10.6, 10.1 (Fe and Mn)	Heron et al. 1994
3.1. Ion exchangeable Fe(II), Mn		Chou and Zhao 1983
3.2. Oxide/sulfide		Hall et al. 1996
3.3. Total Fe(II), Fe(III), Mn		
3.4. Am- Fe(III), Mn-oxides		
3.5. Crys.-Fe(III), Mn-oxides		
4.1. Alkaline sediment digestion for Cr(VI)	10.5	EPA 3060a

Required Data	Analysis (see Table 3.5)	Method
5.1. Batch water leach rate experiment	10.2, 10.3, 10.5	Szecsody et al. 1994
6.1 1-D. Column water leach rate experiment	10.1, 10.2, 10.3, 10.5, 10.8	Qafoku et al. 2004 Szecsody et al. 2013
7.1 1-D. Column no-flow contaminant reduction rate and capacity	10.3, 10.4	Szecsody et al. 2014 Szecsody et al. 2016

Table 3.5. Geochemical analysis methods.

Data and Instrumentation	Constituents Analyzed	Method
10.1. Metals by ICP-OES	Al, Ba, Ca, Fe, K, Mg, Mn, Na, Si, Sr, Cr	EPA 6010D (PNNL-ESL-ICP-OES, Rev. 4)
10.2. U, Tc-99 by ICP-MS	U, Tc-99	EPA 6020B (PNNL-ESL-ICP-MS, Rev. 4)
10.3. Iodine species by ICP-MS	Iodide, iodate	Revision of ESL-ICP-MS, Rev. 4
10.4. Kinetic phosphorescence analysis	U(VI)	Brina and Miller 1992
10.5. Aqueous Cr(VI)	Cr(VI)	Modified Hach 8023; Pflaun and Howick 1956
10.6. Aqueous Fe(II)	Fe(II)	Modified Hach 8147; Viollier et al. 2000
10.7. Aqueous CN ⁻	CN ⁻	EPA 9014
10.8. Aqueous Br ⁻ column effluent/influent ratio by electrode	Br ⁻	EPA 9211 (Szecsody et al. 2016)
10.9. Anions by ion chromatography	Cl ⁻ , F ⁻ , NO ₃ ⁻ , NO ₂ ⁻ , PO ₄ ⁻³ , SO ₄ ⁻²	EPA 9056A (PNNL-ESL-IC, Rev. 1)
10.10. Aqueous pH by electrode	pH	EPA 9040C (PNNL-ESL-pH, Rev. 2)
10.11. Aqueous SpC by electrode	Specific conductance (SpC)	Modified EPA 9050A (use of multiple SpC standards)
10.12. Total carbon and inorganic carbon in water	Total carbon (TC) and total inorganic carbon (TIC)	EPA 9060A
10.13. Total carbon and inorganic carbon in sediment	TC and TIC	Leco 2002

ICP-OES is inductively coupled plasma optical emission spectroscopy;

ICP-MS is inductively coupled plasma mass spectroscopy

3.4.4 Water and Acid Extraction of Contaminants from Sediments

The water extraction (at 1:1 sediment/water ratio) is the aqueous contaminant fraction extracted in deionized water with a 1.0-hour sediment-water contact time (from EPA 9045D, Rhoades 1996). The acid extraction is at a 1:3 dry sediment/water ratio using 8M HNO₃ for 3 hours at 90°C to 95°C. This is a modified method based on EPA 3051a to not include the HCl, as the chloride interferes with U(VI) analysis.

3.4.5 Sequential Extractions and 1000-hour Carbonate Extraction

Six sequential liquid extractions are conducted on a sediment sample. Extraction 1 is the aqueous contaminant fraction, extraction 2 is the adsorbed contaminant fraction, extraction 3 is the “rind-carbonate” contaminant fraction, extraction 4 is the total carbonate contaminant extraction fraction, extraction 5 is the Fe-oxide contaminant fraction, and extraction 6 is defined as the hard-to-extract contaminant fraction. These sequential extractions are conducted at a 1:2 sediment:liquid ratio at room temperature (20°C to 25°C). The extractions use reagents 1 through 6 defined below.

- **Reagent 1 - Artificial groundwater:**

Constituent	Conc. (mg/L)	Mass for 1 L (g)
H ₂ SiO ₃ •nH ₂ O, silicic acid	15.3	0.0153
KCl, potassium chloride	8.20	0.0082
MgCO ₃ , magnesium carbonate	13.0	0.0130
NaCl, sodium chloride	15.0	0.0150
CaSO ₄ , calcium sulfate	67.0	0.0670
CaCO ₃ , calcium carbonate	150	0.1500

- **Reagent 2 - 0.5 mol/L Mg(NO₃)₂:** 128.2 g Mg(NO₃)₂•6H₂O + 30 µL 2 mol/L NaOH to pH 8.0, balance deionized (DI) H₂O to 1.0 liters
- **Reagent 3 - Acetate solution: 2 liters:** 136.1 g sodium acetate•3H₂O + 30 mL glacial acetic acid (17.4 mol/L), pH 5.0, balance DI H₂O to 2.0 liters
- **Reagent 4 - Acetic acid solution:** concentrated glacial acetic acid, pH 2.3; 2 liters: 50.66 mL glacial acetic acid (17.4 mol/L) + 47.2 g Ca(NO₃)₂•4H₂O, pH 2.3, balance DI H₂O to 2.0 liters
- **Reagent 5 - Oxalate solution:** 0.1 mol/L ammonium oxalate, 0.1 mol/L oxalic acid; 1 liter: 9.03 g anhydrous oxalic acid + 14.2 g ammonium oxalate•H₂O, balance DI H₂O to 1.0 liters
- **Reagent 6 - 8.0 mol/L HNO₃:** 502 mL conc. HNO₃ (15.9 mol/L) + 498 mL DI H₂O

In the first extraction, 6 mL of artificial groundwater (reagent 1) is mixed with 3.0 (±0.5) g of sediment for 50 minutes; the tube is then centrifuged at 3000 rpm for 10 minutes, and liquid is drawn off the top of the sediment and filtered (0.45-µm) for analysis. Extractions 2 and 3 are conducted with the same procedure except using reagents 2 and 3, respectively. The fourth extraction uses the same procedure except with a contact time of 5 days and with use of reagent 4. The fifth extraction is conducted the same as extraction 1 except using reagent 5. In the sixth extraction, 6 mL of nitric acid (reagent 6) is added and mixed for 2 hours at 95°C with the sediment; the tube is then centrifuged at 3000 rpm for 10 minutes, and liquid is drawn off the top of the sediment and filtered (0.45-µm) for analysis.

The 1000-hour carbonate extraction is a separate extraction from sequential extractions. The carbonate solution (0.0144M NaHCO₃ + 0.0028M Na₂CO₃ (pH 9.3); 2 liters: 2.42 g NaHCO₃ + 0.592 g Na₂CO₃ + balance DI H₂O to 2.0 liters) is used for the 1000-hour carbonate extractions (Kohler et al. 2004). Sediment (3.0 ±0.5 g) and 6.0 mL of the carbonate solution were placed in 45-mL Teflon or polycarbonate centrifuge tubes, mixed for 1000 hours at 6 rpm, and centrifuged at 3000 rpm for 10 minutes, and liquid is drawn off the top of the sediment and filtered (0.45-µm) for analysis.

3.4.6 Iron and Manganese Extractions

Iron extractions are conducted to quantify ferrous and ferric iron (Gibbs 1976), and manganese that are solubilized by different solutions. These extractions are conducted in an anoxic chamber.

- For the first extraction, sediment samples (2.0 ± 0.5 g) were mixed with 10.0 mL of ion exchange solution (1.0 mM CaCl_2) for 50 minutes at 6 rpm, centrifuged (3000 rpm, 10 minutes), liquid filtered (0.45- μm), and the solution is analyzed for Fe(II) and Mn.
- For the second extraction, sediment samples (2.0 ± 0.5 g) were mixed with 10.0 mL of 0.5M HCl (reagent 10) for 24 hours at 6 rpm, centrifuged (3000 rpm, 10 minutes), liquid filtered (0.45- μm), and the solution was analyzed for Fe(II) and Mn.
- For the third extraction, sediment samples (2.0 ± 0.5 g) were mixed with 10.0 mL of 5.0M HCl for 24 hours at 6 rpm, centrifuged (3000 rpm, 10 minutes), liquid filtered (0.45- μm), and the solution was analyzed for Fe(II) and Mn.
- For the fourth extraction, sediment samples (2.0 ± 0.5 g) were mixed with 10.0 mL of 0.25M $\text{NH}_2\text{OH}\cdot\text{HCl}$ solution for 30 minutes at 50°C , centrifuged (3000 rpm, 10 minutes), liquid filtered (0.45- μm), and the solution was analyzed for total Fe and Mn.
- For the fifth extraction, sediment samples (2.0 ± 0.5 g) were mixed with 10.0 mL of dithionite-citrate-bicarbonate solution (0.3 mol/L Na-citrate, 1.0 mol/L NaHCO_3 , and 0.06 mol/L sodium dithionite), mixed for 30 minutes at 80°C , centrifuged (3000 rpm, 10 minutes), liquid filtered (0.45- μm), and the solution was analyzed for total Fe and Mn.

3.4.7 Batch Leach Experiment

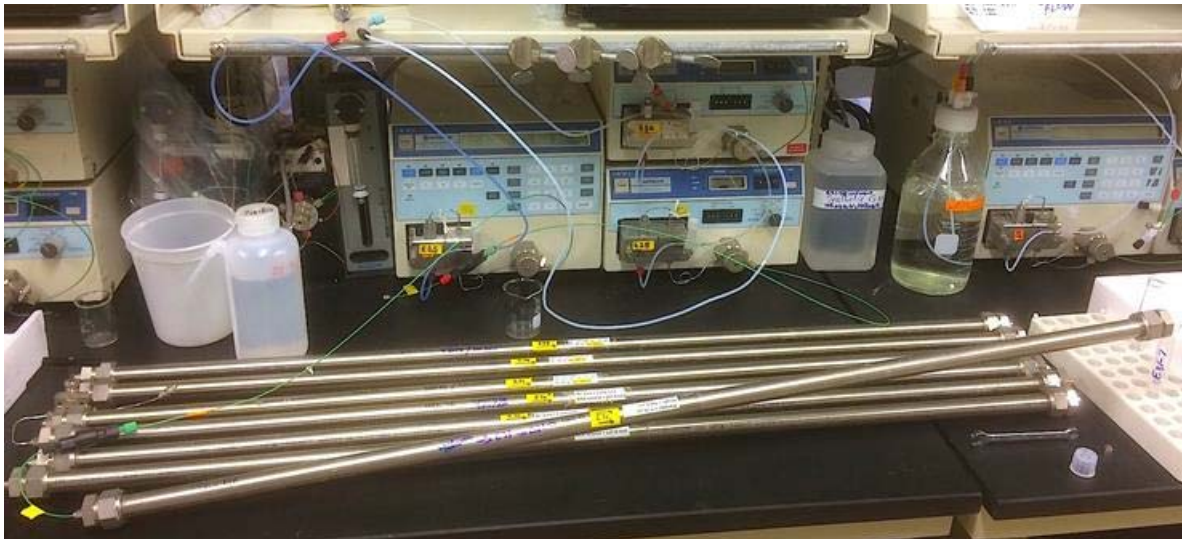
Batch experiments used 50 g of sediment and 200 mL of air-saturated artificial groundwater placed in a 250-mL polyethylene centrifuge bottle (Figure 3.2a). The bottle was placed on a slow (12-rpm) linear mixer with supernatant samples taken at 1, 10, 30, 100, 300, 1000 hours for analysis of the target contaminants. Sampling consisted of (a) centrifuging the bottle at 3000 rpm for 10 minutes, (b) removing 5.0 mL from the bottle, and (c) filtering the liquid (0.45 μm).



(a)



(b)



(c)

Figure 3.2. Images of (a) batch water leach experiments, (b) 1-D column water leaching experiments with continuous flow, and (c) no-flow column reduction rate and capacity experiments.

3.4.8 1-D Column Leach Experiment

Sediment column experiments were conducted with 1-D, vertical, bottom-up flow of injected simulated groundwater solution through contaminated sediment (Figure 3.2b). The concentration of contaminant in the effluent was measured. A non-sorbing, non-reactive tracer (bromide ion) was included in the injection solution and its breakthrough was measured to assess column flow dynamics. The flow rate was set to achieve a residence time of between 1 and 4 hours. Sampling frequency in the effluent was varied based on typical contaminant elution dynamics, with more dynamics present at earlier times (fewer pore volumes).

Stop-flow events ranging from 16 to 300 hours were conducted where the flow rate of solution through the column was stopped to provide time for contaminants present in one or more surface phases on the sediment surface to partition into pore water (i.e., from diffusion from intraparticle pore space or time-dependent dissolution of precipitate phases or slow desorption). Operationally, initiating a stop-flow event involves turning off the pump and plugging both ends of the column (to prevent water movement out of the sediment column). Ending a stop-flow event involves reconnecting the column to the pump, turning on the effluent sample collector, and then turning on the pump. The calculation of the contaminant release rate from sediment (μg contaminant/g of sediment/day) uses the contaminant effluent concentration before and after the stop-flow event, and the length of time of the stop-flow event.

3.4.9 1-D No-Flow Contaminant Reduction Rate Experiment

No-flow experiments were conducted at a high sediment/water ratio to characterize the rate at which specific contaminants [U(VI) and iodate] may be reduced. The high sediment/water ratio of a 1-D column was used to obtain rates in near field conditions. These experiments consisted of (a) packing the 100-cm-long column (Figure 3.2c) with sediment and equilibrating with 10 pore volumes of artificial groundwater (to obtain bulk density and porosity), (b) injecting 20 pore volumes of 100 $\mu\text{g/L}$ Ca-uranyl carbonate and 100 $\mu\text{g/L}$ iodate in artificial groundwater into the column to equilibrate the pore water and sorption sites with U-238 and iodate, (c) at periodic times (1, 10, 30, 100, 300, 1000 hours) injecting $\sim 1/10$ of a pore volume of contaminant-free water at the inlet end and collect $\sim 1/10$ of a pore volume of water at the column effluent end, and (d) analyzing U-238 and iodine species (iodate, iodide) in samples. Previous studies of Hanford sediments show there is a small natural abiotic and/or biotic reductive capacity that can reduce a low concentration of pertechnetate, chromate, and iodate.

3.5 Objective 6: Oxygen and Hydrogen Isotopic Signature of the Pore Water

Isotopic analysis for oxygen and hydrogen can be applied for water samples or water extracted from sediment (Prudic et al. 1997). Within the vadose zone, however, much of the sample water remains bound to the surfaces of soil particles or contained within pore spaces, making isotope measurement challenging. An extraction procedure was used to quantitatively remove water from solid soil samples and ensure minimal isotopic fractionation during the extraction and collection process.

A vacuum distillation apparatus was applied for extraction (Figure 3.3). This apparatus was constructed based on slightly modified versions of those discussed in West et al. (2006) and Goebel and Lascano (2012). In brief, a soil sample was added to one end of the system and then frozen to prevent water migration out of the material. Following establishment of a vacuum, the sample is heated to drive off the native water, which is collected in a cryogen trap cooled by liquid nitrogen. Once the extraction is complete, the water is removed from this cryogen trap and its isotopic content can be analyzed on a separate instrument, offline from the extraction system. Extracted water was analyzed for isotopic ratios using a PNNL operating procedure (OP-DVZ-AFRI-002) for the analytical instrument.

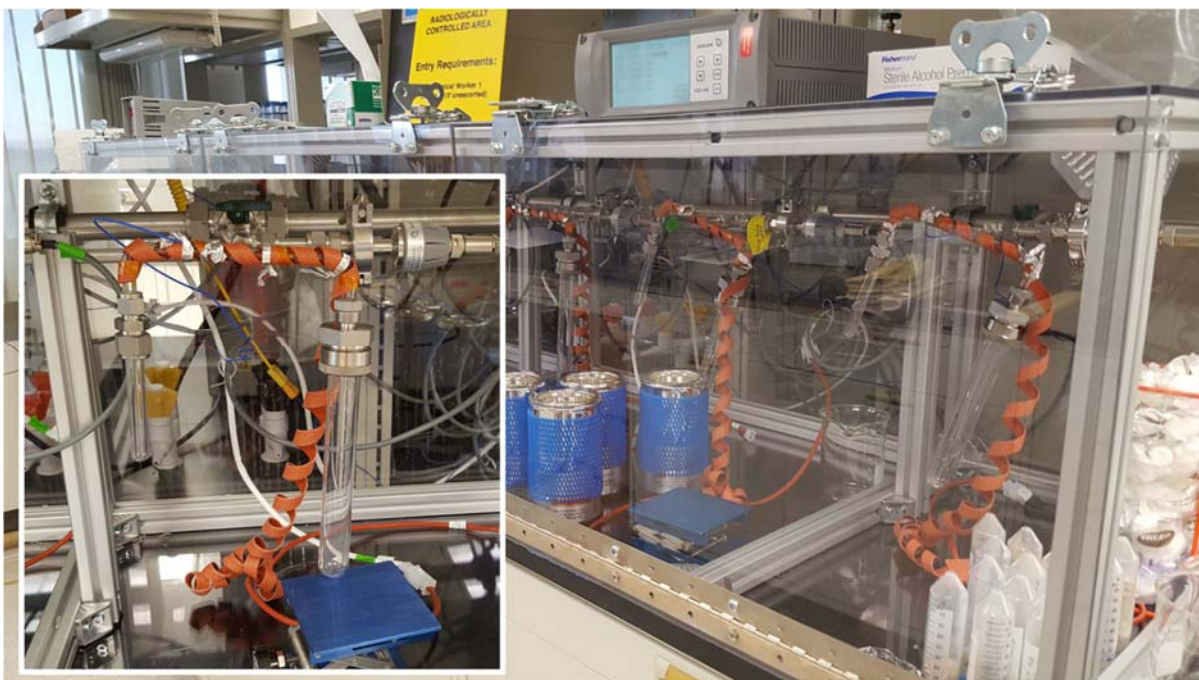


Figure 3.3. Pictures of the water extraction line system. The insert shows a single cell on the line where a sample is placed in the large tube on the right and water is cryogenically trapped in the smaller tube on the left. The backdrop shows the larger system setup, whereby a series of these cells are connected and share access to a common vacuum manifold (the stainless steel line behind the extraction cells).

4.0 Results

The laboratory analysis data are described below and interpreted in relation to the three main objectives of the work (Section 2.0). These objectives were developed to be consistent with EPA guidance for evaluating natural attenuation of contaminants and provide data to support contaminant fate and transport assessments. The sections below present the data for each of the three objectives.

Section 4.1 presents the contaminant distribution data in the context of the hydrologic and biogeochemical setting. This information allows the data collected in this effort to be linked with the 200-DV-1 OU characterization data compiled by CHPRC. Collectively, this information is a foundation for interpreting contaminant distribution, correlations between contaminant data and other types of data, and the conditions at locations used to determine attenuation and transport parameters, and consists of the following:

- 4.1.1 Contaminants and Geochemical Constituents
- 4.1.2 Microbial Ecology
- 4.1.3 Iron and Manganese Characterization
- 4.1.4 Oxygen and Hydrogen Isotopes
- 4.1.5 Sediment Physical Characterization

Section 4.2 presents and interprets data in terms of identifying contaminant attenuation processes and the types of attenuation mechanisms that are suggested by these data, and consists of the following:

- 4.2.1 Sequential Extractions and 1000-hour Carbonate Extraction for U-238, I-127, Tc-99, and Cr
- 4.2.2 Sequential Extractions for Major Cations/Metals (Ca, Mg, K, Na, Al, Si)
- 4.2.3 U(VI) and Iodate Reduction Rate Experiments

Some of these data quantify how contaminants are distributed in different phases within the vadose zone that relate to attenuation processes and contaminant mobility.

Section 4.3 presents contaminant mobility data based on batch or column experiments, as follows:

- 4.3.1 Long-term Contaminant Sediment-Water Partitioning (batch water leach)
- 4.3.2 1-D Water Leach of Contaminants Cr^{VI}, U-238, Tc-99, and I-127
- 4.3.3 1-D Water Leach of Co-Contaminant Ions

These batch and column experiment data provide information to estimate contaminant partitioning and kinetically controlled release rates from sediments. This report provides an initial interpretation of attenuation and transport parameters. The data will also be useful for additional interpretation by others through modeling of the results (e.g., to evaluate surface complexation parameters).

4.1 Contaminant Distribution

4.1.1 Contaminants and Geochemical Constituents

Contaminants are present in vadose zone sediments in pore water, adsorbed on surfaces, and as precipitates. Different extractions were used to remove specific fractions of ions and contaminants from the pore water and sediments. The water extraction (1 mL deionized water/1 g of sediment, 1 hour) was used to evaluate pore water geochemistry (i.e., pH, specific conductance), cations/anions present in pore water, and contaminants of concern that are present in pore water. The water extraction may also remove some fraction of adsorbed ions/contaminants. Due to the short water/sediment contact time (1 hour), there is little slow dissolution of contaminants that are present in precipitates. Time-dependent water extraction of contaminants to 1000 hours (in batch experiments) is described in Section 4.2.2, and time-dependent water elution of contaminants in 1-D columns is described in Section 4.2.3.

An 8M nitric acid extraction (3 mL acid/1 g sediment, 3 hours at 95°C) was used to dissolve most (but not all) surface precipitates that may contain contaminants, and thus was used as a measure of the total contaminant present in pore water, adsorbed, and in surface precipitates. A series of sequential extractions using different solutions was also conducted to quantify contaminants present in aqueous, adsorbed, and specific precipitate phases.

Geochemical characterization of the pore water, based on water-extractable ions (Table 4.1, and in different units in Appendix B) showed that there was significant Na-nitrate contamination in the three depths analyzed in borehole C9552, and small Na-nitrate contamination in C9487 and C9488 borehole samples. The specific conductance of the pore water (normalized to the conductance in the pore water) was a good indicator of ion contamination. Interestingly, pore water pH of the C9552 borehole sediments was near neutral (pH 7.15 to 8.14), yet two depths in the C9487 borehole indicated an alkaline pH (pH 9.94 and 10.0), indicating some contamination. Results from pore water extraction of an uncontaminated vadose zone sediment (ERDF pit, 40-ft depth) from a different project are included for comparison.

There was significant uranium contamination in the two alkaline pH samples from borehole C9487 (Table 4.2), with 0.001 and 0.25 µg/g water-extractable U and 0.38 and 5.5 µg/g acid-extractable U (reported per gram of sediment). The sediment with the highest uranium mass (C9487 58.2-ft depth) did release significant uranium in column studies (Section 4.3.2). These samples did not contain Tc-99. In contrast, the three C9552 sampled depths contained significant water and acid extractable Tc-99, somewhat elevated I-127 concentrations, and lower U-238 concentrations. There were low concentrations of water-extractable cyanide in three C9552 borehole samples (< 0.042 µg/g). Chromium was not detected in water extractions, but significant chromium was present in the acid-extractable fraction (third to last column, Table 4.2) and in the alkaline-extractable solution (second to last column). Batch experiments (described in the following section) also showed some chromium was released over hundreds of hours.

Table 4.1. Geochemical characterization of sediment pore water by water/sediment (1:1) extraction.

Borehole	Depth (ft)	HEIS #	Moisture (g/g)	pH	SpC (mS/cm)	SpC (mS/cm) ^(a)	Ca (μg/g)	Mg (μg/g)	Na (μg/g)	K (μg/g)	Fe (μg/g)	Cl (μg/g)	F (μg/g)	SO ₄ (μg/g)	NO ₃ (μg/g)	NO ₂ (μg/g)	PO ₄ (μg/g)	CO ₃ (μg/g)	TOC (μg/g)
C9552	104.2–105.2	B34H37	0.0308	7.88	7.28	244	43.5	5.05	831	7.75	0.938	20.7	ND	916	3510	ND	ND	33.6	4.24
C9552	134.1–135.1	B34H55	0.0216	8.14	4.66	220	15.6	6.83	478	7.28	0.646	14.8	ND	113	2500	ND	ND	31.3	4.52
C9552	194.2–195.2	B34H79	0.0317	7.15	3.86	126	216	47.1	74.8	9.67	0.394	14.2	ND	34.1	2270	ND	ND	NA	NA
C9487	58.2–59.2	B34W66	0.0367	9.94	0.64	18.1	ND	ND	57.9	14.3	ND	ND	14	26.7	50.9	ND	ND	43.0	4.56
C9487	134.1–135.1	B34WB2	0.0285	10.0	0.201	7.25	ND	ND	21.5	ND	ND	1.77	0.28	4.33	6.13	ND	ND	102	6.05
C9487	230.0–231.0	B354L8	0.2272	8.68	0.605	3.27	2.56	1.14	65.4	ND	ND	15	6.93	78	97.9	5.01	ND	129	NA
C9488	219.3–220.3	B355L3	0.2427	7.93	1.16	5.94	18.5	9.83	86.3	4.72	ND	109	ND	733	1360	ND	7.96	227	2.76
ERDF pit	40' uncontam.		0.0102	8.31		15	36.1	9.7	414	46.9	1.1	465	8.6	230	95	ND	ND		

(a) In pore water volume, as originally in pore water and/or solubilized by water extract. NA = not analyzed ND = not detected SpC = specific conductance

Table 4.2. Water and acid extractable concentration of contaminants in sediments.

Borehole	Depth (ft)	HEIS #	U-238 (μg/kg)	U-238 (μg/kg)	Tc-99 (pCi/g) ^b	Tc-99 (pCi/g) ^b	I-127 (μg/kg)	I-127 (μg/kg)	Cr (μg/kg)	Cr (μg/kg)	Cr ^{VI} (μg/kg)	CN- (μg/kg)
			HNO ₃		HNO ₃		HNO ₃		H ₂ O	HNO ₃	alk.	H ₂ O
			H ₂ O extr.	extr.	H ₂ O extr.	extr.	H ₂ O extr.	extr.	extr.	extr.	extr.	extr.
C9552	104.2 – 105.2	B34H37	0.747	422	78.9	104	2.00	(a)	ND	6430	ND	42
C9552	134.1 – 135.1	B34H55	0.420	328	60.4	79.9	0.931	(a)	ND	6680	ND	36
C9552	194.2 – 195.2	B34H79	0.386	350	29.9	89.1	12.1	(a)	ND	7570	683	ND
C9487	58.2 - 59.2	B34W66	251	5500	ND	ND	1.64	(a)	ND	4790	ND	ND
C9487	134.1 – 135.1	B34WB2	0.961	382	ND	ND	1.36	(a)	ND	8240	1180	ND
C9487	230.0 – 231.0	B354L8	16.1	628	0.80	ND	2.53	(a)	ND	9830	ND	ND
C9488	219.3 – 220.3	B355L3	0.276	599	9.38	ND	3.44	(a)	ND	11200	1280	ND

(a) Aqueous iodine volatilizes as I₂ in acidic matrix, not analyzed.

(b) Tc-99 specific activity 0.017 Ci/g (Reynolds, 1973)

4.1.2 Microbial Ecology

Sediment samples from various depths in boreholes C9487, C9488, and C9552 were analyzed for the density of viable bacteria using both most probable number (MPN) analyses. MPN analyses were also performed to determine the numbers of nitrate-reducing, iron-reducing, and manganese-reducing bacteria. Numbers of aerobic bacteria in the samples was low in sediments from all depths for core C9552 (see Table 4.3). Cores C9487 and C9488, showed aerobic bacteria at greater than 1.1×10^6 cells/g of sediment at depths greater than 200' bgs. Results indicated greater than 1.1×10^6 denitrifying bacteria per gram of sediment, regardless of the depth sampled or borehole from which the sample originated. Density of iron-reducing bacteria increased with depth, and iron-reducing bacteria were present in numbers greater than 1.1×10^6 in sediment taken from deeper than ~134 ft bgs. Analysis of ferrous iron, showed that turbidity in the vials was associated with iron reduction. Numbers of manganese reducing bacteria was low in all samples tested. Initial results for total heterotrophs using plate counts were inconclusive for sediment from borehole C9552, so these analyses are being repeated. Total heterotrophs for sediments from boreholes C9487 and C9488 showed approximately 2×10^6 colony forming units per gram of sediment. These results indicate stimulation of microbial communities in the B-Complex vadose zone can lead to transformation of inorganic contaminants such as nitrate, or metals and radionuclides.

Abundance of bacterial phyla in the B-Complex boreholes (C9552 and C9487) was determined by sequencing DNA extracted from the sediments. Extracted DNA was sent to the Institute for Genomics and Systems Biology Next Generation Sequencing Core Facility at Argonne National Laboratory for processing using an Illumina MiSeq instrument. Raw sequences were processed in silico and percent abundance of phyla in each sample was determined (Figure 4.1). Bacteria in the *Proteobacteria* phylum were dominant in all of the samples, accounting for 68% to 96% of the bacteria in the samples. Other less-dominant but plentiful phyla include *Firmicutes* and *Actinobacteria*. These results indicate that facultative anaerobic bacterial phyla common to sediment environments are present in the B-Complex vadose zone. Facultative anaerobes can grow in oxic as well as anoxic environments using alternate electron acceptors such as nitrate. Phyla found in the samples also contain many bacterial species that are capable of contaminant transformation, which ultimately could affect fate and transport.

The presence of facultative anaerobic bacterial phyla, as well as the capacity to grow using nitrate and iron, indicate the functional capacity for contaminant transformation in the B-Complex vadose zone.

Table 4.3. Nitrate-, iron-, or sulfate-reducing microbial biomass by MPN.

HEIS #	Well	Depth (ft)	Nitrate	Fe-Citrate	MnO ₂	Aerobic
B34H33	C9552	99.2	> 1,100,000	4,600	23	1,100
B34H37	C9552	104.25	150,000	> 1,100	93	240
B34H41	C9552	109.2	> 1,100,000	4,600	23	240
B34H47	C9552	129.3	> 1,100,000	15,000	43	240
B34H55	C9552	134.1	> 1,100,000	7,500	23	240
B34H63	C9552	139.2	> 1,100,000	150,000	460	1,100
B34H71	C9552	189.2	> 1,100,000	> 1,100,000	23	93

B34H79	C9552	194.2	> 1,100,000	> 1,100,000	43	240
B34H87	C9552	199.3	> 1,100,000	> 1,100,000	210	1,100
B34WB3	C9487	134.1	> 1,100,000	1,100,000	2,100	>11,000
B354L2	C9487	227.7	> 1,100,000	> 1,100,000	2,800	>1,100,000
B355L3	C9488	219.3		> 1,100,000	240	>1,100,000

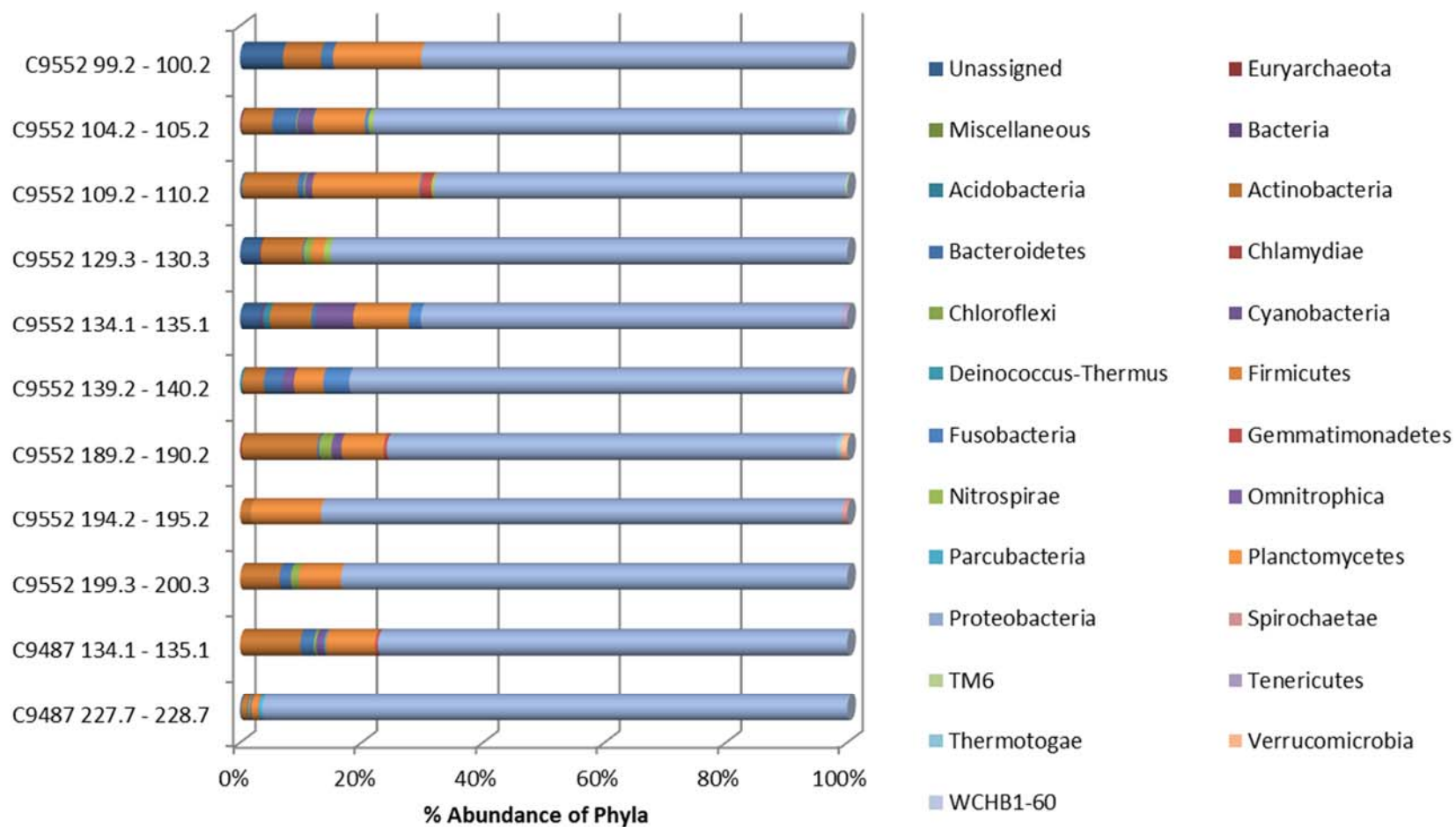


Figure 4.1. Abundance of bacterial phyla based on DNA sequencing of bacteria extracted from sediments.

4.1.3 Iron and Manganese Characterization

The relative distribution of iron and manganese in different forms provides insight into the sorptive and reactive capacity of the sediments. Table 4.4 and Table 4.5 show the results of the extractions and iron and manganese analyses. For context, the information for iron is also plotted, showing the relative portions of different iron forms and the relative amount of redox-active iron and ferrous iron phases (Figure 4.2a) and Mn phases (Figure 4.2b).

Table 4.4. Ferrous and ferric iron phases in sediments based on liquid extractions.

Borehole Depth (ft)	HEIS #	ads. Fe ^{II} (mg/g)	Fe ^{II} CO ₃ , FeS (mg/g)	Other Fe ^{II} (mg/g)	am. Fe ^{III} (mg/g)	crys. Fe ^{III} (mg/g)	Other Fe ^{III} (mg/g)	Total Fe ^{III} (mg/g)
C9552 104.2-105.2	B34H37	< 2.50E-3	1.76	0.18	2.04E-02	0.227	15.3	17.5
C9552 134.1-135.1	B34H55	< 2.50E-3	1.42	0.00	2.11E-02	0.221	16.8	18.4
C9552 194.2-195.2	B34H79	< 2.50E-3	2.17	0.00	3.82E-02	0.287	19.9	22.4
C9487 58.2 - 59.2	B34W66	< 2.50E-3	0.91	4.56	3.43E-03	4.71	7.29	17.5
C9487 134.1-135.1	B34WB2	< 2.50E-3	1.45	1.08	2.12E-02	0.221	15.9	18.7
C9487 230.0-231.0	B354L8	< 2.50E-3	1.06	1.10	1.89E-02	0.980	14.8	18.0
C9488 219.3 – 220.3	B355L3	< 2.50E-3	1.67	0.44	4.32E-03	1.31	16.1	19.5
C9488 219.3 – 220.3	B355L3	< 2.50E-3	1.80	0.33	3.41E-03	1.38	16.1	19.6

Table 4.5. Manganese phases in sediments based on liquid extractions.

Borehole Depth (ft)	HEIS #	ads. Mn ^{II} (mg/g)	Mn ^{II} CO ₃ (mg/g)	am. Mn ^{II+IV} (mg/g)	crys. Mn ^{II+IV} (mg/g)	Other Mn ^{II+IV} (mg/g)	Total Mn ^{II+IV} (mg/g)
C9552 104.2-105.2	B34H37	8.29E-04	0.117	0.058	4.40E-04	0.082	0.252
C9552 134.1-135.1	B34H55	8.16E-04	0.093	0.055	< 1.0E-4	0.146	0.296
C9552 194.2-195.2	B34H79	2.99E-03	0.106	0.054	< 1.0E-4	0.169	0.332
C9487 58.2 - 59.2	B34W66	5.83E-04	0.117	0.031	1.86E-02	0.121	0.288
C9487 134.1-135.1	B34WB2	6.76E-04	0.099	0.053	< 1.0E-4	0.125	0.279
C9487 230.0-231.0	B354L8	1.83E-03	0.125	0.101	< 1.0E-4	0.054	0.281
C9488 219.3 – 220.3	B355L3	5.83E-03	0.152	0.085	2.40E-03	0.067	0.311
C9488 219.3 – 220.3	B355L3	4.69E-03	0.166	0.080	1.89E-02	0.030	0.300

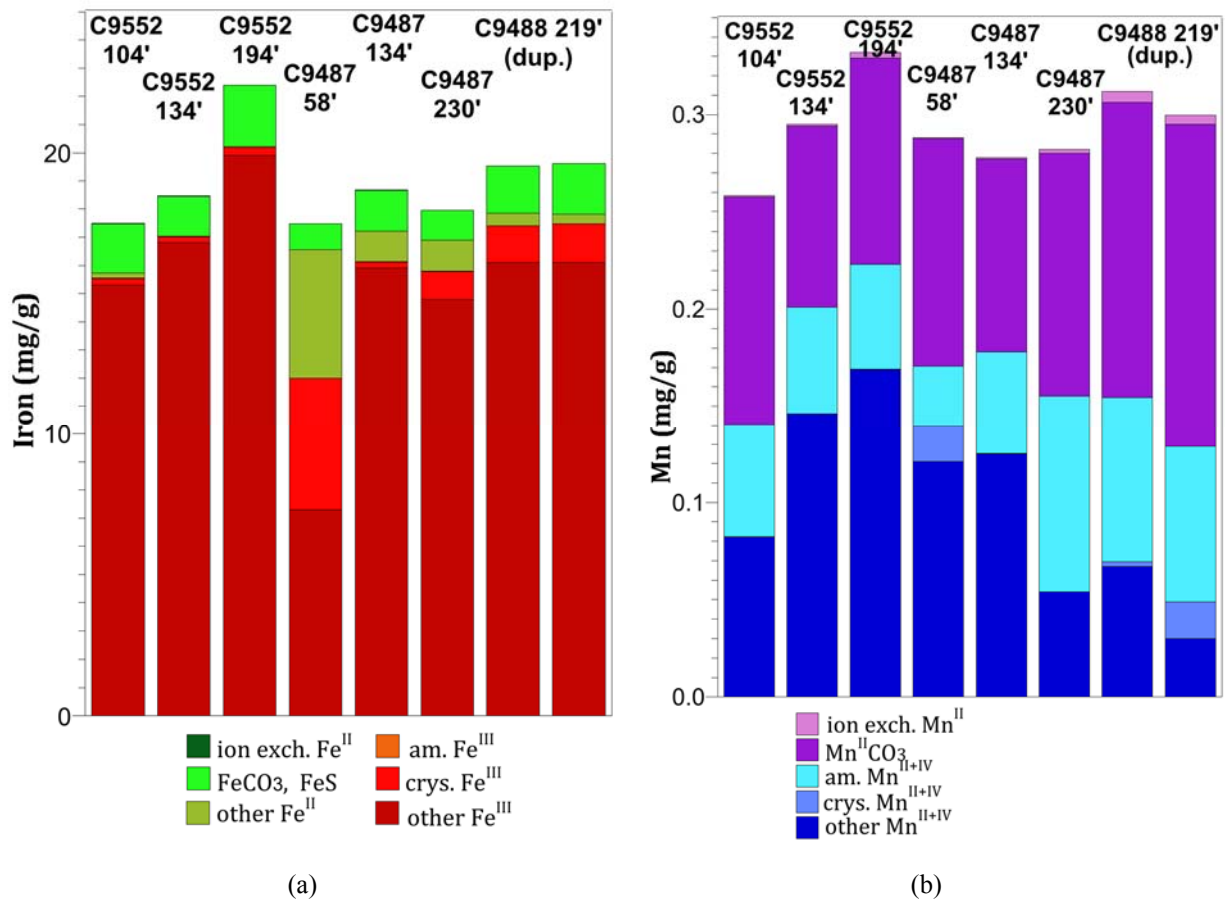


Figure 4.2. Iron (a) and manganese (b) surface phase distributions in sediments, based on liquid extractions.

Iron and manganese extractions were conducted to characterize the potential for contaminant reduction in the sediments. Sediments contained a total of 18 to 22 mg/g extractable iron, based on a 3-week 5M HCl extraction. These B-Complex subsurface sediments contain a mixture of mafic (i.e., sediments derived from basalt) and granitic minerals, with mafic minerals (pyroxenes, amphiboles) and clay minerals containing significant Fe and Mn phases (Table 4.6). The amorphous and crystalline ferric iron oxide phase concentrations were small (< 0.1 mg/g, Table 4.4; available for microbial iron reduction), whereas the majority of ferrous iron was likely in pyroxene and amphibole phases. Ferrous phases accounted for ~13.5% of the total iron (green bars in Figure 4.2a), with little adsorbed ferrous iron (dark green; Table 4.4), minor ferrous iron in carbonates/sulfides (light green), some of which is redox reactive, and the remaining ferrous iron in unidentified phases (likely in clays). The sediment from C9487 at 58' depth had a greater fraction of ferrous iron phases (32%) than other sediments. Although all of these sediments are from the vadose zone, if water saturated, some abiotic reduction can occur (Szecsody et al. 2014) due to the availability of ferrous iron from carbonates/sulfides.

Although the total manganese (II and IV) extracted from the sediment (0.25 to 0.34 mg/g, Table 4.5) was only 1.5% of the total iron in the sediment, there was a greater fraction of potentially redox reactive

Mn^{II}. Ion exchangeable Mn^{II} was small (0.7 to 5.8 µg/g), but the Mn^{II} associated with carbonates (0.09 to 0.17 mg/g) was significant. Mn^{II} phases were 32% to 57% of the total Mn.

Table 4.6. Summary of Hanford mineralogy (Xue et al. 2003).

Mineral	Formula	Both Fm (% wt)	Hanford Fm (% wt)	Ringold Fm (% wt)
Quartz	SiO ₂	37.7 ± 12.4	38.4 ± 12.8	37.03 ± 12.4
Microcline	KAlSi ₃ O ₈	17.0 ± 6.7	15.3 ± 4.4	18.7 ± 8.0
Plagioclase	NaAlSi ₃ O ₈ -CaAl ₂ Si ₂ O ₈	18.7 ± 7.7	22.2 ± 7.2	15.5 ± 6.8
Pyroxenes	(Ca,Mg,Fe)Si ₂ O ₆	3.03 ± 5.99	5.01 ± 7.83	1.14 ± 2.52
Calcite	CaCO ₃	4.97 ± 7.19	1.91 ± 1.71	0.68 ± 0.92
Magnetite	Fe ₃ O ₄	5.09 ± 4.37	4.46 ± 4.12	5.68 ± 4.63
Amphiboles	Ca ₂ (Mg, Fe, Al) ₅ (Al, Si) ₈ O ₂₂ (OH) ₂	5.55 ± 5.97	5.46 ± 5.67	5.64 ± 6.40
Apatite	Ca ₁₀ (PO ₄) ₆ (OH) ₂	0.60 ± 1.04	0.52 ± 0.92	0.67 ± 1.16
Mica ^(a)	(K, Na,Ca)(Al, Mg, Fe) ₂ - 3(Si,Al) ₄ O ₁₀ (O, F, OH) ₂	2.07 ± 4.47	2.46 ± 3.74	1.71 ± 5.15
Ilmenite	FeTiO ₃	2.51 ± 2.66	1.28 ± 1.51	3.67 ± 3.00
Epidote	{Ca ₂ } {Al ₂ Fe ³⁺ } [O OH SiO ₄ Si ₂ O ₇]	1.65 ± 2.98	1.78 ± 3.75	1.52 ± 2.14
(a) Muscovite, biotite, phlogopite, lepidolite, clintonite, illite, phengite				

4.1.4 Oxygen and Hydrogen Isotopes

Isotopic analysis for oxygen and hydrogen are developed and applied for multiple purposes (Prudic et al. 1997). For instance, the stable isotopes of water (δ²H [deuterium] and δ¹⁸O [18-oxygen]) can be used to assist with tracking of underground contaminant plumes or linking a source to a measured water sample. For the 200-DV-1 OU, the pore water in the vadose zone is a mixture of water from previous natural recharge and the anthropogenic water discharges of waste streams. Isotopic data was collected to assess whether the signatures from different areas can be correlated to mixtures of different types of water sources. As shown in Table 4.7, this section includes data for sediment samples collected from the B-Complex (borehole C9552 [BY Cribs waste site], borehole C9487 [B7-AB waste site], and C9488 [B-8 waste site]). To assist interpretation, this section also includes data for sediment samples from the S- and T-Complexes (Truex et al. 2017; borehole C9507 [T-19 waste site], borehole C9510 [T-25 waste site], and borehole C9512 [S-9 waste site]) and for water samples from the perched-water aquifer in the B-Complex (Lee et al. 2017).

Table 4.7. Sediment samples selected for analyses and isotope data values (outliers removed).

Borehole and Liner Designation	Borehole ID	Sample ID	Nominal Geologic Unit	Depth Interval (ft bgs)	Data Source	$\delta^{18}\text{O}$ (‰)	$\delta^2\text{H}$ (‰)
BY Cribs 13A	C9552	B341B1	H2	102.2 – 103.2	This report	-13.48 (0.2)	-128.3 (1.0)
BY Cribs 18A	C9552	B341C1	H2	127.3 – 128.3	This report	-15.13 (1.1)	-134.9 (3.3)
BY Cribs 19A	C9552	B341C3	H2	132.1 – 133.1	This report	-14.18 (0.4)	-130.3 (0.9)
BY Cribs 30A	C9552	B34H74	CCUg	192.2 – 193.2	This report	-16.43 (0.9)	-145.0 (5.7)
B7-AB 17A	C9487	B34WB1	H2	132.1 – 133.1	This report	-19.24 (0.1)	-143.3 (0.1)
B7-AB 35D	C9487	B34WH8	H2/CCUz	220.0 – 221.0	This report	-18.11 (1.8)	-141.8 (9.7)
B7-AB Opt. 12C	C9487	B354L1	CCUz	227.2 – 227.7	This report	-16.19 (0.5)	-127.0 (1.4)
B7-AB Opt. 14C	C9487	B354M3	CCUz	232.0 – 233.0	This report	-17.73 (0.9)	-135.4 (3.5)
B-8 37B	C9488	B355L8	CCUz	222.5 – 225.5	This report	-16.09 (0.9)	-129.4 (5.6)
T19 14A	C9507	B35432	CCUz	92.1-93.1	Truex et al. (2017)	-19.36 (2.0)	-145.5 (7.8)
T19 16A	C9507	B35441	CCUc	102.4-103.4	Truex et al. (2017)	-17.54 (1.0)	-135.1 (6.0)
T-19 Ringold	C9507	B35461	Ringold	139.1-139.6	Truex et al. (2017)	-15.33 (0.3)	-123.9 (1.1)
T-25 14A	C9510	B361M7	H2/CCUz	112.3-113.3	Truex et al. (2017)	-17.16 (0.2)	-138.0 (0.9)
S-9 8A	C9512	B36173	H1/H2	62.2-63.2	Truex et al. (2017)	-21.05 (2.7)	-146.7 (11.5)
S-9 20A	C9512	B361D9	H2/CCUz	122-123	Truex et al. (2017)	-20.54 (1.1)	-143.5 (6.2)
Perched Water	299-E33- 344	B33CV5	Well Samples	NA	Lee et al. (2017)	-15.7 (0.2)	-124.0 (0.8)
Perched Water	299-E33- 350	B35K19	Well Samples	NA	Lee et al. (2017)	-14.7 (0.2)	-119.4 (0.5)
Perched Water	299-E33- 351	B34V09	Well Samples	NA	Lee et al. (2017)	-13.7 (0.3)	-116.1 (1.2)

Isotopic ratios for deuterium and 18-oxygen are reported in delta (δ) notation, defined as

$$\delta = \left(\frac{R_{sa}}{R_{std}} - 1 \right) \times 1000$$

where R is the ratio of the abundance of the heavy to light isotope (i.e., $^2\text{H}/^1\text{H}$, $^{18}\text{O}/^{16}\text{O}$), *sa* denotes the sample, and *std* indicates the standard (McKinney et al. 1950). Delta values are reported in per mil (‰), with $\delta^2\text{H}$ and $\delta^{18}\text{O}$ values relative to Vienna Standard Mean Ocean Water ($\delta^2\text{H} = 0\text{‰}$, $\delta^{18}\text{O} = 0\text{‰}$).

Isotopic analysis for oxygen and hydrogen are typically plotted as shown in Figure 4.3, which also shows the global meteoric water line (Craig 1961), an assembled regional meteoric water line (Graham 1983), and the rough isotope region reported for Columbia River surface water at this location (Spane and Webber 1995) for comparison to the values of water extracted and measured in this study. Error bars correlate to the standard deviation resulting from a minimum of triplicate extraction replicates, each isotopically analyzed using multiple analytical replicates ($n \geq 9$). All data is shown in Figure 4.3a, while Figure 4.3b contains a culled data set in which a Modified Thompson Tau test was used to eliminate outliers in the data that may have resulted from a combination of inherent sample heterogeneity and/or inefficient water extraction. Note that while this statistical application may have reduced the size of associated error bars, the overall trends discussed below remain intact. As such, the additional data discussion is based on the revised data set resulting from the statistical rejection of outlier data points (at the 95% confidence interval). In addition to the vadose zone sediment samples analyzed, isotopic ratios

are plotted for water extracted from the perched-water aquifer in the B-Complex (errors bars correlate to the standard deviation of the analytical replicates, $n \geq 9$).

The global meteoric water line (Craig 1961) shows the average relationship, worldwide, between $\delta^2\text{H}$ and $\delta^{18}\text{O}$ in natural terrestrial waters (e.g., rivers, lakes) and precipitation. The deviation between the local and global meteoric water lines is attributed to evaporative processes coupled to the typically short precipitation durations and semi-arid nature of the local region (Graham 1983). There is overlap between the local meteoric water correlation for each of the extracted water samples and nearly all of the perched water samples, suggesting close connection between regional precipitation and the samples. There is also an interesting relationship between the data from boreholes containing three or more data points (C9507 [Truex et al. 2017], C9552, and C9487). In each of these cases, the data show strong correlation between the two isotopes (R^2 of 1.00, 0.97, and 0.91 respectively) as would be expected, and the linear fit to each of these data sets show a show respective slopes of 5.46, 5.74, and 5.62. These relationships show strong connection to both previous measurements of vadose zone water (DePaolo et al. 2004; identified a slope of ~ 5) and to the regional meteoric precipitation line (slope of ~ 5.8). More revealing, however, is the offset between sample data sets whereby samples from C9552 are noticeably shifted to the right in the isotope plots, likely indicating more extensive evaporation history in these samples than in the others.

A trend was observed between the measured vadose zone samples and depth (Figure 4.4), but there are different behaviors of this trend in different boreholes. For instance, in the T and S complex samples, the total data set displayed a correlation with R^2 of only 0.42; removal of just point B361D9 increased this correlation to R^2 of 0.96, and the three samples within core C9507 also showed a strong correlation with depth (R^2 of 0.96) (Truex et al. 2017). The trend toward isotopic enrichment (less negative values) with increased sample depth apparent in the vadose zone samples is qualitatively consistent with the observations of Hearn et al. (1989), who cited upwelling of isotopically enriched deeper waters for this trend in their analyses. However, the much shallower nature of these samples (<45 m compared to >1200 m) combined with the nature of vadose versus groundwater samples make it difficult to invoke a similar mechanism here. It is possible, however, that barometric mixing effects (similar to those described by Spane [1999]) induced mixing of underlying groundwater vapor with overlaying vadose zone water.

In contrast, DePaolo et al. (2004) suggest that strong evaporative effects in upper Hanford soil columns can create significant (e.g., 2-6 ‰ shift in $\delta^{18}\text{O}$) isotopic enrichment in resulting vadose zone moisture. This mechanism likely helps explain the enriched isotope values observed in samples from C9552 and C9488. This effect is generally confined to only the upper couple meters (or less) of soil. While slight isotopic enrichment may be expected compared to precipitation values below this surface enrichment, that process would not account for the more depleted values being found at shallow depths within the C9507 borehole (Truex et al. 2017). In a core exhumed from the 200 West area in 1999, DePaolo et al. (2004) also observed a negative isotopic anomaly in water extracted from a surface to groundwater depth profile. They attributed this excursion to leaking industrial process water that subsequently focused at the boundary of a coarser-grained layer underlain by a finer-grained layer. While a similar mechanism considered here would be consistent with the negative isotopic values observed in sample B35432 (Truex et al. 2017), a more continuous depth profile would be required to validate this hypothesis. Interestingly, samples B35441, B35461/B36H08 (Truex et al. 2017), and B361M7 are consistent with the absolute isotopic values DePaolo et al. (2004) observed in their study, but samples including B36173 and B361D9 (both from borehole C9512; Truex et al. 2017) are isotopically depleted in comparison to this previous study. Winter precipitation is known to have a more depleted isotopic

composition, but ranges around a $\delta^{18}\text{O}$ of $\sim -18\text{‰}$ and $\delta^2\text{H}$ of $\sim -138\text{‰}$ (DePaolo et al. 2004), so seasonality on its own cannot explain these data.

These observations are more confounding in that evaporative enrichment (e.g., observed by DePaolo et al. [2004] and Singleton et al. [2004]) typically propagates down core, thus isotopically enriching the entire core. Evidence of this is seen in the perched water data whereby these samples show isotopic enrichment consistent with near-surface evaporative processes (Lee et al. 2017). A potential hypothesis for explaining the depletion of the C9512 samples may rest in release of industrial condensate generated from intentional evaporitic enrichment of wastes to reduce their volumes (Truex et al. 2017). As noted in DOE/RL-92-93 (DOE 1992), such condensate would exhibit an isotopic depletion as an inverse to the enrichment observed in residual fluid following evaporation (as would be required by conservation of mass). Discharge of industrial condensate near C9512 could potentially explain both the inherent depleted isotopic content of these samples as well as the deviation of these samples from the more generalized correlation between $\delta^{18}\text{O}$ versus depth; large-scale release of industrial condensate would likely overprint existing isotopic trends within the vadose depth profile. In support of this, there is noted historical release of process condensate from the D-2 receiver tank within the 202-S Building that resulted from condensation of evaporate used to concentrate decontamination waste at this location (DOE 2016). The sharp negative isotope deviation in vadose zone water within this location could represent an isotopic signature of this process that may be useful for tracking regional migration of the resulting plume. A similar process may also contribute to the most extreme isotopic signature within the C9507 T19 borehole, notably B35432 (Truex et al. 2017), as there was noted release of process and steam condensate from the 242 T evaporator in this region but also release of additional tank waste and waste supernate (DOE 2016). It is unclear whether a similar mechanism can explain the depleted isotope signatures in C9487 (specifically B34WB1), but it remains a leading hypothesis regarding the extracted water in this sample having an isotopic composition more depleted than annual precipitation extremes or observed groundwater.

The isotope measurements of the S and T complex samples were plotted against measured nitrate concentrations (Figure 4.5; Truex et al. 2017). Two immediate features were observed. First, there is a linear relationship between the nitrate concentration and isotope data that also correlates to increasing depth in the borehole. The patterns seen in C9507 are in contrast to the data from C9512, however, which shows minimal variation in isotope values or nitrate over a fairly large vertical column (~ 60 ft).

Taken together, the stable isotope data provide a few interesting observations on these systems. First, most boreholes having multiple data points show covariance of the two measured isotopes, suggesting strong input from regional precipitation (e.g., C9507 [Truex et al. 2017], C9487, C9552, and the suite of perched water samples [Lee et al. 2017]). While each of these data sets shows isotopic signatures associated with evaporation, samples from C9552 show a significant increase in this feature, suggesting a stronger evaporative history than in the other samples. In contrast to evaporative enrichment, some samples show negative isotope excursions suggestive of inclusion of condensate-derived moisture in the vadose zone. While this is most notable in samples B36173 and B361D9 (Truex et al. 2017), the mechanism may also help explain observations from samples from the C9507 (Truex et al. 2017) and C9487 boreholes.

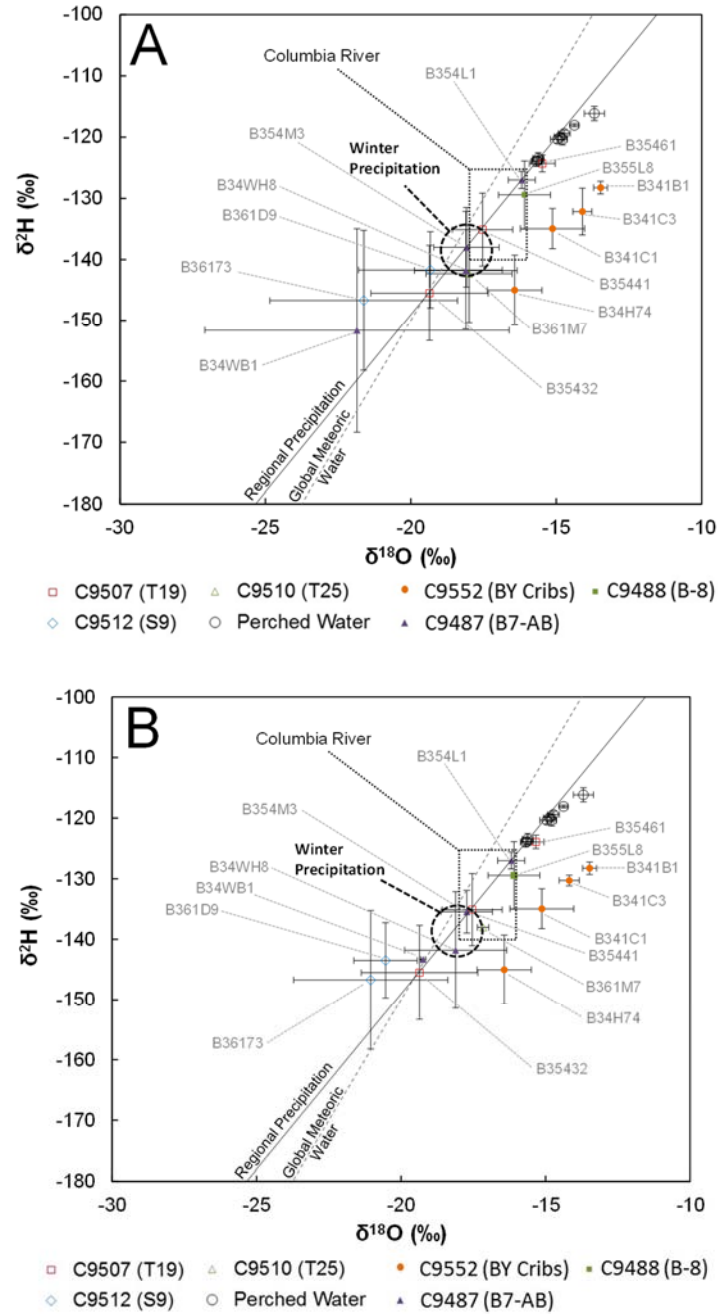


Figure 4.3. Isotope data for vadose zone sediment and perched water analyses. (A) Data resulting from the full data set. (B) Data refined by a Modified Thompson Tau test to remove outlier points (continued on next page). Depiction of winter precipitation is after DePaolo et al. (2004) with a nominal value of $\delta^{18}\text{O}$ of $\sim -18\text{‰}$ and $\delta^2\text{H}$ of $\sim -138\text{‰}$.

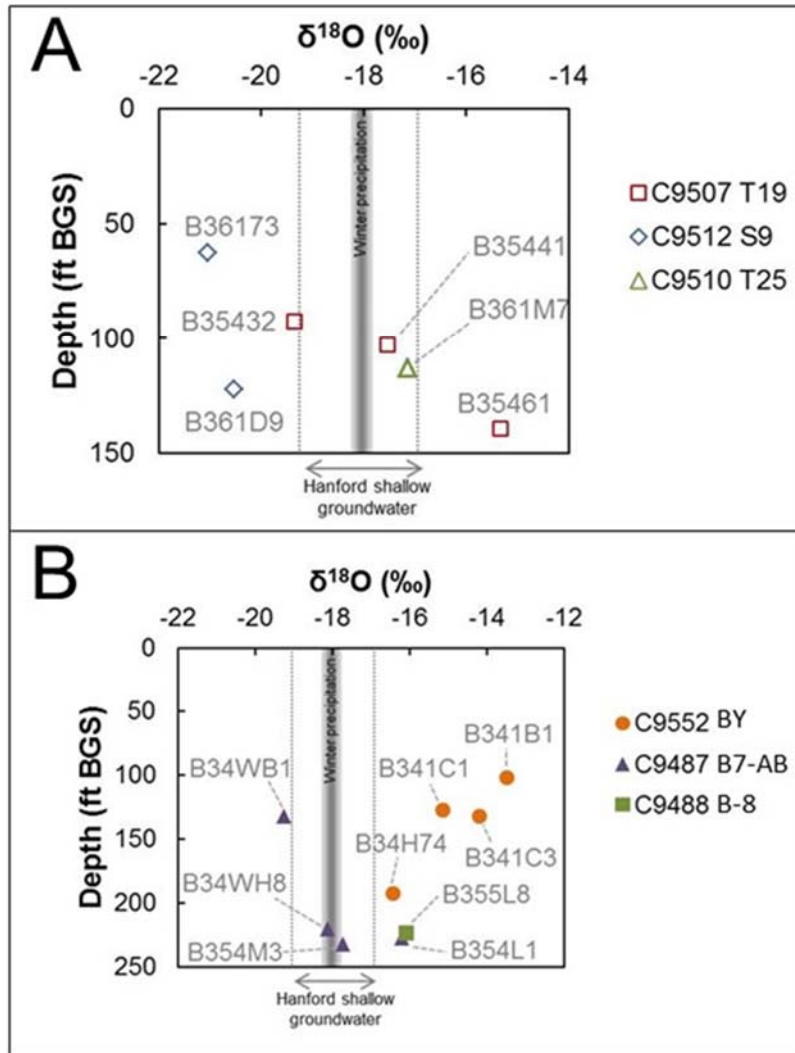


Figure 4.4. $\delta^{18}\text{O}$ relating to sample depth, average local winter precipitation, and local shallow groundwater within the Hanford Site. (A) Sample data from the T and S Complex. (B) Sample data from the B-Complex.

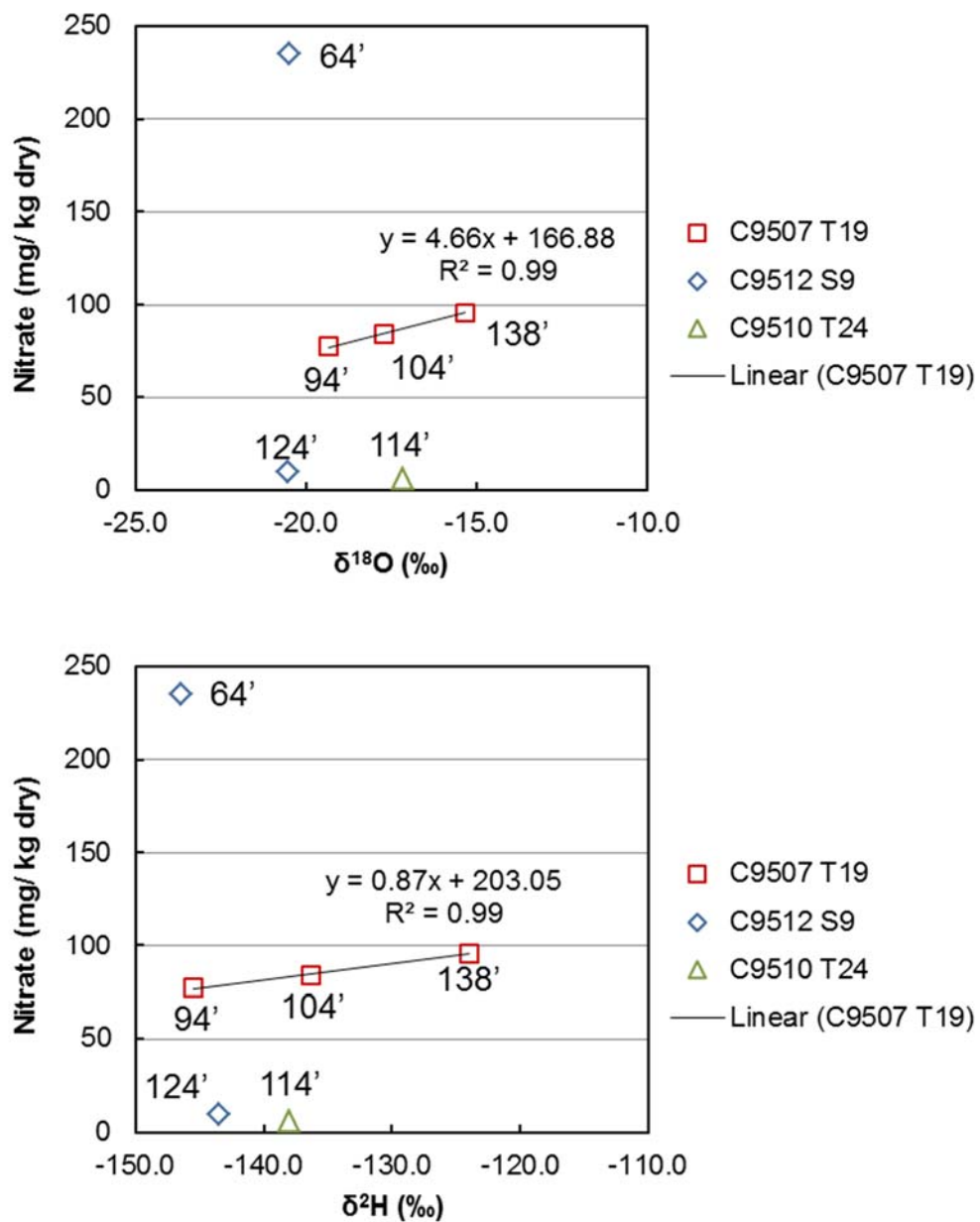


Figure 4.5. Correlation of isotopic ($\delta^2\text{H}$ and $\delta^{18}\text{O}$) analysis and measured nitrate concentration from T and S Complex samples.

4.1.5 Sediment Physical Characterization

Physical characterization of sediments (objective 1) involved measurement of intact core air permeability, dry bulk density, porosity, and moisture content. Air permeability was measured on field moist cores following ASTM D6539. After these measurements, the grain size distribution was measured using a laser particle size analyzer and mechanical sieves (for larger particle sizes). Sediments were mainly medium to coarse sand or gravelly sand, with two sediments (at 220 to 230 ft depth) being sandy silt units with lower permeability (Table 4.8 and Table 4.9) from Hanford and Cold Creek Unit formations. Bulk densities ranged from 1.60 to 2.18 cm³/g, and porosities from 0.203 to 0.408. Measured permeability in the sand and sandy gravel units was 23 to 59 darcy, and units within finer grained infill were 0.04 to 0.059 darcy (Table 4.8). Grain size distributions are in Appendix A.

Table 4.8. Physical characterization of sediments.

Borehole	Depth (ft)	HEIS #	Dry Bulk Density (cm ³ /g)	Porosity (cm ³ /cm ³)	Moisture (g/g)	Air Permeability (m ²)	(darcy) ^a	Formation ^b	Lithology
C9552	103.2 – 104.2	B34H36	1.86	0.316	0.0402	2.16E-11	21.9	Hanford H2	S
C9552	133.1 – 134.1	B34H53	1.88	0.315	0.0203	2.01E-11	20.4	Hanford H2	S
C9552	193.2 – 194.2	B34H77	2.18	0.203	0.0834	3.58E-14	0.036	CCU _g	msG
C9487	59.5 – 60.0	B34WN7	1.68	0.370	0.0435	3.31E-11	33.5	Hanford H2	S
C9487	133.1 – 134.1	B34WB2	1.84	0.322	0.0238	5.27E-11	53.4	Hanford H2	S
C9487	228.7 – 229.7	B354L3	1.75	0.356	0.1806	5.19E-14	0.053	CCU _z	sS
C9488	218.3 – 219.3	B355L2	1.60	0.408	0.2341			CCU _z	sS
			± 0.01	± 1E-3	± 1E-4	± 1%	± 1%		
(a)	conversion using 1 darcy = 9.869233E-13 m ²								
(b)	fine grained Cold Creek Unit (CCU _z) or coarse grained Cold Creek Unit (CCU _g), Serne et al., 2010.								

Table 4.9. Description of sediment grain size distribution.

Borehole	Depth (ft)	HEIS #	Clay (%)	Silt (%)	Sand (%)	Gravel (%)	Grain Size Description
C9552	103.2 – 104.2	B34H36	0.97	6.03	92.70	0.30	Medium to coarse sand with trace of clay and gravel
C9552	133.1 – 134.1	B34H53	1.34	6.20	92.46	0.00	Medium to coarse sand with trace of clay
C9552	193.2 – 194.2	B34H77	2.30	7.46	32.72	57.52	Sandy gravel with some silt and trace of clay
C9487	59.5 - 60.0	B34WN7	2.36	8.50	86.12	3.02	Sand with some silt and trace of gravel and clay
C9487	133.1 - 134.1	B34WB2	0.20	7.19	92.61	0.00	Medium to coarse sand with some silt
C9487	228.7 - 229.7	B354L3	1.42	46.03	52.55	0.00	Fine silty sand
C9488	218.3 - 219.3	B355L2	1.56	35.39	63.05	0.00	Fine silty sand with trace of clay
			±0.01	±0.01	±0.01	±0.01	

Sediments used in geochemical experiments were adjacent to cores used for physical characterization (Table 4.10). The physical parameters of these < 2-mm sediments repacked into columns (Table 4.10) show slightly greater porosities and slightly lower dry bulk densities than intact cores (Table 4.8). Images of sediments in borehole C9552 show units of relatively uniform medium to coarse sand at 104 and 134 ft depths and sandy gravel at 194 ft depth (Figure 4.6).

Table 4.10. Physical characterization of sediments used in 1-D column experiments.

#	Borehole	Depth (ft)	HEIS #	Dry Bulk Density (cm ³ /g)	Porosity (cm ³ /cm ³)	Field Moisture (g/g)	Column Volume (cm ³)	Pore Volume (cm ³)
E21	C9552	104.2 – 105.2	B34H37	1.408	0.493	0.0308	50.7	25.0
E22	C9552	134.1 – 135.1	B34H55	1.428	0.405	0.0216	50.7	20.5
E23	C9552	194.2 – 195.2	B34H79	1.588	0.373	0.0317	50.7	18.9
E27	C9487	58.2 – 59.2	B34W66	1.714	0.333	0.0367	50.7	21.2
E24	C9487	134.1 – 135.1	B34WB3	1.513	0.456	0.0285	50.7	23.1
E25	C9487	230.0 – 231.0	B345L8	1.545	0.386	0.2272	50.7	19.6
E26	C9488	219.3 – 220.3	B355L3	1.535	0.425	0.2427	59.4	25.3
E28	C9488	219.3 – 220.3	B355L3	1.608	0.394	0.2421	59.4	23.4
				±0.01	± 1E-3	±1E-4	± 0.1	±0.1

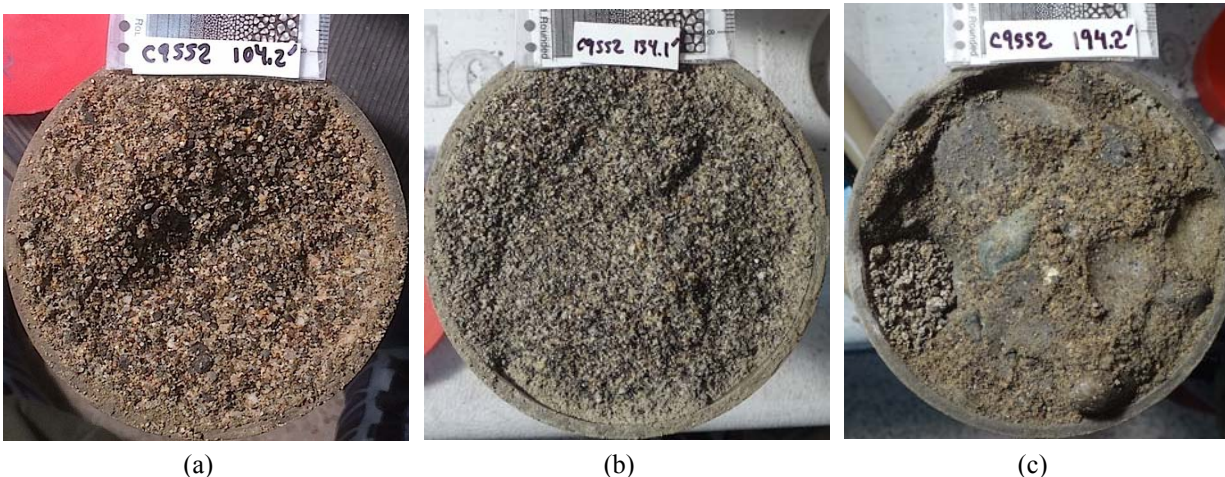






**Figure 4.6.** Core images in borehole C9552 of: a) and b) Hanford formation, and c) Cold Creek Unit.

4.2 Observation of Attenuation Processes

4.2.1 Sequential Liquid Extraction of Contaminants in Sediments

Identifying attenuation processes involves collecting data that can be used to demonstrate whether contaminants have interacted with sediments in a way that changes their mobility. One type of data is from sequential extractions (Table 4.11). In this process, a sediment sample is sequentially exposed to more harsh extraction solutions and the contaminant concentration in each solution is measured. These data show how the contaminant mass in a sediment sample is distributed among different water- and sediment-associated phases. Analysis for geochemical constituents was also conducted for each extraction solution to help interpret the types of sediment constituents mobilized or dissolved by each solution for the specific sediment sample. It was not possible to measure iodine species (iodate and iodide) in extracted samples.

Table 4.11. Sequential extraction of contaminants from sediment samples.

Extraction Solution	Hypothesized Targeted Sediment Components	Interpreted Contaminant Mobility of Extracted Fraction	Color Code
1. Aqueous: uncontaminated Hanford groundwater	Contaminants in pore water and a portion of sorbed uranium	Mobile phase	
2. Ion exchange: 1M Mg-nitrate	Readily desorbed contaminants	Readily mobile through equilibrium partitioning	
3. Acetate pH 5: 1 hour in pH 5 sodium acetate solution	Contaminants associated with surface-exposed carbonate precipitates and other readily dissolved precipitates	Moderately mobile through rapid dissolution processes	
4. Acetate pH 2.3: 1 week in pH 2.3 acetic acid	Dissolution of most carbonate compounds, and sodium boltwoodite (a hydrous uranium silicate)	Slow dissolution processes for contaminant release from this fraction; mobility is low with respect to impacting groundwater	
5. Oxalic acid: 1 hour	Dissolution of some aluminosilicates and oxides	Slow dissolution processes are associated with contaminant release; mobility is very low with respect to impacting groundwater	
6. 8M HNO ₃ : 2 hours in 8M nitric acid at 95°C	Considered to represent total contaminant extraction for this study (though not completely dissolving the sediment particles)	Very slow dissolution processes are associated with contaminant release; functionally immobile; some or all of the contaminants in this phase may be naturally occurring	

Sequential extraction contaminant results for each sample for uranium (Figure 4.7), iodine (Figure 4.8), Tc-99 (Figure 4.9), and chromium (Figure 4.10) show surface phase distributions before and after leach experiments, as well as the 1000-hour carbonate extraction. Results are also shown in Table 4.12. Cations/metals released during sequential extractions (Figure 4.11 and Figure 4.12) aid in interpretation of extracted phases. These B-Complex sediments ranged in U-238 contamination from 0.4 to 54 µg/g. Sediments with higher U-238 contamination generally had a higher fraction of mobile uranium. Sequential extractions showed that 3% to 12% of uranium was aqueous/adsorbed (highly mobile), 4% to 40% was carbonate associated (somewhat mobile), and 40% to 80% was associated with oxides and silicates (generally not very mobile). Groundwater leaching for 100 pore volumes removed all the aqueous/adsorbed, and about half of carbonate-associated U. Post-leach extractions showed the lesser fraction of the more mobile phases. Pre-leach extraction contaminant masses were equivalent (within 20%) of post leach extractions (including leached mass) for all sediments except C9487 at 58' depth. The uranium mass in the leached sediment sample (total 58 ug/g in Figure 4.7e) was substantially greater than the uranium mass in the pre-leach sediment sample (total 6.6 ug/g in Figure 4.7e and Table 4.13).

The B-Complex sediments had low iodine contamination, with total I-127 in sediments ranging from 0.014 to 0.054 µg/g. Sequential extractions at these low concentrations had no measureable aqueous or adsorbed iodine, with 60% to 75% carbonate associated iodine, and 25% to 40% Fe/Mn/Al oxide associated iodine. It was not possible to measure iodine in the 8M nitric acid extraction. Groundwater

leaching for 100 pore volumes removed 60% to 80% of the total iodine and post-leach extractions showed less carbonate-associated iodine.

Some B-Complex sediments had low Tc-99 contamination ($<0.013 \mu\text{g/g}$), which pre-leach sequential extractions showed was all in aqueous and adsorbed phases. Leaching removed nearly all Tc-99 from sediments, as post-leach extractions had no reportable Tc-99. The 1000-hour carbonate extraction removed a third to half of the Tc-99. The distribution coefficient (K_d) was calculated from the aqueous (extraction 1) and adsorbed (extraction 2) concentrations and sediment/water ratio in the extraction.

Table 4.12. Contaminant distribution in sequential liquid extracted sediments and 1000-hour carbonate extraction for U-238, I-127, Tc-99, and Cr.

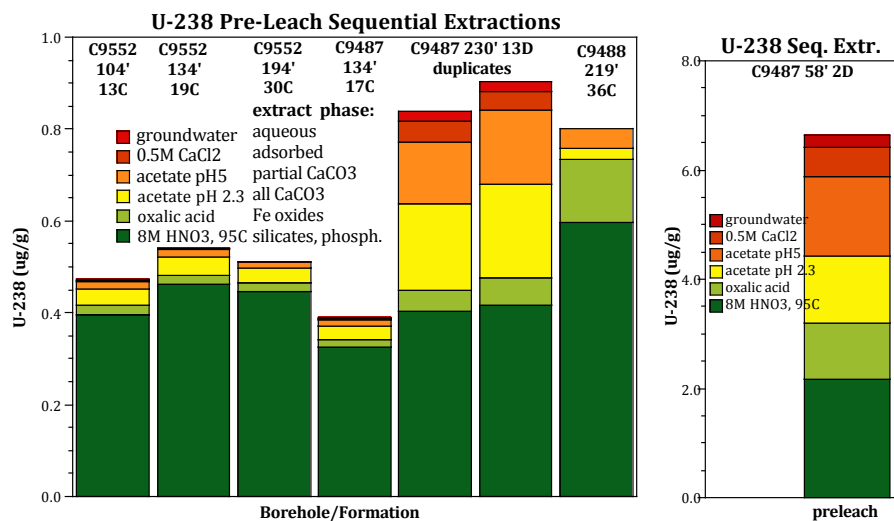
		----- U-238 (all $\mu\text{g/g}$) -----								K_d (mL/g)
Borehole Depth (ft)	HEIS #	extr. 1	extr. 2	extr. 3	extr. 4	extr. 5	extr. 6	total	1000 h	
C9552 104.2	B34H37	0.00127	0.00169	0.0161	0.0358	0.0208	0.396	0.472	0.0246	2.79
C9552 134.1	B34H55	0.00072	0.00168	0.0161	0.0407	0.0172	0.464	0.540	0.0159	5.05
C9552 194.2	B34H79	0.00079	0.0000	0.0118	0.0322	0.0198	0.446	0.511	0.0104	
C9487 58.2	B34W66	0.220	0.529	1.464	1.217	1.040	2.16	6.631	0.0158	5.03
C9487 134.1	B34WB3	0.00317	0.0043	0.0133	0.0288	0.0160	0.325	0.390	0.0158	2.78
C9487 230.0	B354L8	0.0218	0.0474	0.1335	0.1873	0.0454	0.404	0.840	0.12	5.19
C9487 230.0	B354L8	0.0238	0.0381	0.1633	0.2025	0.0613	0.416	0.905	no dup	4.26
C9488 219.3	B355L3	0.0000	0.0000	0.0424	0.0264	0.1357	0.597	0.802	0.0193	

		----- I-127 (all $\mu\text{g/g}$) -----							
Borehole Depth (ft)	HEIS #	extr. 1	extr. 2	extr. 3	extr. 4	extr. 5	extr. 6	total	1000 h
C9552 104.2	B34H37	0.000	0.000	3.25E-03	4.89E-03	5.46E-03	0.000	1.36E-02	0.00469
C9552 134.1	B34H55	0.000	0.000	0.0000	4.66E-03	2.79E-03	0.000	7.44E-03	0.00263
C9552 194.2	B34H79	0.000	0.000	4.68E-03	9.31E-03	4.68E-03	0.000	1.87E-02	0.0173
C9487 58.2	B34W66	0.000	0.000	4.57E-03	3.21E-02	1.58E-02	0.000	5.25E-02	0.00307
C9487 134.1	B34WB3	0.000	0.000	0.0000	2.94E-03	0.0000	0.000	2.94E-03	0.00404
C9487 230.0	B354L8	0.000	0.000	3.49E-03	3.76E-03	0.0000	0.000	7.25E-03	no dup
C9487 230.0	B354L8	0.000	0.000	4.40E-03	3.70E-03	0.0000	0.000	8.10E-03	0.00281
C9488 219.3	B355L3	0.000	0.000	5.71E-03	8.25E-03	6.38E-03	0.000	2.03E-02	0.00483

		----- Tc-99 (all $\mu\text{g/g}$) -----								K_d (mL/g)
Borehole Depth (ft)	HEIS #	extr. 1	extr. 2	extr. 3	extr. 4	extr. 5	extr. 6	total	1000 h	
C9552 104.2	B34H37	5.88E-03	7.33E-04	0.000	0.000	0.000	0.000	6.61E-03	0.00499	0.263
C9552 134.1	B34H55	3.89E-03	0.0000	0.000	0.000	0.000	0.000	3.89E-03	0.00379	
C9552 194.2	B34H79	2.23E-03	0.0000	0.000	0.000	0.000	0.000	2.23E-03	0.00245	
C9487 58.2	B34W66	0.0000	0.0000	0.000	0.000	0.000	0.000	0.000	0.00	
C9487 134.1	B34WB3	0.0000	0.0000	0.000	0.000	0.000	0.000	0.000	0.00	
C9487 230.0	B354L8	0.0000	0.0000	0.000	0.000	0.000	0.000	0.000	no dup	
C9487 230.0	B354L8	0.0000	0.0000	0.000	0.000	0.000	0.000	0.000	0.00	
C9488 219.3	B355L3	3.60E-04	0.0000	0.000	0.000	0.000	0.000	3.60E-04	0.00	

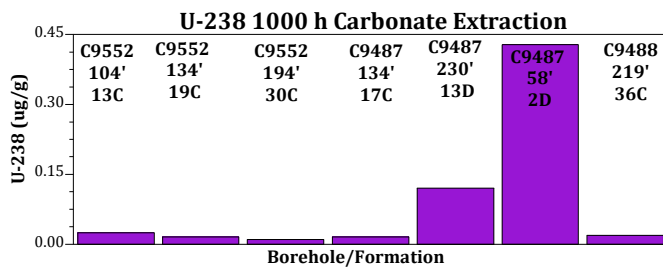
		----- Cr (all $\mu\text{g/g}$) -----							
Borehole Depth (ft)	HEIS #	extr. 1	extr. 2	extr. 3	extr. 4	extr. 5	extr. 6	total	
C9552 104.2	B34H37	0.000	0.000	0.000	0.0548	0.0807	11.55	11.68	
C9552 134.1	B34H55	0.000	0.000	0.000	0.0931	0.0927	12.99	13.18	

C9552	194.2	B34H79	0.000	0.000	0.000	2.653	0.6191	11.01	14.29
C9487	58.2	B34W66	0.000	0.000	0.000	0.0610	0.133	6.63	6.82
C9487	134.1	B34WB3	0.000	0.000	0.000	0.105	0.104	11.34	11.55
C9487	230.0	B354L8	0.000	0.000	0.000	0.627	0.600	17.41	18.64
C9487	230.0	B354L8	0.000	0.000	0.000	0.983	0.866	17.16	19.01
C9488	219.3	B355L3	0.000	0.000	0.000	0.0000	1.074	19.30	20.38



(a)

(b)



(c)

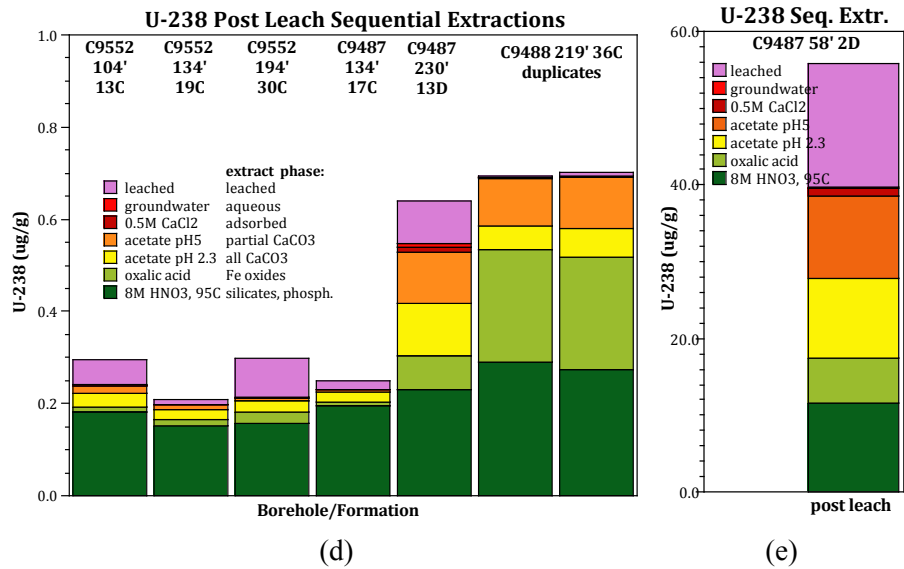
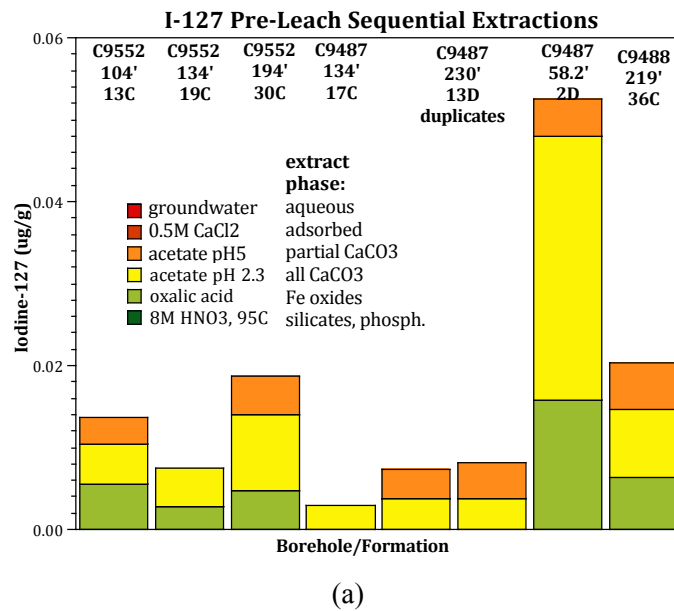
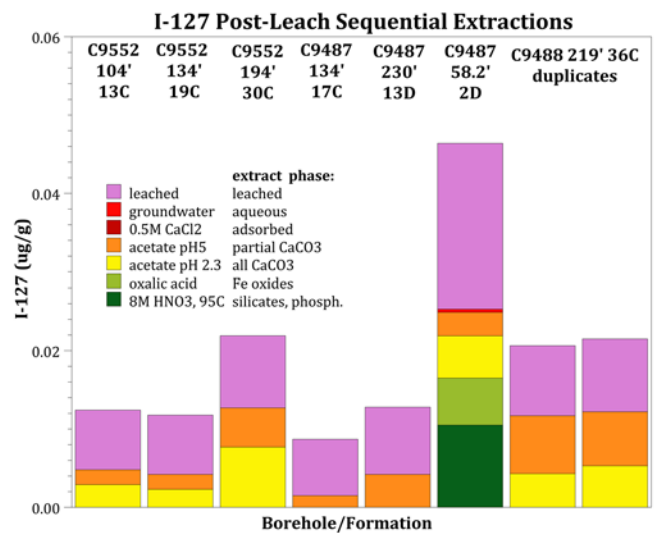
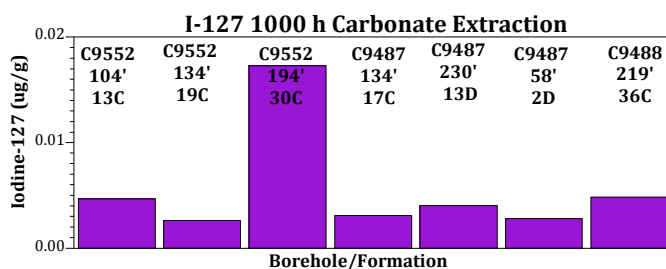


Figure 4.7. U-238 extractions: (a) and (b) sequential extractions pre-leach, (c) 1000-hour extraction pre-leach, (d) and (e) sequential extractions post-leach.





(b)



(c)

Figure 4.8. Iodine-127 sequential extractions conducted: (a) pre-leach, (b) post-leach, and (c) 1000-hour extraction conducted on pre-leach sediments.

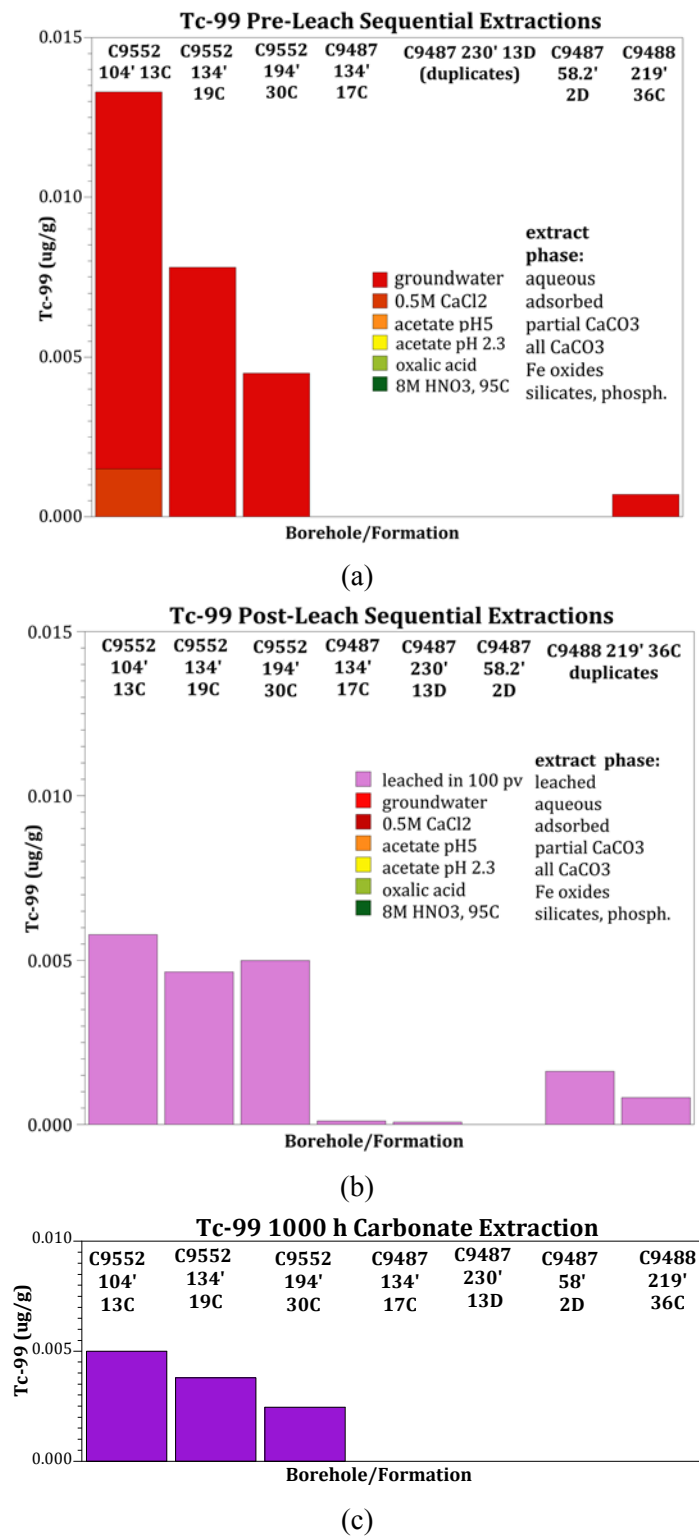
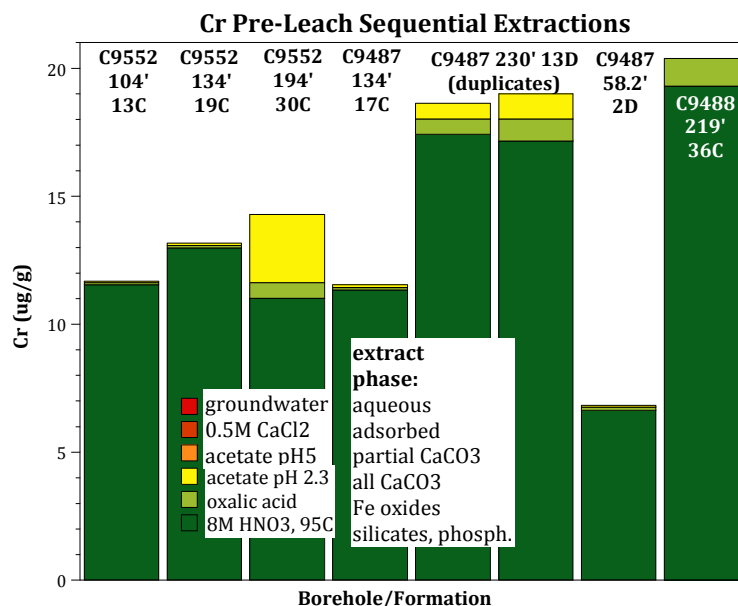
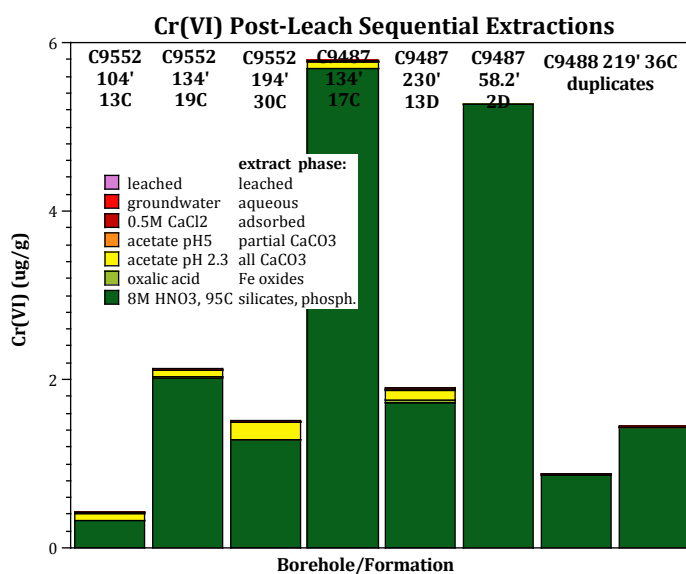


Figure 4.9. Tc-99 sequential extractions conducted: (a) pre-leach, (b) post leach, and (c) 1000-hour extraction conducted on pre-leach sediments.



(a)



(b)

Figure 4.10. Chromium sequential extractions conducted: (a) pre-leach with total Cr analysis, and (b) post-leach with Cr(VI) analysis.

4.2.2 Sequential Extractions for Major Cations/Metals

Cations and metals measured in sequential extractions represent aqueous (extraction 1) or adsorbed cations (extraction 2), then extractions 3 through 6 represent cations or metals from dissolved minerals and/or anthropogenic precipitates (NaNO_3 , NaSO_4 , NaCO_3). Cations presented in stack bar graphs (Figure 4.11) show major ion changes with extractions between sediments. In general, significant Na, Ca, and Mg are removed in the first four extractions. Extraction 6 (8M HNO_3) dissolves a number of different phases, with Al, Mg, and Ca (and other) ions at concentrations ~5 times that of other extractions.

Carbonates are dissolved in the pH 5 sodium acetate solution (extraction 3, partial dissolution of some carbonates), and the pH 2.3 acetic acid solution (extraction 4). The Ca, Mg, and Sr concentrations in extractions 3 and 4 are high (Figure 4.12a, b, and c). Other than high anthropogenic Na in aqueous and adsorbed phases (extractions 1 and 2), high Na in extractions 5 and 6 are likely from plagioclase and clay/mica dissolution (Figure 4.12d). High K in extraction 6 (Figure 4.12e) is likely from microcline and clay/mica dissolution (Table 4.6). Trace element Ba is high in extraction 6 (Figure 4.12f), and parallels Cr, and thus may represent naturally occurring Ba-chromate. Iron and manganese phases (i.e., magnetite, Fe, Mn in clays/mica, pyroxenes, Fe, Mn oxides, ilmenite) are dissolved primarily in extractions 5 and 6 (Figure 4.12g and Figure 4.12h). Dissolution of minerals containing Si and Al are shown in Figure 4.12i (Si), j (Al), and k (Si/Al). Dissolution of clays should have a Si/Al ratio of 1 to 2. Dissolution of microcline should have a Si/Al ratio of 3, plagioclase 1 to 3, and amphiboles 1 to 2. Quartz dissolution contains no Al. No major minerals at Hanford contain Al without Si (Table 4.6). The Si/Al ratio (Figure 4.12k) shows Si/Al ratio of 1 to 2 for most sediments except C9487 58' (sediment E7), C9487 230' (sediment E6), and C9488 219' (sediment E6 and E8 in Figure 4.12), which had significantly lower Al concentrations (Figure 4.12j). These three sediments had the highest U contamination (Figure 4.7). Extraction 6 dissolved significant Al from an unknown phase in all sediments (Figure 4.12j).

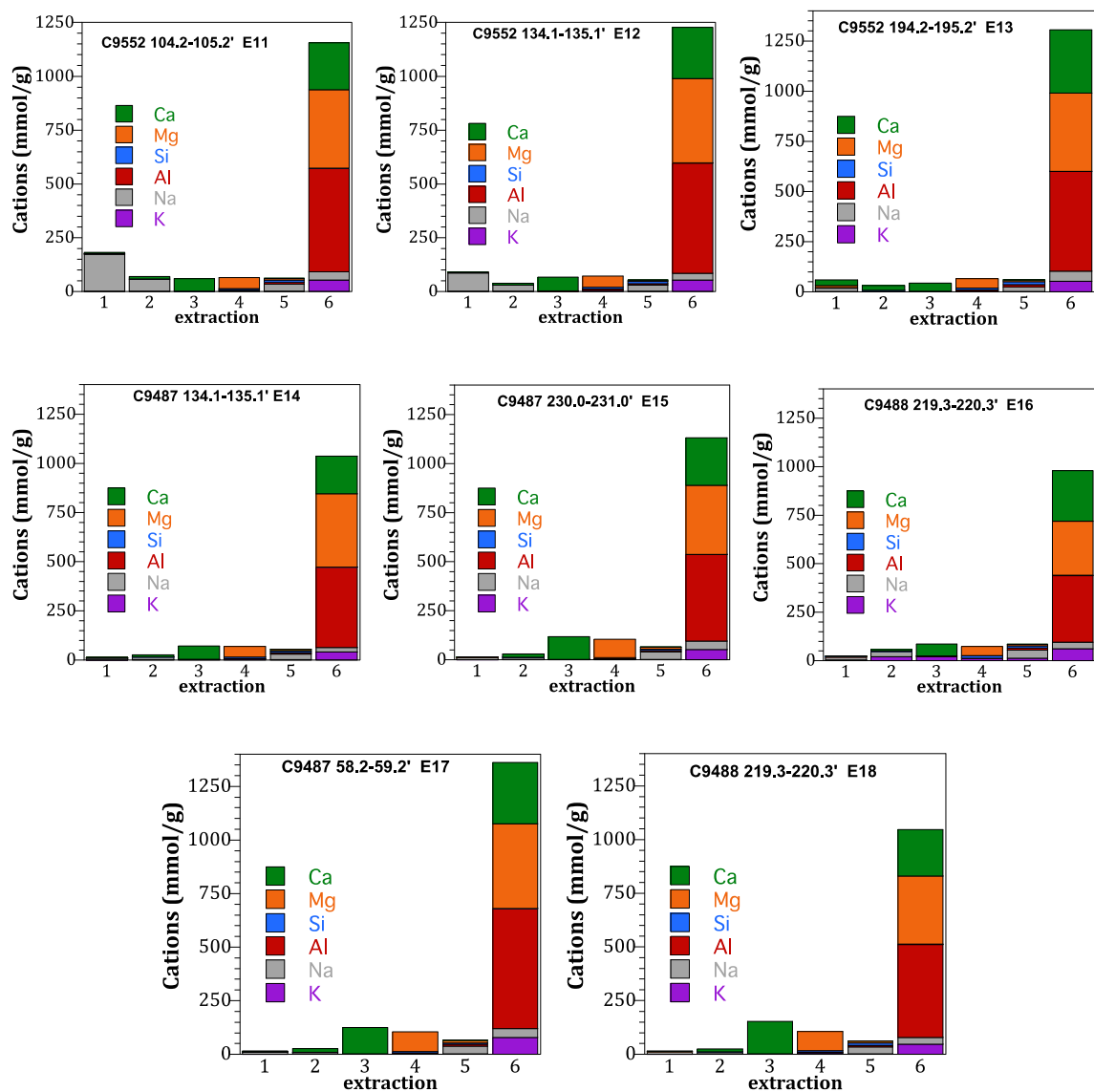


Figure 4.11. Cations/metals distribution measured in sequential extraction solutions. Cations are not reported for extraction solutions that contain that cation (i.e., Mg for extractions 2 and 3, Na for extractions 3 and 4, and Ca for extraction 4).

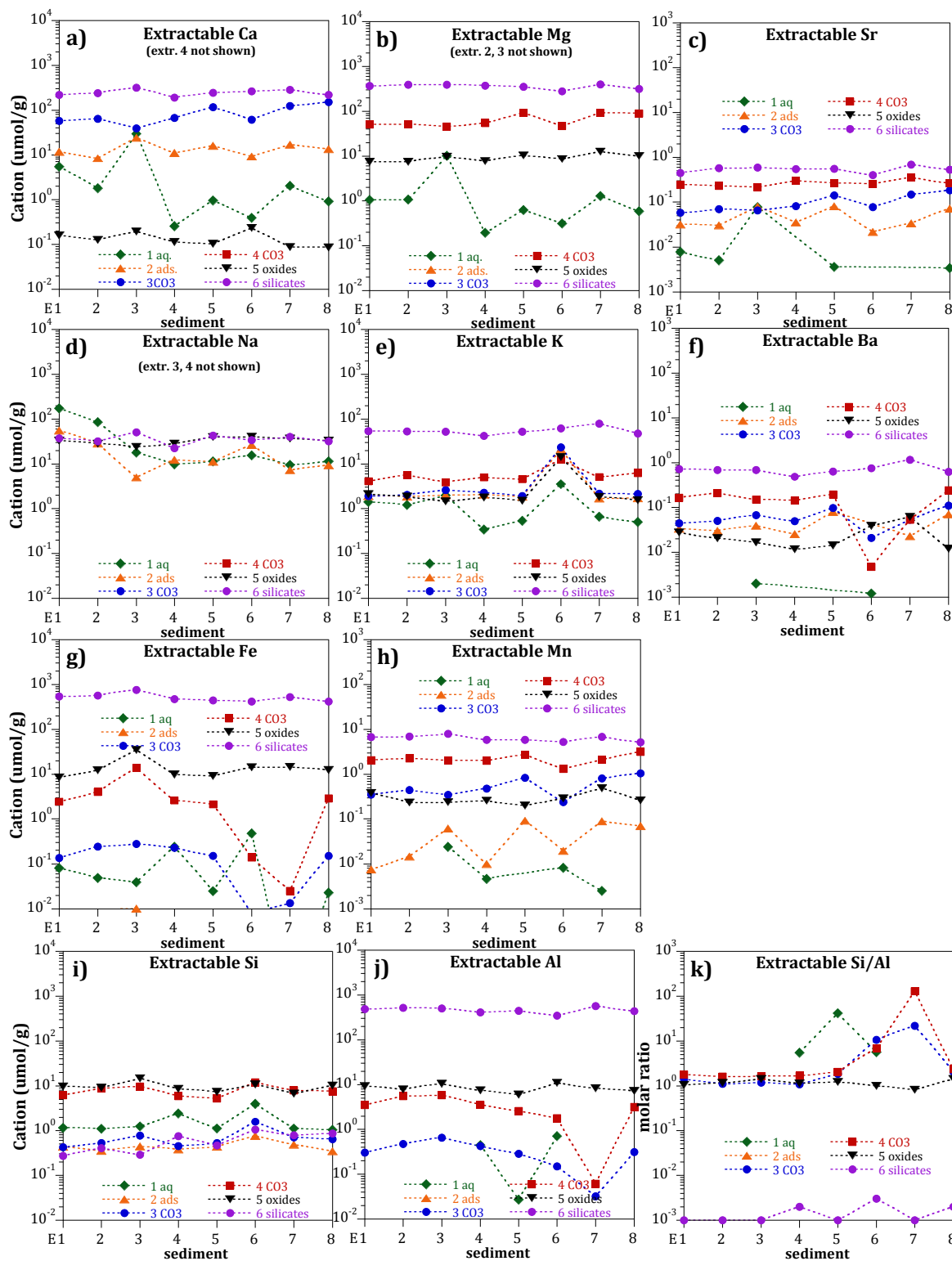


Figure 4.12. Major and trace cations/metals measured in sequential extractions: (a) Ca, (b) Mg, (c) Sr, (d) Na, (e) K, (f) Ba, (g) Fe, (h) Mn, (i) Si, (j) Al, and (k) Si/Al ratio. Sediments are: C9552 13C (E1), C9552 19C (E2), C9552 30C (E3), C9487 17C (E4), C9487 13D (E5 and E6), C9487 2D (E7), and C9488 36C (E8).

4.2.3 U(VI) and Iodate Reduction Rate Experiments

Experiments were conducted to evaluate the U(VI) and iodate reductive capacity and rate of B-Complex sediments, as previous studies of Hanford 200 vadose zone and 100D area saturated zone sediments have shown sufficient abiotic (i.e., iron/manganese) or biotic reductive capacity that pertechnetate, chromate, and iodate have been reduced. In these sediments, 100 µg/L iodate and 100 µg/L Ca-uranyl-carbonate in artificial groundwater was pre-equilibrated into sediment columns by ~20 pore volumes of injection. This was sufficient to reach equilibrium of iodate aqueous and sorbed phases, but may not have been sufficient for uranium species.

Experimental results show a similar pattern of iodate behavior in all sediments, as a result of sorption and iodate reduction to iodide (Figure 4.13). In all sediments, the total I-127 decreased in tens to hundreds of hours, then in four of eight sediments, the I-127 increased. Iodine speciation shows that all I-127 was initially iodate, but iodine increased in five of eight sediments, clearly showing reduction. Four sediments did show a decrease in I-127 and iodate, but no quantitative corresponding increase in iodide.

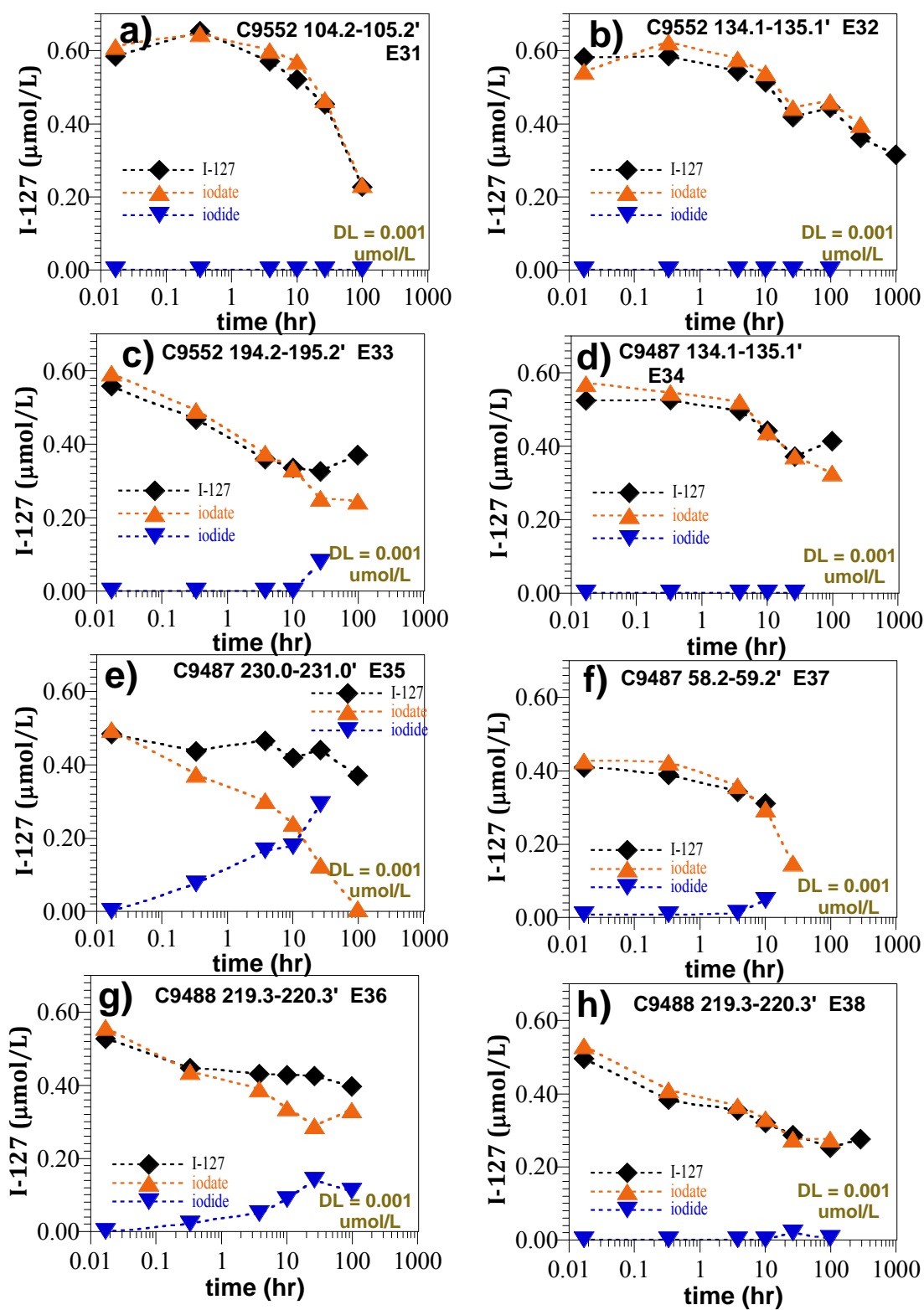


Figure 4.13. Iodate reduction experiments with the addition of 100 μg/L iodate into no-flow sediment columns.

For U(VI) present as multiple aqueous Ca-uranyl-carbonate complexes (neutral and negatively charged), removal of U-238 from aqueous solution may be the result of sorption (if sorption equilibrium was not reached) or U(VI) reduction and precipitation of $U^{IV}O_2$. With the exception of one sediment with very high uranium contamination (Figure 4.14f, C9487 58' depth), all sediments showed a decrease in aqueous uranium concentration. In all cases, the decrease was rapid (<1 h), and thus was likely caused by additional sorption of Ca-uranyl-carbonate complexes and not the predicted slow (hundreds of hours time scale) U(VI) reduction. For three sediments (Figure 4.14a, b, and d), the aqueous U(VI) concentration increased in hundreds of hours, which may reflect some dissolution of uranium in carbonates in these field-contaminated sediments.

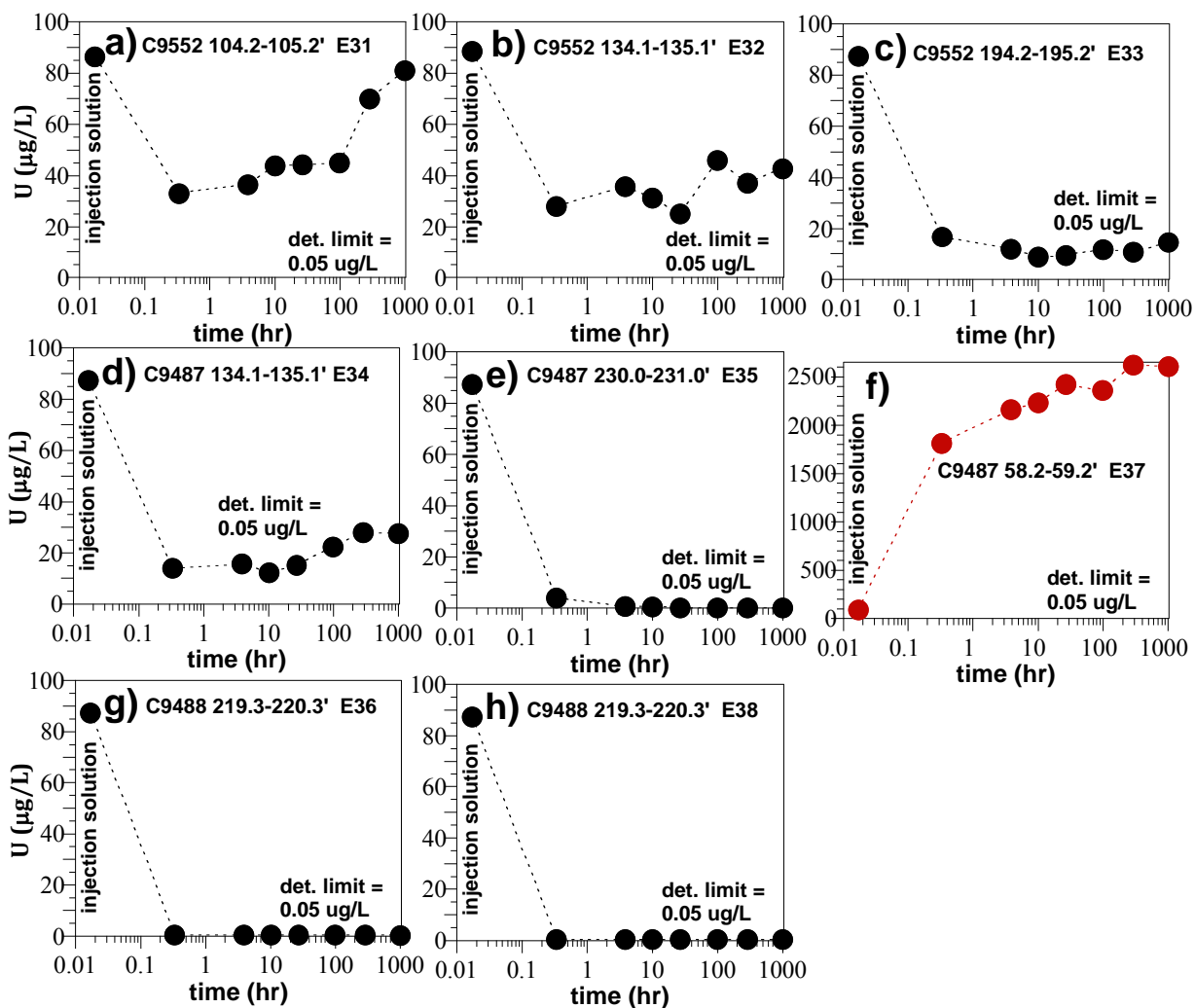


Figure 4.14. Rate of uranium removal from aqueous solution in no-flow 1-D columns after injection of 20 pore volumes of artificial groundwater containing 100 µg/L U (as Ca-uranyl-carbonate aqueous complexes) and 100 µg/L iodate.

4.3 Contaminant Mobility

4.3.1 Long-Term Contaminant Leaching in Batch Experiments

To evaluate the rate of release of contaminants, long-term (to 1000 hours) batch experiments (described in this section) and 1-D column experiments (described in the next section) were used. Batch leach experiments consisted of mixing 50 g of sediment with 200 mL of contaminant-free artificial groundwater on a linear mixer and sampling the aqueous solution at selected times ranging from 1 to 1000 hours. Samples were analyzed for U-238, technetium, I-127, iodine species, and Cr(VI). Although Cr(VI) concentrations in most samples were below detection limits (10 $\mu\text{g/L}$), Cr(VI) was released from some sediments into solution over the long term (100 to 1000 hours) with concentrations as high as 24 $\mu\text{g/L}$ (Figure 4.15a). An aqueous Cr(VI) concentration of 24 $\mu\text{g/L}$ is equivalent to 0.1 $\mu\text{g/g}$ Cr in the sediment. There was some interference in the colorimetric method due to yellow color in some samples (indicated by * on graphs) due to the high Na-nitrate co-contaminant concentration.

In contrast, there was no additional time release of Tc-99 from sediments (Figure 4.15b); the 1000-hour concentration was nearly the same as the 1-hour concentration for most sediments. This Tc-99 behavior was consistent with sequential extractions (Figure 4.9), which showed Tc-99 all in aqueous or adsorbed surface phases, and could readily be nearly all leached. One sediment (C9487, 58' depth) showed a Tc-99 (pertechnetate in aqueous solution) decrease, which may be the result of reduction (and precipitation of $\text{Tc}^{\text{IV}}\text{O}_2$). This sediment also has the ability to reduce iodate within 10s of hours (Figure 4.13) although two other sediments that also showed significant iodate reduction (C9488 219' and C9487 230') had very low Tc-99 aqueous concentrations. This batch release rate data for Tc-99 is consistent with Tc-99 release rates calculated in 1-D columns (described later in this section) during stop-flow events, where there was little change in the Tc-99 release rate between different sediments and over time. Based on equilibrium redox potentials, iodate reduction should occur first (or be the most rapid), followed by chromate, then pertechnetate.

Uranium-238 was present in all sediments, either naturally occurring (low concentration, typically $<0.3 \mu\text{g/g}$ or in these batch experiments $\sim 2 \mu\text{g/L}$) or anthropogenic. Uranium-238 present mainly as natural uranium generally showed a slow release rate from sediment (Figure 4.15c), whereas two sediments with low (Figure 4.15c, C9487 230') and very high uranium contamination (Figure 4.15d) showed a rapid uranium release (within hours), followed by little slower release in hundreds of hours. This U-238 behavior was consistent with sequential extractions, which showed a higher fraction of mobile uranium (i.e., aqueous, adsorbed, and carbonate phases) for these two sediments compared with the other sediments. These data are also consistent with U-238 release rates calculated in 1-D columns (described later in this section) during stop-flow events; namely, the sediments with moderate to high uranium released uranium more rapidly and released a higher uranium mass, and that release rate decreased significantly over time.

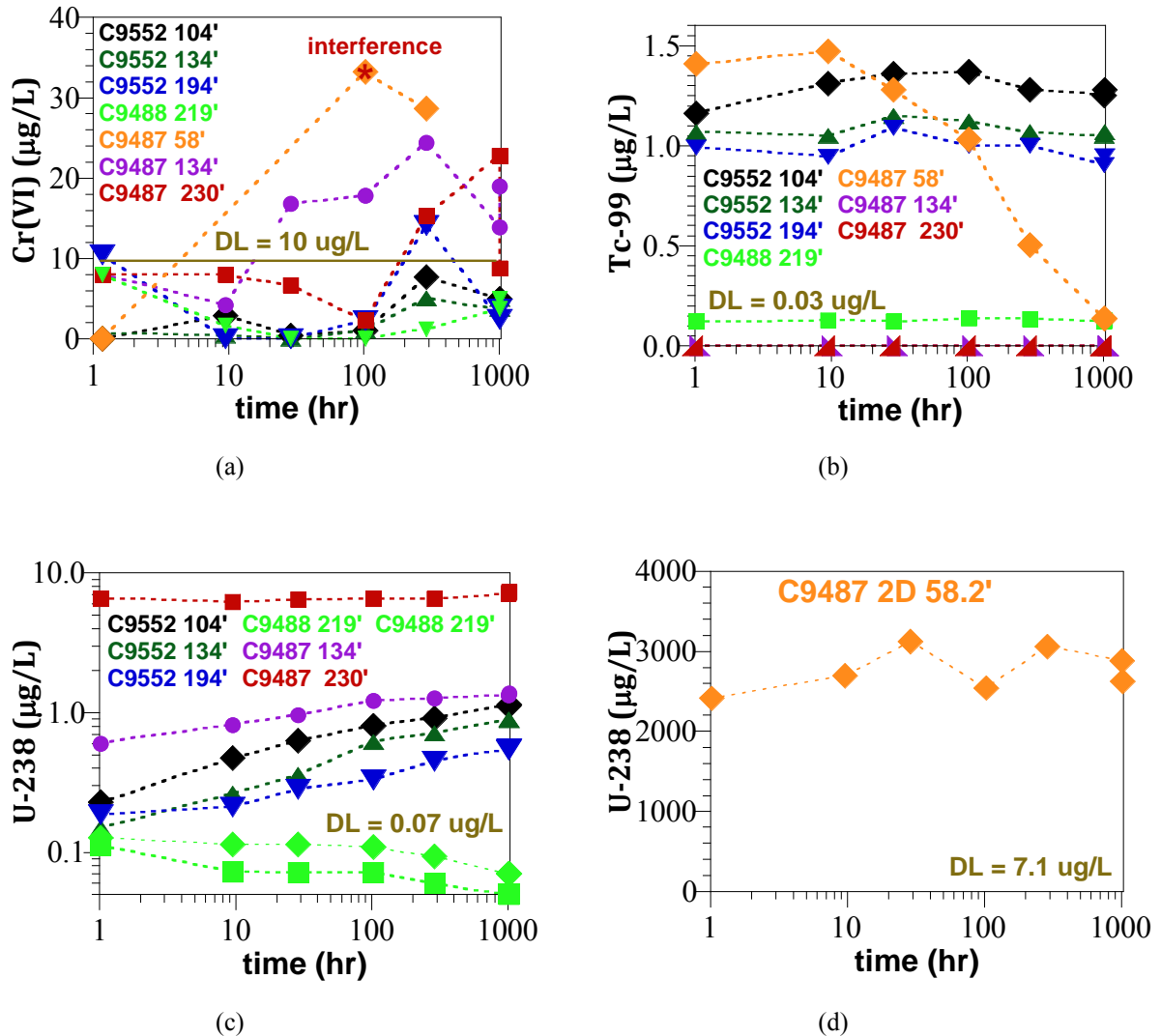


Figure 4.15. Long-term leaching of contaminants from sediments in batch systems showing: (a) Cr(VI) release, (b) Tc-99 release, (c) U-238 for six sediments, and (d) U-238 for C9487 58'.

Iodine-127 initially present in sediment at a low concentration was slowly released from sediment (Figure 4.16), as concentrations increased 50% to 200% by 1000 hours. This was consistent with sequential extraction data (Figure 4.8), which showed little I-127 present in aqueous or adsorbed phases but most I-127 present in carbonate phases (which may slowly exchange I-127 out of the carbonate into solution as carbonates dissolve/reprecipitate). There were significant challenges to analyzing iodine species in these field-contaminated sediments, because other ions (primarily nitrate and sulfate) interfere with the iodide and iodate separation. Previous studies with low field contamination had analytical detection limits of iodate and iodide near 1 µg/L. In this study, samples had to be diluted to decrease nitrate/sulfate concentrations, which increases the analytical detection limit. For the sediment with the lowest ion co-contaminants (C9487 58'; see cations/anions in the 1-D column section), iodine species were analyzed (Figure 4.16b). This showed initially primarily iodate (80%), which decreased in tens of hours (with 60% iodide), then increased again by 1000 hours (for 65% iodate). Two processes may

account for the some of the observed changes: iodate reduction and carbonate dissolution. Iodate reduction for this sediment was quantified (Figure 4.13) to occur in tens of hours, so the increase in iodide could be due to aqueous (or sorbed) iodate reduction. Carbonates incorporate iodate, so the slow dissolution over hundreds of hours should release additional iodate into solution, which is consistent with observations. However, the iodide concentration decreases between 30 and 1000 hours, which cannot be accounted for by these two processes. If real, this could be caused by biotic or abiotic oxidation of iodide. For one additional sediment (C9488 219'), iodine speciation showed 83% iodide at 9.6 h, which decreased to 55% iodide by 103 hours. For another sediment (C9552 104'), iodine speciation showed 62% iodide at 103 hours.

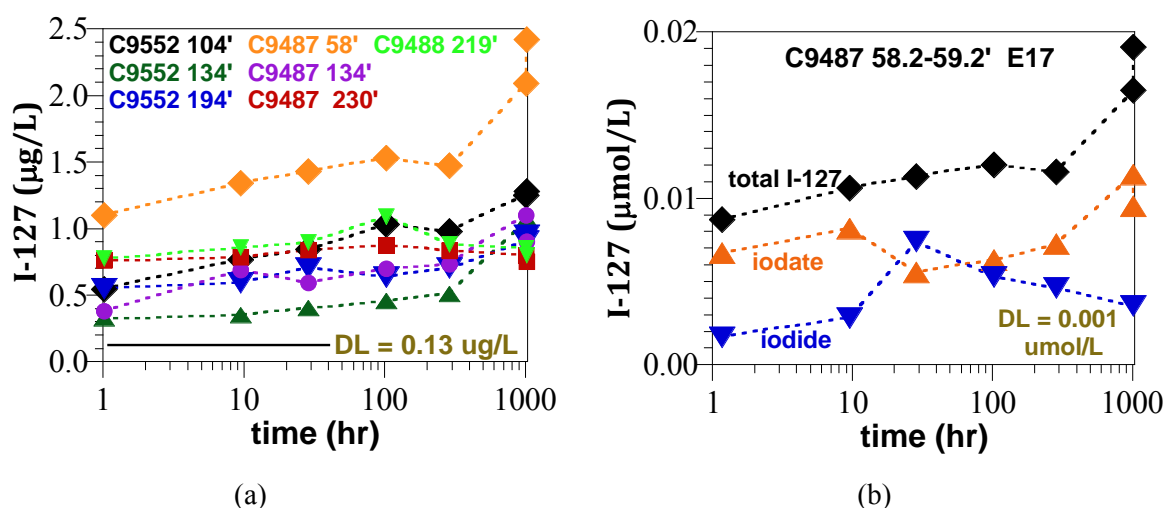


Figure 4.16. Long-term leaching of contaminants from sediments in batch systems showing (a) total I-127, and (b) iodine speciation for C9487 58'. Iodine speciation for most experiments was below analytical detection limits, with the exception of C9487 58' and single points in three experiments, which showed 62% iodide (C9552 104' at 103 hours), 55% iodide (C9488 219' at 103 hours), and 83% iodide (C9488 219' at 9.6 hours).

Rates of I-127 and U-238 released from sediments during the 24- to 1000-hour range were calculated from the batch experimental data (Table 4.13). Rates for I-127 were small (maximum of 0.05 $\mu\text{g/kg/day}$), whereas U-238 release rates varied considerably from 0.0016 to 13.4 $\mu\text{g/kg/day}$. Negative rates reflected net uptake of I-127 or U-238 due to slow sorption (for uranium) or reduction (for iodate, Figure 4.13).

Table 4.13. Calculated release rates of I-127 and U-238 in long-term batch experiments.

Borehole Depth (ft)	HEIS #	I-127 ($\mu\text{g/kg/d}$)	U-238 ($\mu\text{g/kg/d}$)
C9552 104.2-105.2	B34H37	3.05E-02	2.83E-02
C9552 134.1-135.1	B34H55	5.64E-02	2.32E-02
C9552 194.2-195.2	B34H79	2.30E-02	1.73E-02
C9487 58.2 - 59.2	B34W66	6.06E-02	9.36E+01
C9487 134.1-135.1	B34WB3	3.18E-02	1.09E-02
C9487 230.0-231.0	B354L8	-7.00E-03	6.94E-02
C9488 219.3–220.3	B355L3	-1.30E-02	-4.60E-03
C9488 219.3–220.3	B355L3	-4.02E-03	-1.04E-02

4.3.2 Long-Term Leaching of Contaminants from Sediments in 1-D Columns

The seven sediments (Table 3.1) were subjected to long-term leaching with artificial groundwater in 1-D column studies to evaluate the rate at which contaminants were released from the sediment. These experiments consisted of leaching a total of 95 to 136 pore volumes of artificial groundwater through the sediment at a constant flow rate, with collection of effluent samples that were analyzed for U-238, Tc-99, I-127, iodine species, chromate (selected samples), cations (on selected samples), anions (on selected samples), and a tracer (bromide). In addition, three stop-flow events were used to further evaluate the contaminant release rate from the sediment at 3, 16, and 100 pore volumes. The stop-flow intervals ranged from 24 hours (at 3 pore volumes), to 72 hours (at 16 pore volumes), and 195 hours (at 75 to 130 pore volumes). For some of the data interpretation, data from Truex et al. (2017) for boreholes in the S-Complex and T-Complex are included on figures.

Tracer (bromide) breakthrough in the 1-D columns (Figure 4.17) showed that injected groundwater flowed through the sediment with little breakthrough tailing, indicating even flow. The retardation coefficient of the bromide ranged from 0.946 to 1.21 for the eight columns (seven sediments with one duplicate).

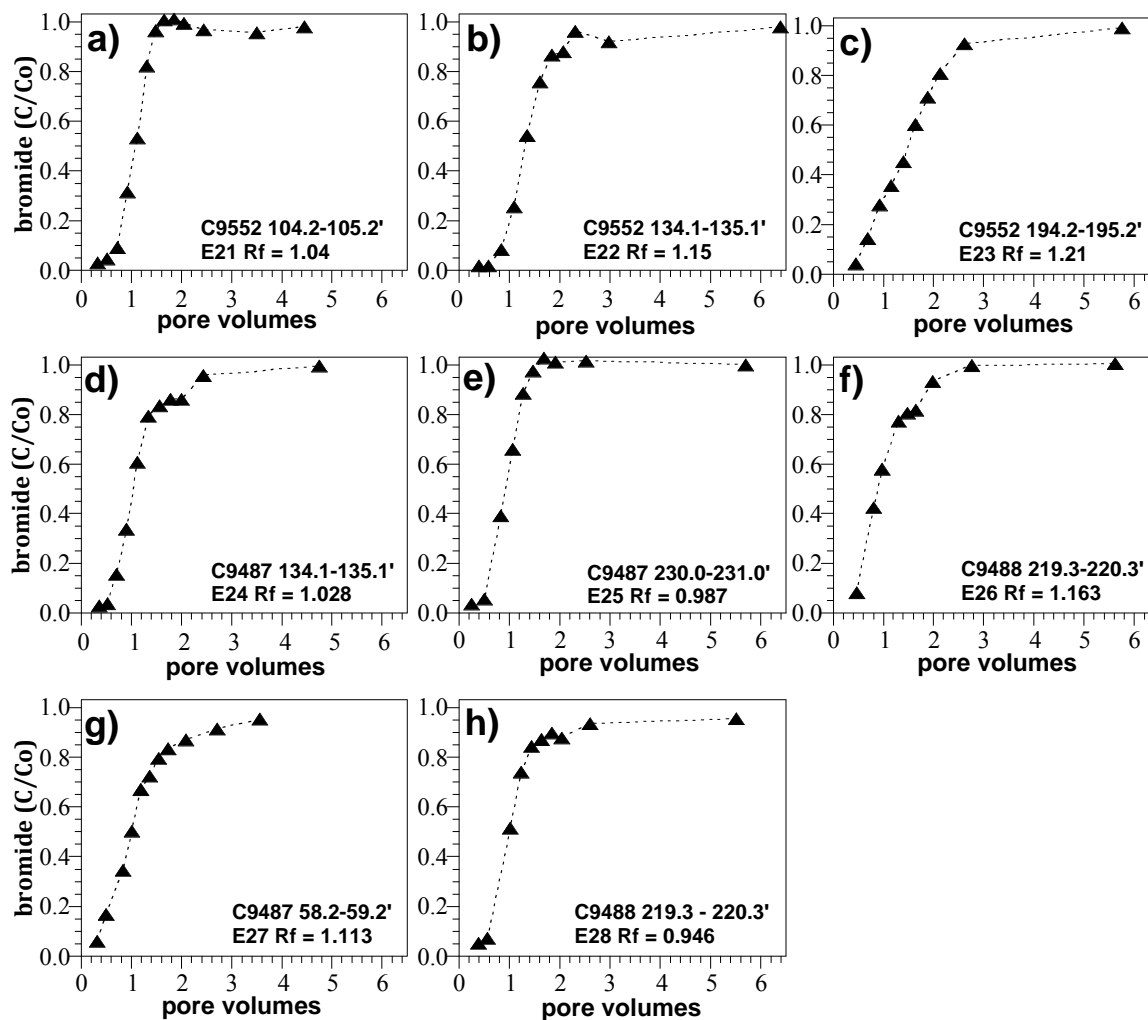


Figure 4.17. Added tracer (bromide) breakthrough in 1-D column experiments.

Aqueous Cr(VI) [i.e., chromate] and total Cr were measured in selected samples by a colorimetric method with detection limits of 10 $\mu\text{g/L}$ (Figure 4.18). There was no reportable Cr in any sediment for any effluent sample. Although Cr(VI) analysis is preferred over Cr analysis, there was significant interference from other ions in solution that rendered the ferrozine colorimetric Cr(VI) analysis not useful. This is in contrast to previous studies in 100D groundwater sediments, where hundreds of Cr(VI) analyses had low detection limits (5 to 10 $\mu\text{g/L}$), although that groundwater had low co-contaminant concentrations.

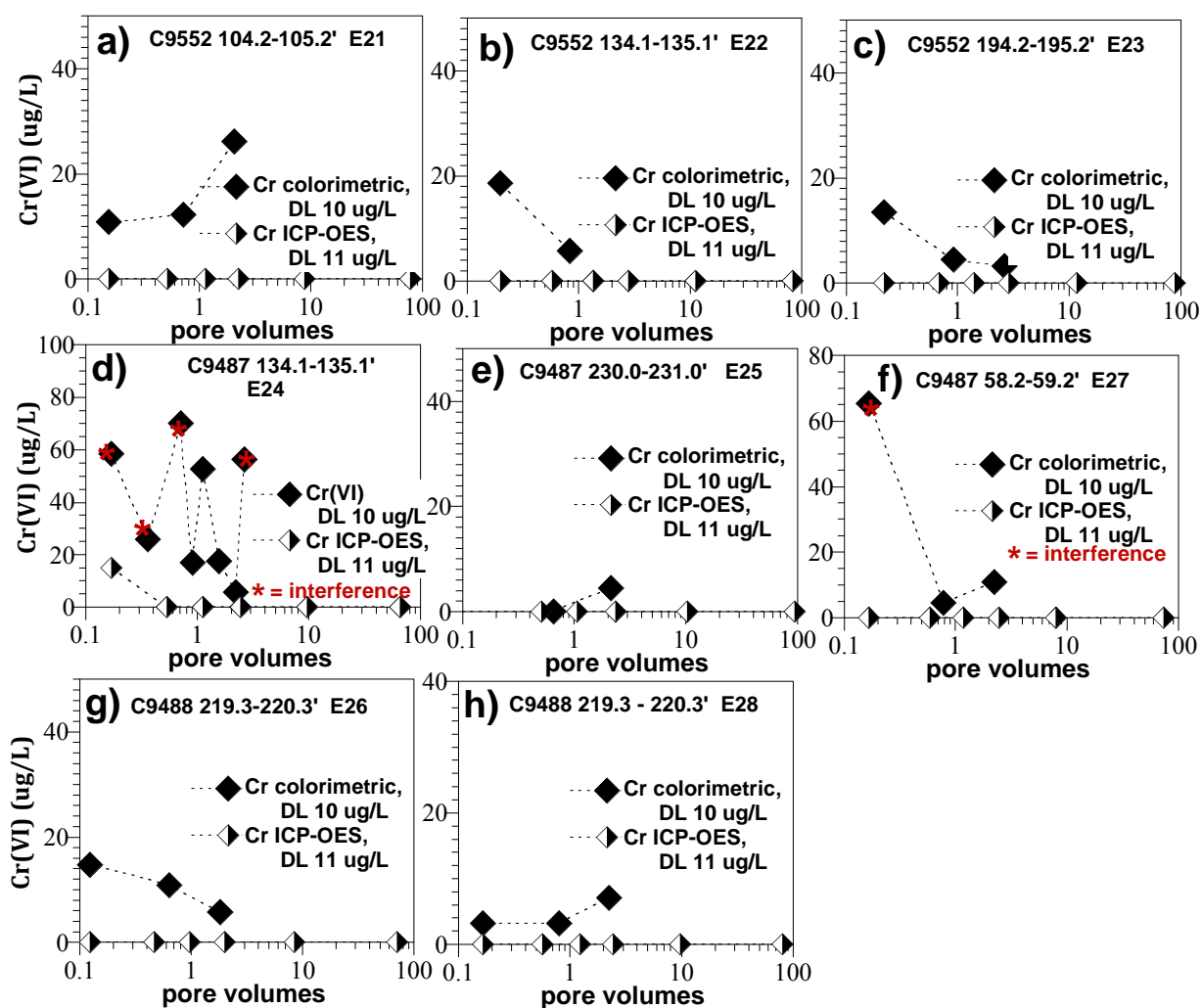


Figure 4.18. Chromate breakthrough in 1-D column leaching experiments.

Aqueous Tc-99 leaching from B-Complex sediments released nearly all Tc-99 in the first few pore volumes, with little additional mass over the next 80 to 130 pore volumes for all sediments (Figure 4.19). This rapid Tc-99 release behavior was consistent with sequential extractions, showing all Tc-99 was present in aqueous and sorbed phases (Figure 4.20a), and none was present in extractions conducted after these column experiments (Figure 4.20b). The 1000-hour carbonate extraction removed all Tc-99, as did the 1-D column leaching (Figure 4.20c). This rapid Tc-99 release behavior was also consistent with long-term batch studies (Figure 4.15b). The cumulative Tc-99 (purple triangles in Figure 4.19) is most indicative of essentially all mass released quickly, which is in contrast to U-238 and I-127 (described on the following pages). Tc-99 analysis had little interference with ionic co-contaminants.

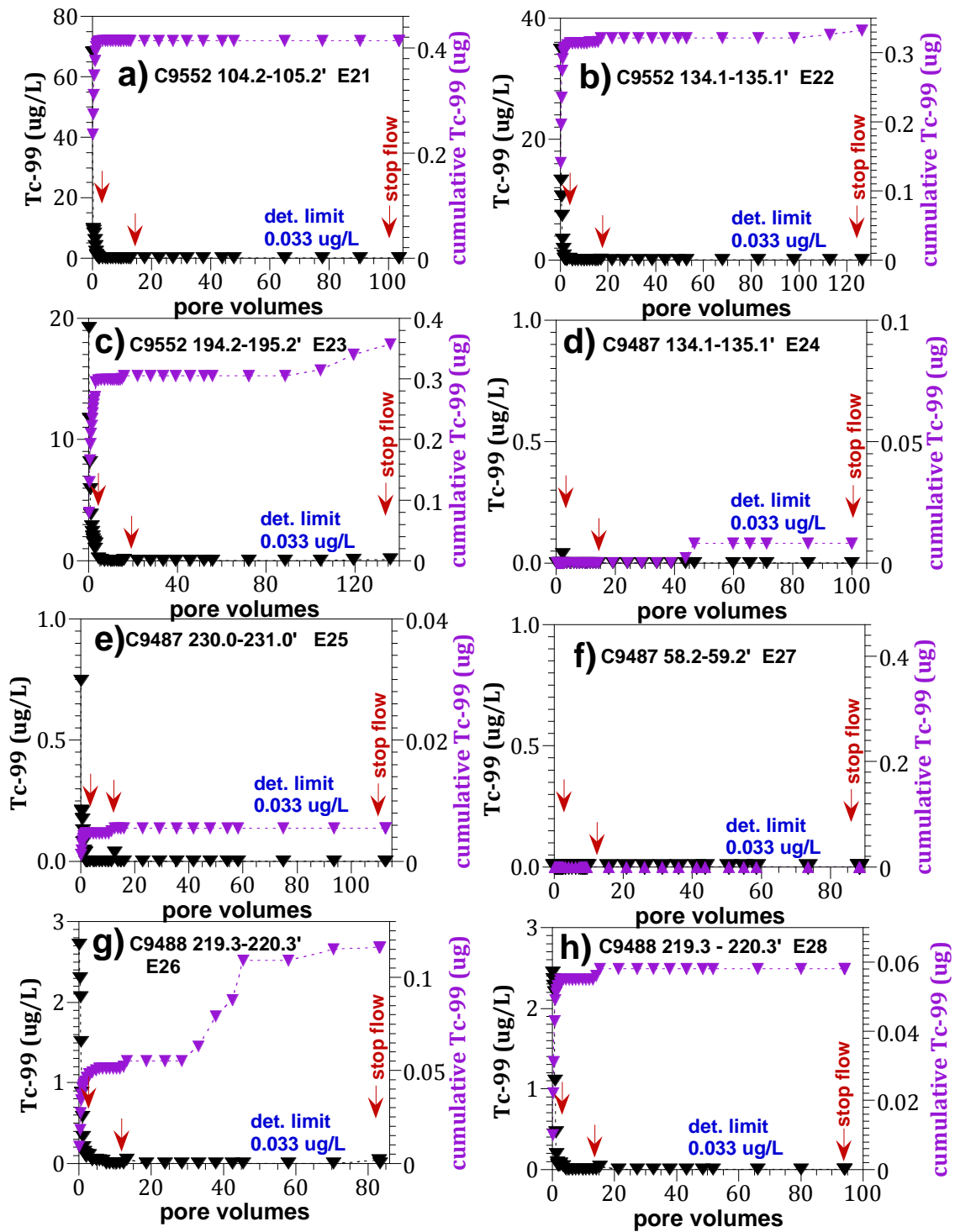


Figure 4.19. Tc-99 breakthrough in 1-D column leaching experiments. Effluent Tc-99 (black triangles) and cumulative Tc-99 mass (purple triangles) are shown.

The Tc-99 release rate from sediments was calculated from stop-flow events at 2.5, 10, and 100 pore volumes. During a stop-flow (16 to 300 hours), if additional Tc-99 is released from the sediment, the Tc-99 effluent concentration increases. For Tc-99, the two sediments with the highest Tc-99 contamination (C9552, 134' and 194') showed a decrease in the release rate for higher leached pore volumes (Figure 4.20a), which may indicate initial release from aqueous/adsorbed surface phases, and slower release at later times from a precipitate phase such as TcO_2 or possibly pertechnetate incorporated into carbonate. These sediments with the highest release rate also leached greater Tc-99 mass (Figure 4.20b). A sediment with an order of magnitude lower Tc-99 also showed a decrease in release rate at higher leach pore volumes (C9488 219' data from duplicate experiments, Figure 4.20)

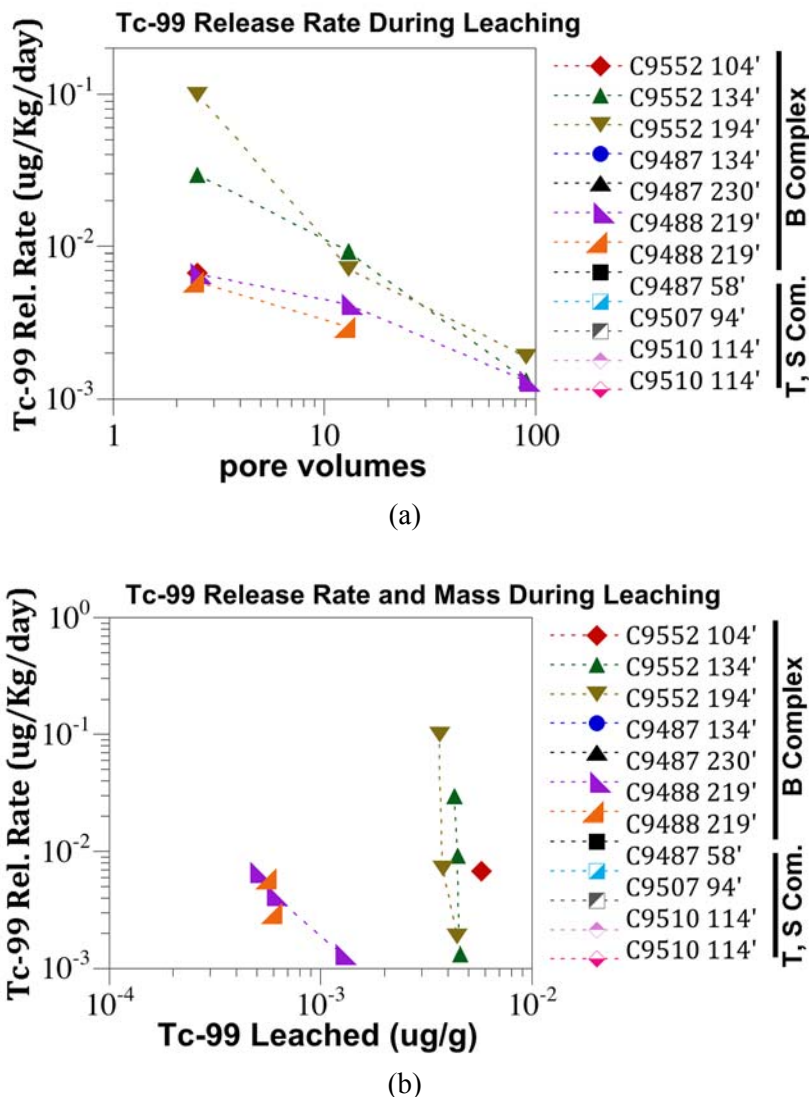


Figure 4.20. Tc-99 release rates calculated from stop-flow events in 1-D column leach experiments showing (a) Tc-99 release rate change with pore volumes, and (b) Tc-99 release rate and mass leached.

Uranium (U-238) leaching from B-Complex sediments shows a combination of significant initial release in the first few pore volumes followed by substantial cumulative additional U-238 over the next 80 to 130 pore volumes (Figure 4.21). This complex behavior is likely caused by uranium presence in multiple

surface phases. Sequential extractions on sediments prior to leaching indicated 5% to 10% aqueous/adsorbed, 15% to 50% carbonate-associated uranium, and 50% to 80% hard-to-extract phases (i.e., hard to mobilize, Figure 4.22a, b). Sequential extractions on sediments after leaching indicated the aqueous, adsorbed, and a portion of carbonate-associated uranium leached (Figure 4.7c, d). The 1000-hour carbonate extraction (Figure 4.7e) on pre-leach sediments removed approximately the same uranium mass as 100 pore volumes of groundwater.

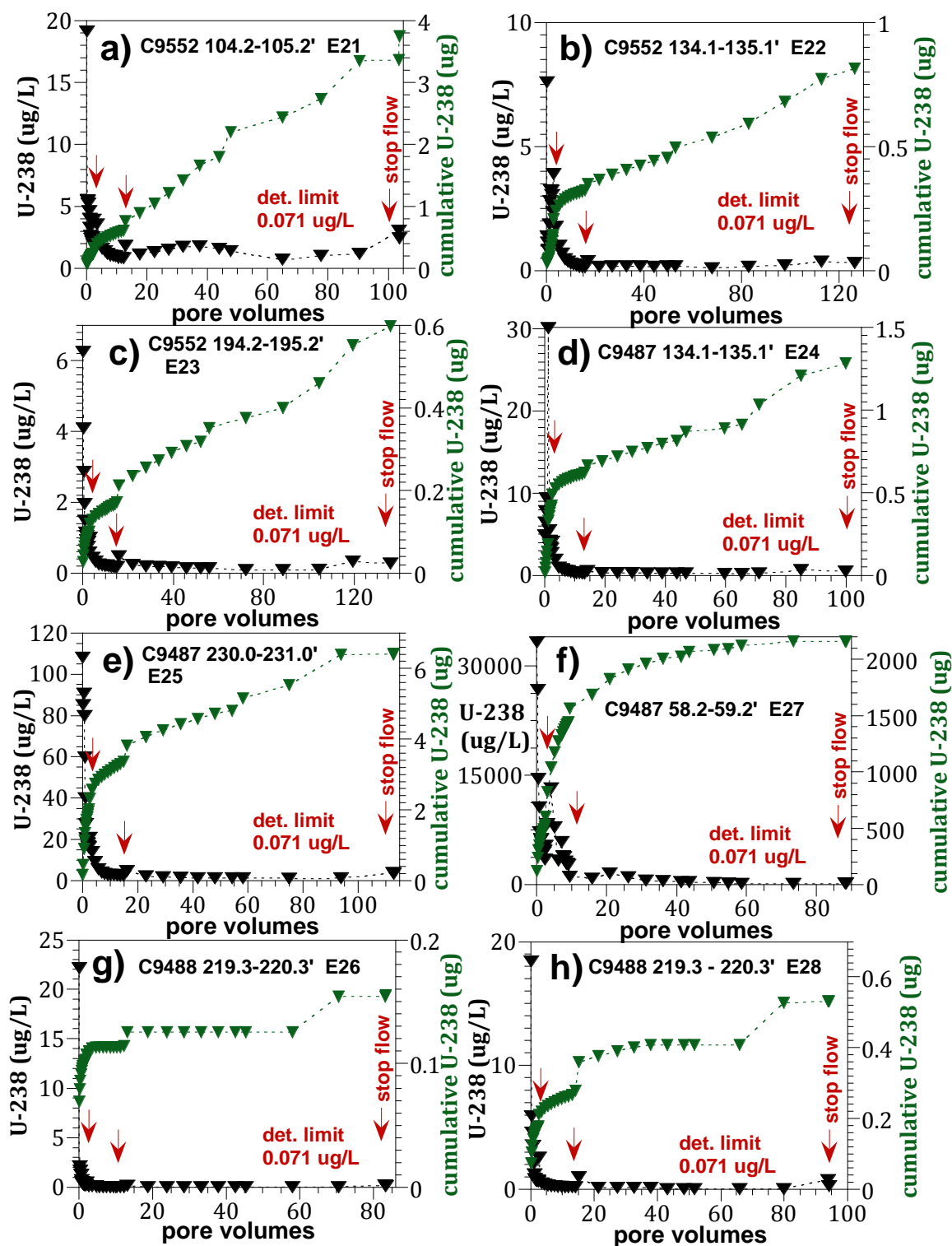


Figure 4.21. U-238 breakthrough in 1-D column leaching experiments. Effluent U-238 (black triangles) and cumulative U-238 mass (green triangles) are shown.

The three stop-flow events in 1-D leach columns provide additional insight into uranium release behavior. The U-238 release rate from sediments calculated from stop-flow events at 2.5, 10, and 100 pore volumes showed predominantly decreasing rates for higher leached pore volumes (Figure 4.22a). There was a good correlation between the U-238 release rate from sediment and leached mass (Figure 4.22b). This is consistent with sequential extraction data (Figure 4.7a, b), which showed the more highly U-238 contaminated sediments had a higher percentage of aqueous/adsorbed uranium (and as a consequence initially released that at a higher rate). Sediments with a very low U-238 leached mass (such as C9488 219' and C9552 134') are likely dominated by naturally occurring uranium; thus, uranium surface phases are in near equilibrium with pore water, and release rates are low and are not changing as with leached water injected compared with sediments containing high uranium contamination.

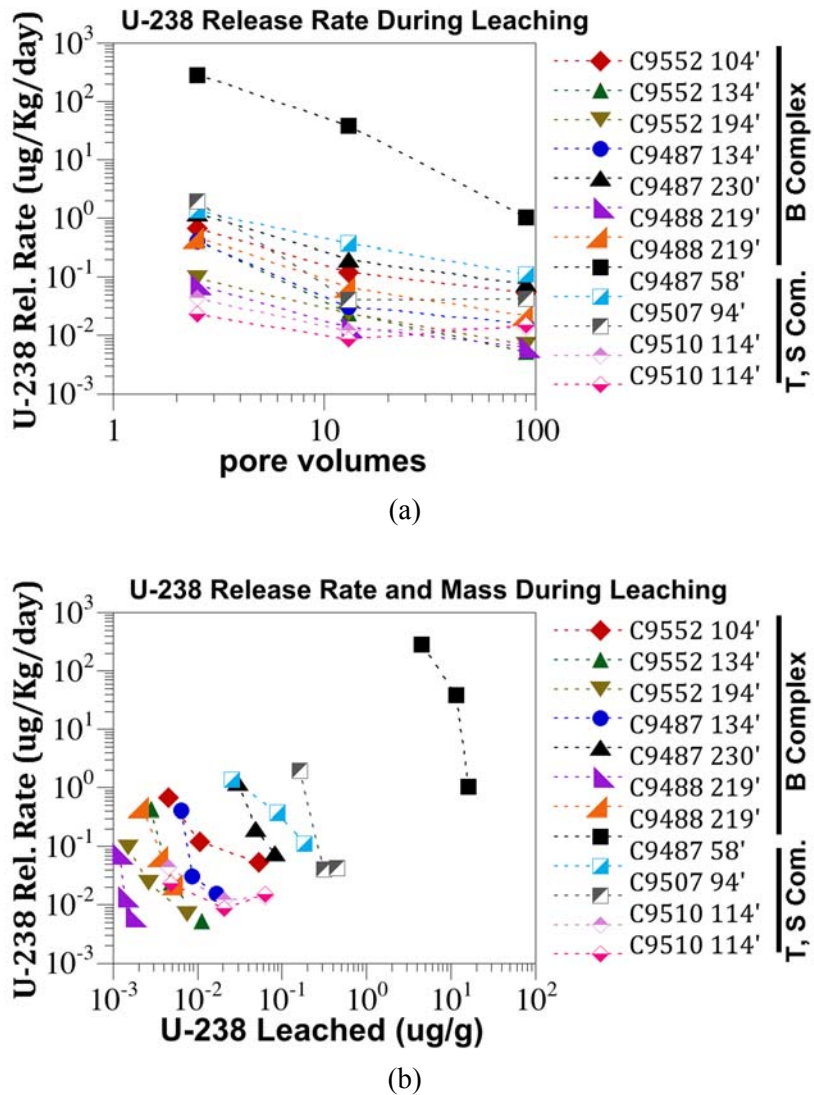


Figure 4.22. U-238 release rates calculated from stop-flow events in 1-D column leach experiments showing (a) U-238 release rate change with pore volumes, and (b) U-238 release rate and mass leached.

Iodine (I-127) leaching from B-Complex sediments shows a combination of significant initial release in the first few pore volumes followed by additional leaching over the next 80 to 130 pore volumes (Figure 4.23). This complex behavior is likely caused by iodine presence in multiple surface and aqueous phases. Sequential extractions on sediments prior to leaching indicated no aqueous/adsorbed, 20% to 30% rind carbonate-associated iodine, 30% to 60% total carbonate associated iodine, and 0% to 30% hard-to-extract phases (i.e., hard to mobilize, Figure 4.8a). Leaching mobilized 40% to 60% of the iodine (Figure 4.8b), indicating about half of iodine in carbonates was mobilized. The 1000-hour carbonate extraction (Figure 4.8c) on pre-leach sediments removed approximately the same iodine mass as 100 pore volumes of groundwater. Iodine speciation was only possible on some effluent samples due to high nitrate contamination and low iodine concentrations (Figure 4.24). For five sediments, initial samples were iodide dominated (< 2 pore volumes), followed by a smaller peak of iodate (1 to 3 pore volumes). Note that $\mu\text{g/L}$ concentrations are shown (i.e., comparing molar concentrations as in Figure 4.25 reduces the relative iodate concentration by a third). In two sediments, the iodate concentration dominated iodine speciation (Figure 4.24d and f).

Cumulative iodine speciation plots even more clearly show dominance of iodide or iodate in different pore volumes and sediments (Figure 4.25). Initial leaching (< 1 pore volume) is dominated by iodide in all seven experiments, with later breakthrough of iodate. This is consistent with previous studies indicating iodate sorption to sediment is generally found to be about four times greater than iodide sorption. However, the total I-127 breakthrough is dominated mainly by iodide in three sediments (Figure 4.25a, b, and c), and mainly dominated by iodate in two sediments (Figure 4.25d and g). For the other two sediments, iodide and iodate mass did not quantitatively come close to total I-127 (Figure 4.25e and f). Again, there was significant analytical difficulty analyzing initial (< 5 pore volume) leach samples due to the presence of high ion co-contaminants, which likely contributed to the lack of iodine species mass balance. Cations and anions present during leaching are described in the following section.

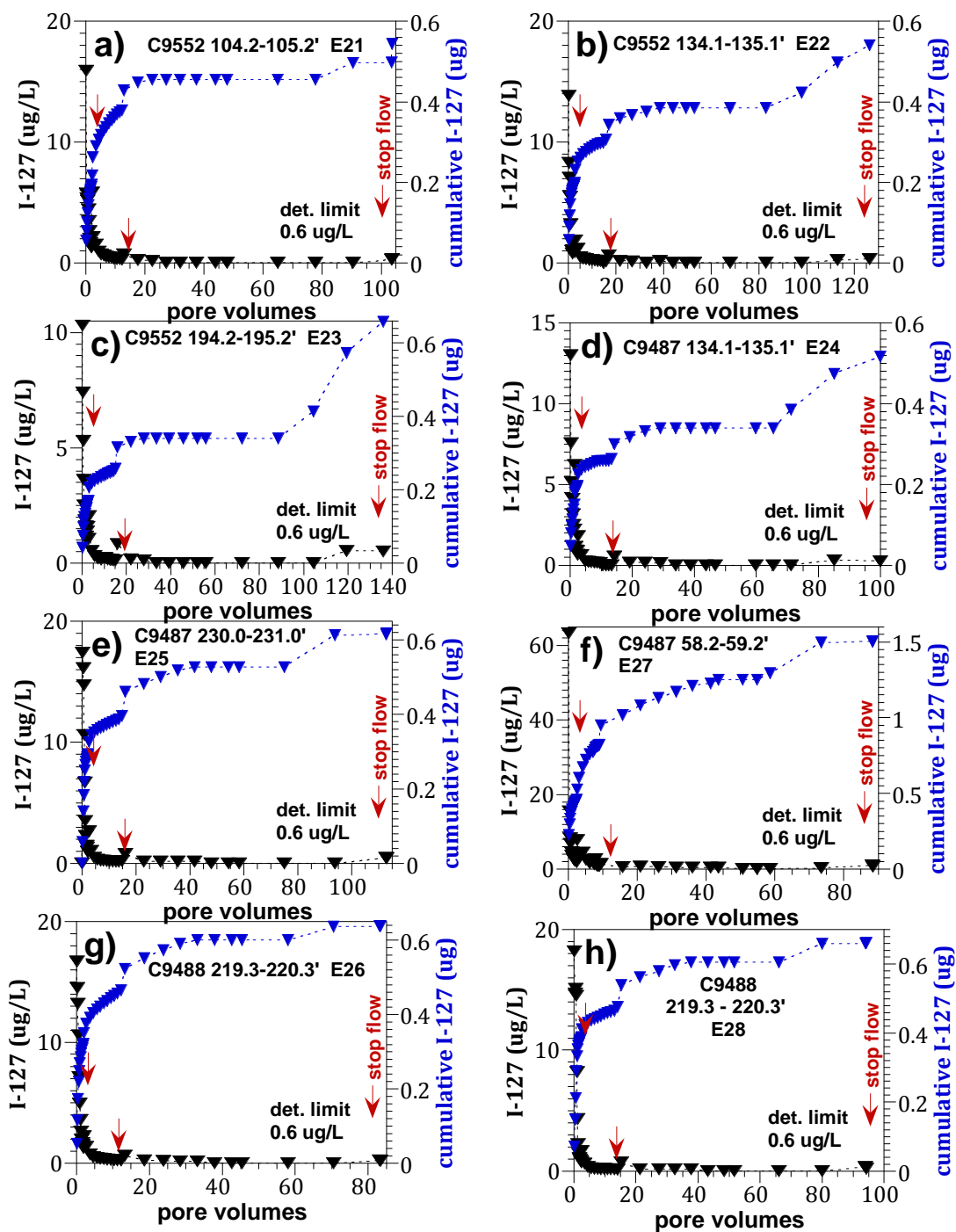


Figure 4.23. I-127 breakthrough in 1-D column leaching experiments. Effluent I-127 (black triangles) and cumulative I-127 mass (blue triangles) are shown.

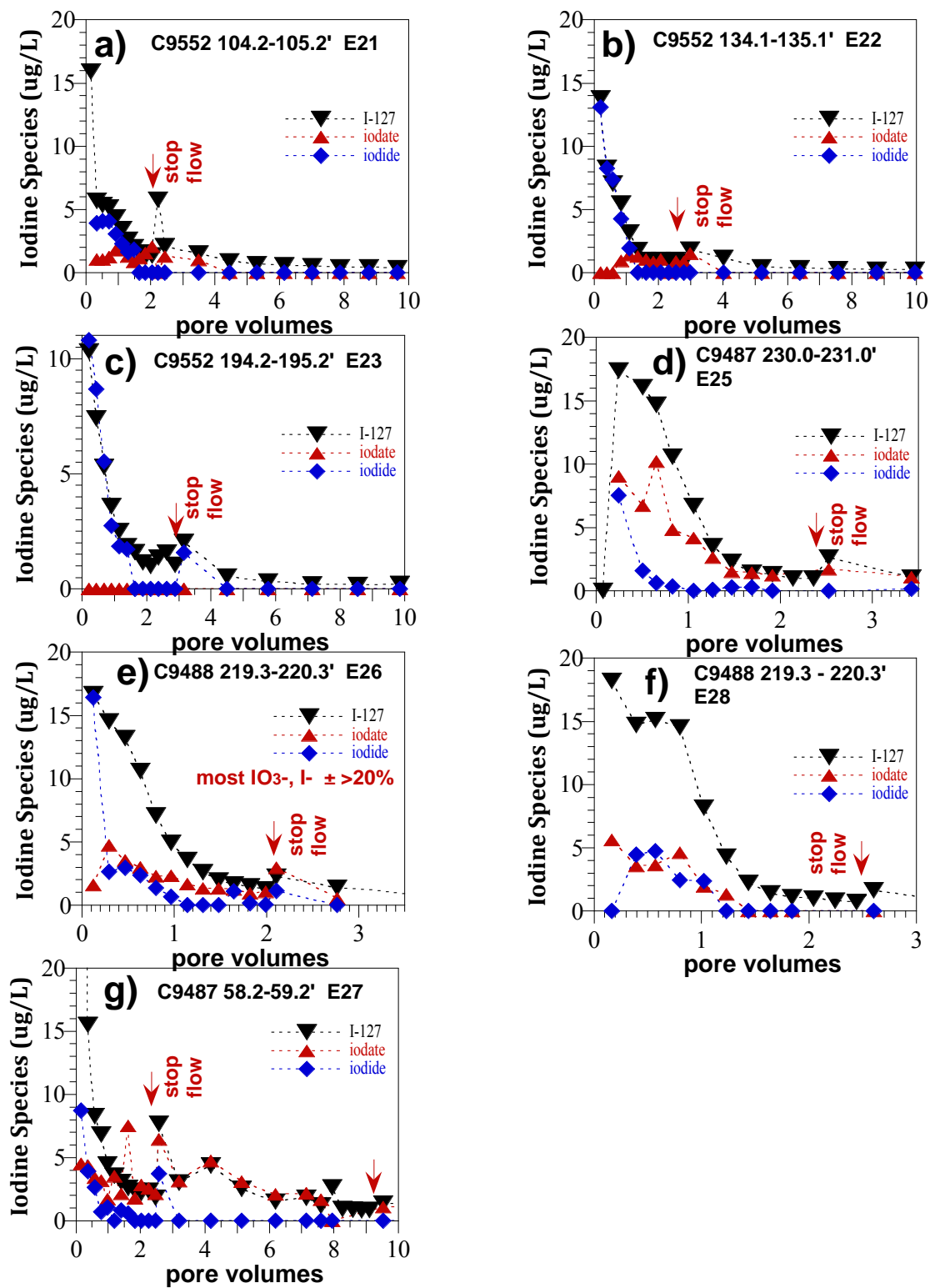


Figure 4.24. Iodine speciation breakthrough in 1-D column leaching experiments for selected samples with speciation analysis. Iodine speciation on C9487 134' was below detection limits.

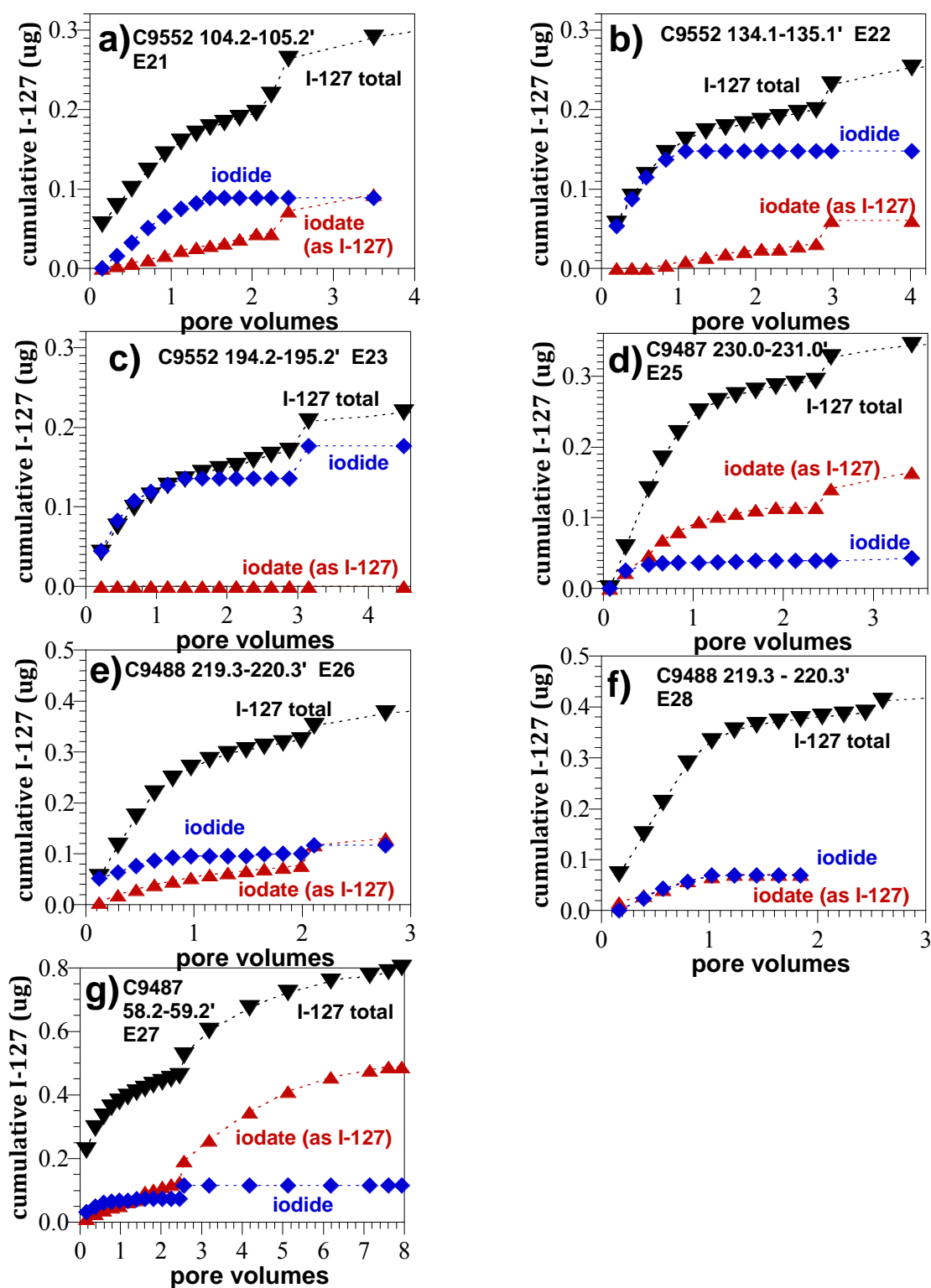


Figure 4.25. Cumulative iodine speciation breakthrough in 1-D column leaching experiments for selected samples with speciation analysis. Iodine speciation on C9487 134' was below detection limits.

The three stop-flow events in 1-D leach columns provide additional insight into iodine release behavior. The I-127 release rate from sediments calculated from stop-flow events at 2.5, 10, and 100 pore volumes showed predominantly decreasing rates for higher leached pore volumes (Figure 4.26a), similar to U-238 rate data (Figure 4.22a). In contrast to U-238 (Figure 4.22b), there was only a minor correlation between the I-127 release rate from sediment and leached mass (Figure 4.26b). This is consistent with sequential extraction data (Figure 4.8a, b), which showed nearly the same fraction of I-127 dominantly in carbonate-extractable phases; thus, there was little difference in surface phases between sediments. There was a fair correlation of sediments with somewhat greater leached I-127 mass had slightly greater release rates, similar to the correlation with uranium leached concentration and release rate.

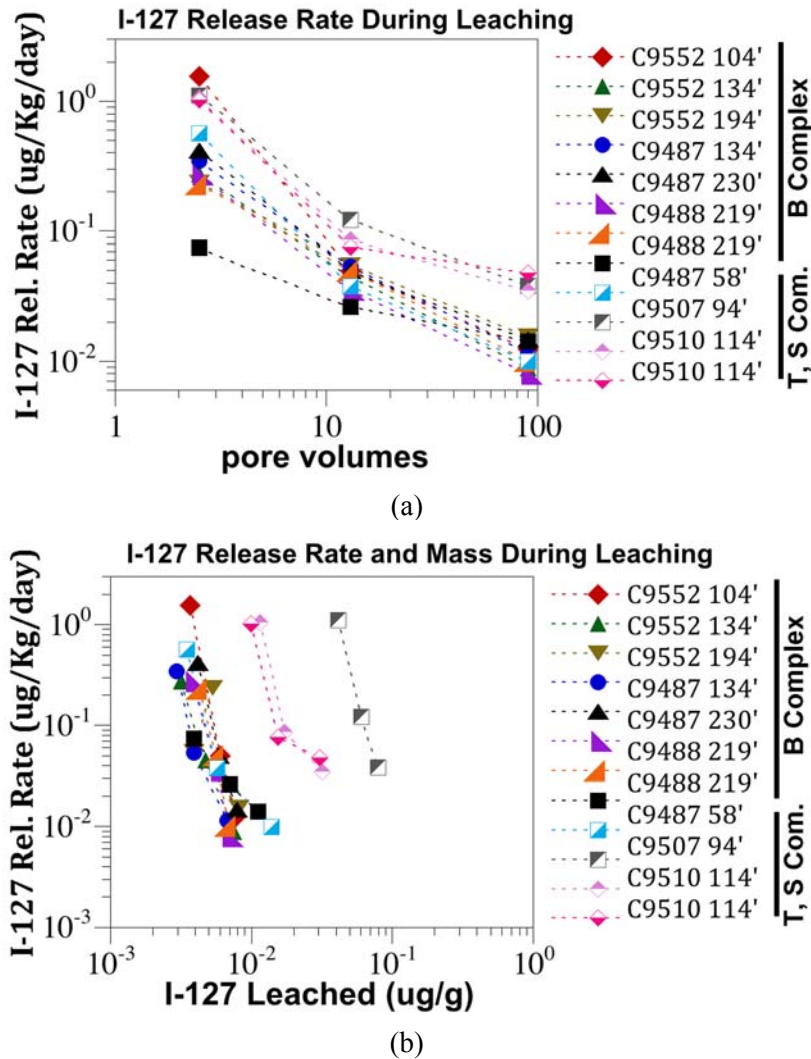


Figure 4.26. I-127 release rates calculated from stop-flow events in 1-D column leach experiments showing (a) I-127 release rate change with pore volumes, and (b) I-127 release rate and mass leached.

4.3.3 1-D Water Leach of Co-Contaminant Ions

During 1-D water leach of contaminants (described in the previous section), there are additional significant changes in co-contaminant ions that can have little influence on specific contaminants (i.e., Tc-99 as pertechnetate) or can have a significant influence (i.e., U^{VI} as Ca-uranyl-carbonate aqueous complexes adsorption changes with ionic strength and presence of specific ions). To address the co-contaminant ion issue, selected samples from 0.1 to 100 pore volumes were analyzed for major cations (Figure 4.27) and anions (Figure 4.28).

The general breakthrough behavior of major cations for six of the seven sediments was initial dominance by high Na, which slowly decreased (over tens of pore volumes) to the composition of the artificial groundwater. The initial Na concentration varied from 10 to 400 mmol/L, which is equivalent to 25 mmol/L to 4.5 mol/L in the original pore water. One sediment (C9552, 194', Figure 4.27c) was initially dominated by Ca (90 mmol/L) with 60 mmol/L Na. Another sediment (C9487 58') had unusually high potassium concentration (8 mmol/L initially). Advection of these cations out of the sediment and replacement by inflowing low ionic strength Ca, Mg-carbonate groundwater occurs by ion exchange, which is concentration and ion dependent. Initially, Na at high ionic strength can be rapidly ion exchanged off surfaces by inflowing divalent Ca and Mg, but as the ionic strength decreases, the exchange process slows. For example, measured Ca retardation in sediment in groundwater is ~125 (11 mmol/L ionic strength), but decreases to 15 at 50 mmol/L ionic strength, and to 3.7 at 200 mmol/L ionic strength. Therefore, ion exchange in these column leaches is increasingly slow with a greater number of pore volumes due to the decreasing ionic strength. This behavior is observed, as ~100 pore volumes of injected groundwater is needed for reach near equilibrium of ions in the sediment.

In contrast, the general breakthrough behavior of major anions for five of seven sediments was initial dominance by nitrate, with one sediment with initially high nitrite and sulfate (Figure 4.28). Anion equilibrium was reached more quickly than cation equilibrium, as most adsorb weakly, as shown by near groundwater equilibrium likely by 10 pore volumes.

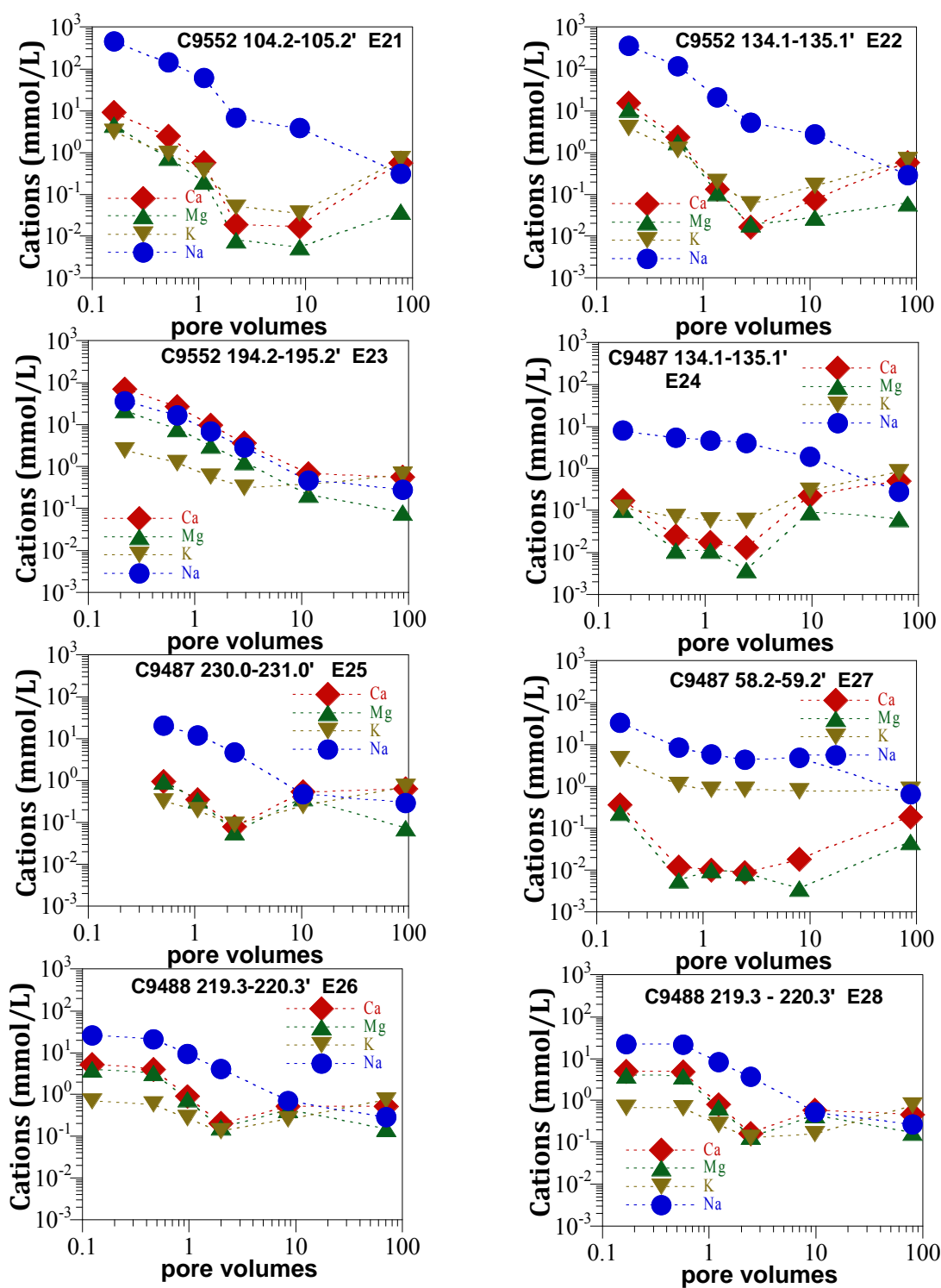


Figure 4.27. Change in major cations leaching from sediments in 1-D column leach experiments.

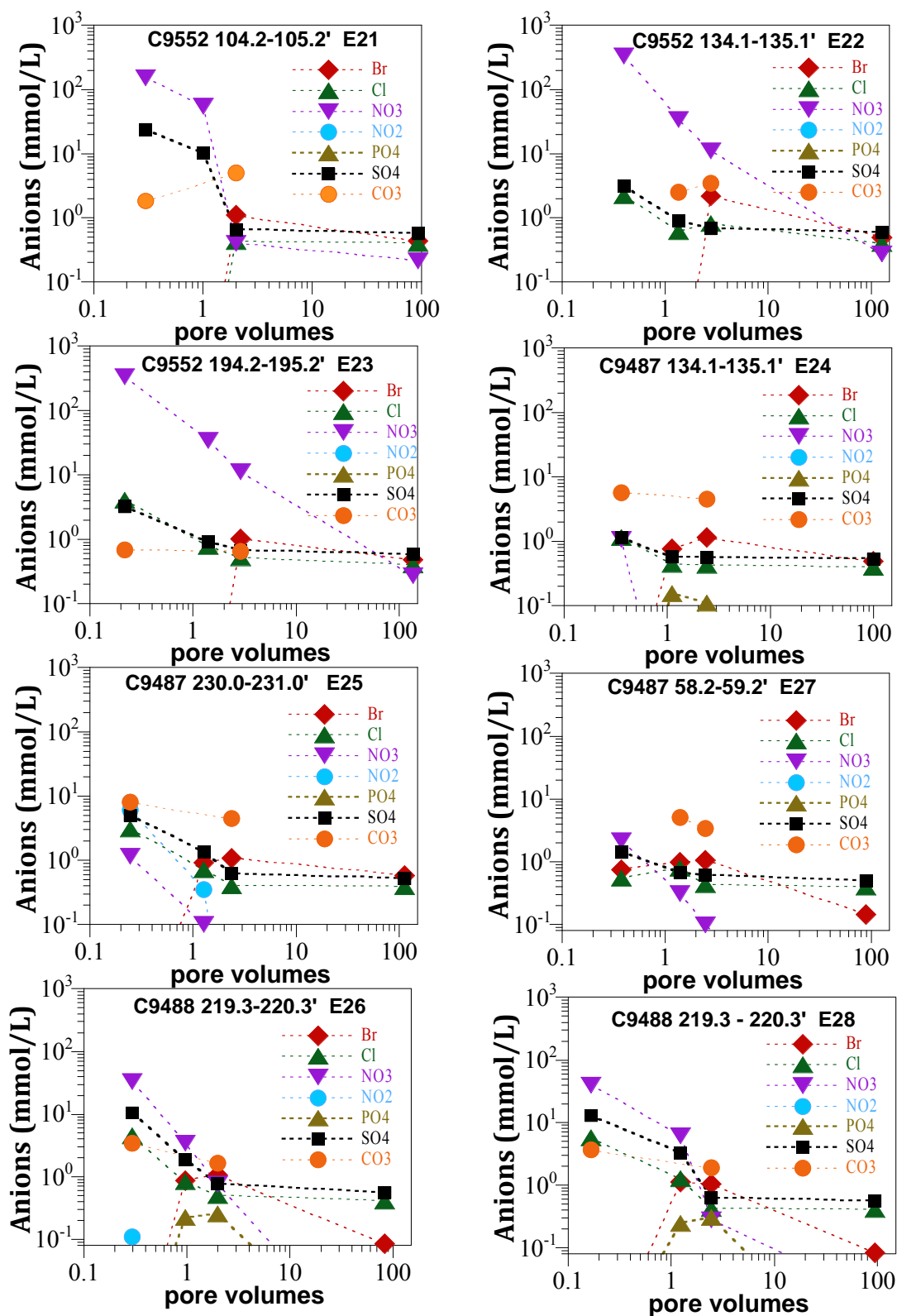


Figure 4.28. Change in major anions leaching from sediments in 1-D column leach experiments.

5.0 Conclusions and Implications for Field Transport of Contaminants

This report describes geochemical, microbial, and physical characterization of Hanford vadose zone boreholes C9552, C9487, and C9488 (located in the BY Cribs, B-7AB, and B-8 waste sites, respectively). Targeted mobile contaminants (uranium, technetium, iodine species, chromate, cyanide, and nitrate) were measured and attenuation processes and other factors that affect transport of these contaminants were evaluated. The objectives of this study were to (a) quantify contaminant distribution and geochemical, microbial, and physical setting; (b) identify attenuation processes; and (c) quantify mobility of contaminants, based on EPA guidance (EPA 2015). Geochemical characterization included short- (i.e., hours) and long-term (1000-hour) reactions of sediments with groundwater and other solutions designed to remove contaminants from surface phases, characterization of contaminant leaching from sediments in 1-D columns, measurement of Fe- and Mn-oxide surface phases, and measurement of uranium(VI) and iodate reduction rate and extent. Microbial characterization included characterization of microbial biomass, and the ability of the natural sediment consortium to reduce contaminants of concern (i.e., uranium as Ca-uranyl-carbonate aqueous species, pertechnetate, chromate, iodate, and nitrate). Physical characterization of the sediment included measurement of intact core bulk density, porosity, air permeability, field moisture content, lithology, and grain size distribution. Finally, stable isotopes ($\delta^2\text{H}$ [deuterium] and $\delta^{18}\text{O}$ [18-oxygen]) were measured in the pore water to evaluate natural and anthropogenic water sources at different locations.

Water extractions of B-Complex sediment cores had moderate U-238, Tc-99, and iodine contamination, trace cyanide contamination, and high Na-nitrate contamination. The 58-ft depth in borehole C9487 contained significant (54 $\mu\text{g/g}$) uranium contamination. Sediments with higher U-238 (as U^{VI} complexes) contamination generally had a higher fraction of mobile uranium. Sequential extractions showed that 3% to 12% of uranium was aqueous/adsorbed (highly mobile), 4% to 40% was carbonate associated (slow-release mobility), and 40% to 80% was associated with oxides and silicates (functionally immobile). Batch reaction of sediments with groundwater for 1 to 1000 hours showed significant increase in uranium release. This behavior was shown more clearly during 1-D column leaching, where initial (5 pore volume) release from aqueous and adsorbed phases accounted for 20% to 70% of the total mass released, then significant additional U was released over the following 100 pore volumes, likely from slow carbonate dissolution. Post-leach extractions showed the lesser uranium fraction of the more mobile phases. Stop-flow events provided further insight into uranium release behavior. Sediments with high contamination released uranium more rapidly to 150 $\mu\text{g/kg/day}$ (similar to batch experiment release rates), whereas sediments with low uranium leached mass (likely dominated by natural uranium in equilibrium with pore water) had slow uranium release rates (0.05 $\mu\text{g/kg/day}$). Release rates also decreased with further leaching.

The I-127 contamination in these B-Complex sediments ranged from 0.014 to 0.054 $\mu\text{g/g}$. Sequential extractions at these low concentrations had no measureable aqueous or adsorbed iodine, with 60% to 75% carbonate-associated iodine, and 25% to 40% Fe/Mn/Al oxide-associated iodine. It was not possible to measure iodine in the 8M nitric acid extraction. Long-term (1000-hour) batch experiments showed a slow increase in aqueous iodine, likely from carbonate dissolution (most of the increased mass was iodate). Experiments in which 100 $\mu\text{g/L}$ iodate was added to field sediments all showed a decrease in iodate concentration, with some experiments showing a corresponding increase in iodide concentration. Groundwater leaching for 100 pore volumes removed 60% to 80% of the total iodine, and post-leach

extractions showed smaller carbonate-associated iodine. Iodine speciation in most sediments showed initial leaching of iodide, followed by later release of iodate. This behavior is consistent with low reported adsorption of iodide (i.e., $K_d < 0.1 \text{ cm}^3/\text{g}$) and moderate sorption of iodate (i.e., $K_d \sim 0.4 \text{ cm}^3/\text{g}$). The leached mass in most sediments was dominated by iodide, with two sediments dominated by iodate. The iodine release rates calculated during stop-flow events in 1-D leaching decreased up to an order of magnitude between 2 and 100 pore volumes, which is consistent with initial leaching of aqueous/adsorbed iodide and iodate, followed by later slow release of iodate in carbonate.

Some B-Complex sediments had low Tc-99 contamination ($<0.013 \text{ } \mu\text{g/g}$), which was all in aqueous and adsorbed phases. Leaching removed nearly all Tc-99 from sediments as post-leach extractions had no reportable Tc-99. The 1000-hour carbonate extraction removed a third to half of the Tc-99. Long-term (1000-hour) batch experiments showed no increase in Tc-99 concentration, and column leaching (100 pore volumes) showed nearly no increase in Tc-99 mass released from sediments after the first few pore volumes. The Tc-99 release rates calculated from stop-flows did not change, indicating a similar release mechanism (i.e., aqueous and adsorbed Tc-99 was advected).

These B-Complex sediments contained no aqueous, adsorbed, or carbonate-associated Cr, but did contain significant Cr in oxide and silicate phases. That oxide/silicate Cr was likely natural, as no Cr leached from sediment during 1000-hour batch leach and 100 pore volume groundwater leach. Low cyanide ($<0.042 \text{ } \mu\text{g/g}$) was measured in three water-extracted C9552 borehole sediments.

Cations and metals measured in water leaching show aqueous or adsorbed ions present, then sequential liquid extractions representing cations or metals from dissolved minerals and/or anthropogenic precipitates (NaNO_3 , NaSO_4 , NaCO_3). All cores have elevated cation and anion concentrations relative to natural pore water. The initial Na concentration varied from 10 to 400 mmol/L, which is equivalent to 25 mmol/L to 4.5 mol/L in the original pore water in six cores, with one core with high K (8 mmol/L). Anions were dominated by high nitrate (to 500 mmol/L), with one core initially high in sulfate. There were low concentrations of nitrite in some samples, indicating minimal reduction of the high nitrate. Cation and anion concentrations measured during the 100 pore volume groundwater leach of sediments showed significant leaching is required to reach cation equilibrium (due to high ion exchange of cations), but anion concentrations were close to equilibrium by 10 pore volumes of leaching. The total ferrous iron phases in sediments was 40% to 50%, and Mn^{II} phases were 35% to 60% of the total Mn. While there was no measureable ion-exchangeable Fe^{II} and little Mn^{II} (0.5 to $5.5 \text{ } \mu\text{g/g}$), ferrous iron in $\text{Fe}^{\text{II}}\text{CO}_3/\text{FeS}$ phases was significant (1.7 to 22.3 mg/g) and Mn^{II} a carbonate was minor (0.09 to 0.17 mg/g).

Microbial characterization indicates greater than 1.1×10^6 denitrifying bacteria per gram of sediment for all sediments. The density of iron-reducing bacteria increased with depth, and iron-reducing bacteria were present in numbers greater than 1.1×10^6 in sediment taken from deeper than ~ 134 ft bgs. Sulfate-reducing bacteria were present in similar density in sediment from borehole C9487. The abundance of bacterial phyla determined by sequencing DNA extracted from the sediments indicates *Proteobacteria* phylum were dominant in all of the samples, accounting for 68% to 96% of the bacteria in the samples. Less dominant but plentiful phyla include *Firmicutes* and *Actinobacteria*. These results indicate that facultative anaerobic bacterial phyla common to sediment environments are present in the B-Complex vadose zone.

Overall, sediments showed significant Na-nitrate and uranium contamination and moderate technetium and iodine (iodide and iodate) contamination, with differences in rate of contaminant release. Contaminant mobilization is related to differing release rates from aqueous, adsorbed, carbonate, and other surface phases. Characterized differences in abiotic and microbial reduction potential also influence some contaminants such as iodate.

6.0 Quality Assurance

The PNNL Quality Assurance (QA) Program is based upon the requirements as defined in DOE Order 414.1D, *Quality Assurance*, and 10 CFR 830, *Energy/Nuclear Safety Management*, Subpart A, Quality Assurance Requirements. PNNL has chosen to implement the following consensus standards in a graded approach:

- ASME NQA-1-2000, *Quality Assurance Requirements for Nuclear Facility Applications*, Part 1, Requirements for Quality Assurance Programs for Nuclear Facilities.
- ASME NQA-1-2000, Part II, Subpart 2.7, Quality Assurance Requirements for Computer Software for Nuclear Facility Applications, including problem reporting and corrective action.
- ASME NQA-1-2000, Part IV, Subpart 4.2, Guidance on Graded Application of Quality Assurance (QA) for Nuclear-Related Research and Development.

The procedures necessary to implement the requirements are documented through PNNL's "How Do I...? (HDI), a system for managing the delivery of laboratory-level policies, requirements, and procedures.

The *DVZ-AFRI Quality Assurance Plan* (QA-DVZ-AFRI-001) was applied as the applicable QA document for this work under the NQA-1 QA program. This QA plan conforms to the QA requirements of DOE Order 414.1D and 10 CFR 830, Subpart A. This effort is subject to the *Price Anderson Amendments Act*.

The implementation of the Deep Vadose Zone – Applied Field Research Initiative QA program is graded in accordance with NQA-1-2000, Part IV, Subpart 4.2, Guidance on Graded Application of Quality Assurance (QA) for Nuclear-Related Research and Development. The technology level defined for this effort is Applied Research, which consists of developing information that will be used directly by the Hanford Site to support remediation decisions.

This work was conducted under the Applied Research level to ensure the reproducibility and defensibility of these experimental results. As such, reviewed calculation packages are available upon request except where experimental information is denoted as a scoping or preliminary study.

This work used PNNL's Environmental Sciences Laboratory (ESL) for chemical analyses. The ESL operates under a dedicated QA plan that complies with the *Hanford Analytical Services Quality Assurance Requirements Document* (HASQARD; DOE/RL-96-68), Rev. 3. ESL implements HASQARD through *Conducting Analytical Work in Support of Regulatory Programs* (CAWSRP). Data quality objectives established in CAWSRP were generated in accordance with HASQARD requirements. Chemical analyses of testing samples and materials were conducted under the ESL QA Plan.

QA reviews of data and analyses were conducted for this work in accordance with the QA plan. There were no reportable QA issues with the data included in this report.

7.0 References

- 10 CFR 830, *Energy/Nuclear Safety Management*. U.S. Code of Federal Regulations, as amended.
- APHA, AWWA, WEF. 2012. *Standard Methods for the Examination of Water and Wastewater*. 22nd Edition, American Public Health Association, Washington, D.C.
- ASME NQA-1-2000, *Quality Assurance Requirements for Nuclear Facility Applications*. American Society of Mechanical Engineers, New York, New York.
- Beckett P. 1989. "The use of extractants in studies on trace metals in soils, sewage sludges, and sludge-treated soils." In *Advances in Soil Science*, Volume 9, Springer-Verlag, New York, NY, pp. 144-176.
- Benson DA, K Clark, I Karsch-Mizrachi, DJ Lipman, J Ostell, and EW Sayers. 2015. "GenBank." *Nucleic Acids Research* 43(Database issue): D30-D35.
- Brina R and AG Miller. 1992. "Direct detection of trace levels of uranium by laser induced kinetic phosphorimetry." *Analytical Chemistry* 64(13):1413-1418.
- Chao T and L Zhou. 1983. "Extraction techniques for selective dissolution of amorphous iron oxides from soils and sediments." *Soil Science Society of America Journal* 47(2):225-232.
- Cole JR et al. 2013. "Ribosomal Database Project: data and tools for high throughput rRNA analysis." *Nucleic Acids Research*: gkt1244.
- Callos Y, F Mornet, A Sciandra, N Waser, A Larson and PJ Harrison. 1999. "An optical method for the rapid measurement of micromolar concentrations of nitrate in marine phytoplankton cultures." *Journal of Applied Phycology* 11(2):179-184.
- Craig H. 1961. "Isotopic variations in meteoric waters." *Science* 133:1702-1703.
- DePaolo DJ, ME Conrad, K Maher, GW Gee. 2004. "Evaporation effects on oxygen and hydrogen isotopes in deep vadose zone pore fluids at Hanford, Washington." *Vadose Zone Journal* 3:220-232.
- DOE Order 414.1D, *Quality Assurance*. U.S. Department of Energy, Washington, D.C.
- DOE. 1992. *Hanford Site Groundwater Background*. DOE/RL-92-23, U.S. Department of Energy, Richland Operations Office, Richland, Washington.
- DOE. 2016. *Remedial Investigation/Feasibility Study and RCRA Facility Investigation/Corrective Measures Study Work Plan for the 200-DV-1 Operable Unit*. DOE/RL-2011-102, U.S. Department of Energy, Richland Operations Office, Richland, Washington.
- DOE/RL-96-68, *Hanford Analytical Services Quality Assurance Requirements Document*, Rev. 3. U.S. Department of Energy, Richland Operations Office, Richland, Washington.

- EPA. 2004. *Quality Assurance/Quality Control Guidance for Laboratories Performing PCR Analyses on Environmental Samples*. EPA/815/B-04/001, U.S. Environmental Protection Agency, Washington, D.C.
- EPA. 2007a. *Monitored Natural Attenuation of Inorganic Contaminants in Ground Water- Volume 1, Technical Basis for Assessment*. EPA/600/R-07/139, U.S. Environmental Protection Agency, Washington, D.C.
- EPA. 2007b. *Monitored Natural Attenuation of Inorganic Contaminants in Ground Water- Volume 2, Assessment for Non-Radionuclides Including Arsenic, Cadmium, Chromium, Copper, Lead, Nickel, Nitrate, Perchlorate, and Selenium*. EPA/600/R-07/140, U.S. Environmental Protection Agency, Washington, D.C.
- EPA. 2010. *Monitored Natural Attenuation of Inorganic Contaminants in Ground Water- Volume 3, Assessment for Radionuclides Including Tritium, Radon, Strontium, Technetium, Uranium, Iodine, Radium, Thorium, Cesium, and Plutonium-Americium*. EPA/600/R-101093, U.S. Environmental Protection Agency, Washington, D.C.
- EPA. 2015. *Use of Monitored Natural Attenuation for Inorganic Contaminants in Groundwater at Superfund Sites*. OSWER Directive 9283.1-36, U.S. Environmental Protection Agency, Office of Solid Waste and Emergency Response, Washington, D.C.
- Gibbs C. 1976. "Characterization and Application of Ferrozine Iron Reagent as a Ferrous Iron Indicator." *Analytical Chemistry* 48(8):1197-1200.
- Gleyzes C, S Tellier, and M Astruc. 2002. "Fractionation studies of trace elements in contaminated soils and sediments: a review of sequential extraction procedures." *Trends in Analytical Chemistry* 21:(6 & 7):451-467.
- Gould W, M Stichbury, M Francis, L Lortie, and D Blowes. 2003. "An MPN method for the enumeration of iron-reducing bacteria." In *14th International Symposium on Environmental Biogeochemistry: Mining and the Environment Conference*.
- Graham DL. 1983. *Stable isotopic composition of precipitation from the Rattlesnake Hills area of south-central Washington State*. RHO-BW-ST-44 P, Rockwell Hanford Operations, Richland, Washington.
- Grebel JE, JA Charbonnet, and DL Sedlak. 2016. "Oxidation of organic contaminants by manganese oxide geomedia for passive urban stormwater treatment systems." *Water Research* 88:481-491.
- Goebel TS and RJ Lascano. 2012. "System for high throughput water extraction from soil material for stable isotope analysis of water." *Journal of Analytical Sciences, Methods and Instrumentation* 2:203-207.
- Hall G, J Vaive, R Beer, and N Hoashi. 1996. "Selective leaches revisited, with emphasis on the amorphous Fe oxyhydroxides phase extraction." *Journal of Geochemical Exploration* 56:59-78.

Hearn PP, Jr., WC Steinkampf, DG Horton, GC Solomon, LD White, and JR Evans. 1989. "Oxygen-isotope composition of ground water and secondary minerals in Columbia Plateau basalts: Implications for the paleohydrology of the Pasco Basin." *Geology* 17:606-610.

Heron G, C Crozet, AC Bourg, and TH Christensen. 1994. "Speciation of Fe(II) and Fe(III) in contaminated aquifer sediments using chemical extraction techniques." *Environmental Science and Technology* 28:1698-1705.

Kohler M, DP Curtis, DE Meece, and JA Davis. 2004. "Methods for estimating adsorbed uranium (VI) and distribution coefficients of contaminated sediments." *Environmental Science and Technology* 38: 240-247.

Larner B, A Seen, and A Townsend. 2006. "Comparative study of optimized BCR sequential extraction scheme and acid leaching of elements in certified reference material NIST 2711." *Analytica Chimica Acta* 556:444-449.

Leco. 2002. Method of organic and inorganic carbon analysis. Leco Corporation, Saint Joseph, Michigan.

Lee, BD, J. Moran, MK Nims, and DL Saunders. 2017. Letter Report: Stable Hydrogen and Oxygen Isotope Analysis of B-Complex Perched Water Samples. PNNL-26341, Pacific Northwest National Laboratory, Richland, Washington.

Massop K and C Davison. 2003. "Comparison of original and modified BCR sequential extraction procedures for the fractionation of copper, iron, lead, manganese, and zinc in soils and sediments." *Analytica Chimica Acta* 478:111-118.

McKinney CR, JM McCrea, S Epstein, HA Allen, and HA Urey. 1950. "Improvements in mass spectrometers for the measurement of small differences in isotope abundance ratios." *Review of Scientific Instruments* 21:724-730.

O'Leary NA, MW Wright, JR Brister, S Ciufo, D Haddad, R McVeigh, B Rajput, B Robbertse, B Smith-White, D Ako-Adjei, A Astashyn, A Badretdin, Y Bao, O Blinkova, V Braver, V Chetvernin, J Choi, E Cox, O Ermolaeva, CM Farrell, T Goldfarb, T Gupta, D Haft, E Hatcher, W Hlavina, VS Joardar, VK Kodali, W Li, D Maglott, P Masterson, KM McGarvey, MR Murphy, K O'Neill, S Pujar, SH Rangwala, D Rausch, LD Riddick, C Schoch, A Shkeda, SS Storz, H Sun, F Thibaud-Nissen, I Tolstoy, RE Tully, AR Vatsan, C Wallin, D Webb, W Wu, MJ Landrum, A Kimchi, T Tatusova, M DiCuccio, P Kitts, TD Murphy, and KD Pruitt. 2015. "Reference sequence (RefSeq) database at NCBI: current status, taxonomic expansion, and functional annotation." *Nucleic Acids Research*: gkvl189.

Pflaum RT and LC Howick. 1956. "The chromium-diphenylcarbazide reaction. *Proceedings of the American Chemical Society* 78:4862-2866.

Prudic D, D Stonestrom, and R Streigl. 1997. *Tritium, Deuterium, and Oxygen-18 in Water Collected from Unsaturated Sediments near a Low-Level Radioactive-Waste Burial Site South of Beatty, Nevada*. Water Resources Investigations Report 97-4062, U.S. Geological Survey, Reston, Virginia.

- Qafoku NP, CC Ainsworth, JE Szecsody, and OS Qafoku. 2004. "Transport-controlled kinetics of dissolution and precipitation in the sediments under alkaline and saline conditions." *Geochimica et Cosmochimica Acta* 68(14):2981-2995.
- Rehm HL, SJ Bale, P Bayrak-Toydemir, JS Berg, KK Brown, JL Deignan, MJ Friez, BH Funke, MR Hegde, E Lyon, and the Working Group of the American College of Medical Genetics. 2013. "ACMG clinical laboratory standards for next-generation sequencing." *Genetics in Medicine* 15(9):733-747.
- Reynolds, S.A., 1973. "Theoretical and practical specific activities and other properties of common radionuclides. Oak Ridge National Laboratory, ORNL-TM-4167, 21p.
- Rhoades, JD. 1996. *Methods of Soil Analysis Part 3. Chemical Methods*. Soil Science Society of America, Madison, WI.
- Serne, RJ, BN Bjornstad, JM Keller, PD Thorne, DC Lanigan, JN Christensen, and GS Thomas. 2010. *Conceptual models for migration of key groundwater contaminants through the vadose zone and into the unconfined aquifer below the B-Complex*. PNNL-19277, Pacific Northwest National Laboratory, Richland, Washington.
- Singleton MJ, EL Sonnenthal, ME Conrad, DJ DePaolo, and GW Gee. 2004. "Multiphase reactive transport modeling of seasonal infiltration events and stable isotope fractionation in unsaturated zone pore water and vapor at the Hanford site." *Vadose Zone Journal* 3:775-785.
- Spane FA Jr. 1999. *Effects of Barometric Fluctuations on Well Water-Level Measurements and Aquifer Test Data*. PNNL-13078, Pacific Northwest National Laboratory, Richland, Washington.
- Spane FA, Jr. and WD Webber. 1995. *Hydrochemistry and Hydrogeologic Conditions within the Hanford Site Upper Basalt Confined Aquifer System*. PNL-10817, Pacific Northwest National Laboratory, Richland, Washington.
- Sutherland R and F Tack. 2002. "Determination of Al, Cu, Fe, Mn, Pb, and Zn in certified reference materials using the optimized BCR sequential extraction procedure." *Analytica Chimica Acta* 454:249-257.
- Szecsody JE, D Jansik, JP McKinley, and N Hess. 2014. "Influence of alkaline waste on technetium mobility in Hanford formation sediments." *Journal of Environmental Radioactivity* 135:147-160.
- Szecsody J, M Truex, N Qafoku, D Wellman, T Resch, and, L Zhong. 2013. "Influence of acidic and alkaline co-contaminants on uranium migration in vadose zone sediments." *Journal of Contaminant Hydrology* 151:155-175.
- Szecsody J, M Truex, N Qafoku, and T Resch. 2016. "Persistence of Chromate Reduction in Natural Oxidic Aquifer Sediments: Role of Abiotic and Biotic Reactions." *Chemosphere* (in preparation).
- Szecsody J, J Zachara, and P Bruckhart. 1994. "Adsorption-Dissolution Reactions Affecting the Distribution and Stability of Co(II)-EDTA in Fe-oxide Sand." *Environmental Science and Technology* 28:1706-1716.

Truex MJ and KC Carroll. 2013. *Remedy Evaluation Framework for Inorganic, Non-Volatile Contaminants in the Deep Vadose Zone*. PNNL-21815, Pacific Northwest National Laboratory, Richland, Washington.

Truex MJ, JE Szecsody, N Qafoku, and JR Serne. 2014. *Conceptual Model of Uranium in the Vadose Zone for Acidic and Alkaline Wastes Discharged at the Hanford Site Central Plateau*. PNNL-23666, Pacific Northwest National Laboratory, Richland, Washington.

Truex, MJ, M Oostrom, and GD Tartakovsky. 2015. *Evaluating Transport and Attenuation of Inorganic Contaminants in the Vadose Zone for Aqueous Waste Disposal Sites*. PNNL-24731, Pacific Northwest National Laboratory, Richland, Washington.

Truex, MJ, JE Szecsody, NP Qafoku, CE Strickland, JJ Moran, BD Lee, MM Snyder, AR Lawter, CT REsch, BN Gartman, L Zhong, MK Nims, DL Saunders, BD Williams, JA Horner, II Leavy, SR Baum, BB Christiansen, RE Clayton, EM McElroy, D Appriou, KJ Tyrell, and ML Striluk. 2017. Contaminant Attenuation and Transport Characterization of 200-DV-1 Operable Unit Sediment Samples. PNNL-26208/RPT-DVZ-AFRI-037, Pacific Northwest National Laboratory, Richland, Washington.

Um W, J Serne, M Truex, A Ward, M Valenta, C Brown, C Iovin, K Geiszler, I Kutnyakov, E Clayton, H Chang, S Baum, R Clayton, and D Smith. 2009. *Characterization of Sediments from the Soil Desiccation Pilot Test (SDPT) Site in the BC Cribs and Trenches Area*. PNNL-18800, Pacific Northwest National Laboratory, Richland, Washington.

Viollier E, P Inglett, K Hunter, A Roychoudhury, and P Van Cappellen. 2000. "The ferrozine method revisited: Fe(II)/Fe(III) determination in natural waters." *Applied Geochemistry* 15:785-790.

West AG, SJ Patrickson, and JR Ehleringer. 2006. "Water extraction times for plant and soil materials used in stable isotope analysis." *Rapid Communication in Mass Spectrometry* 20:1317-1321.

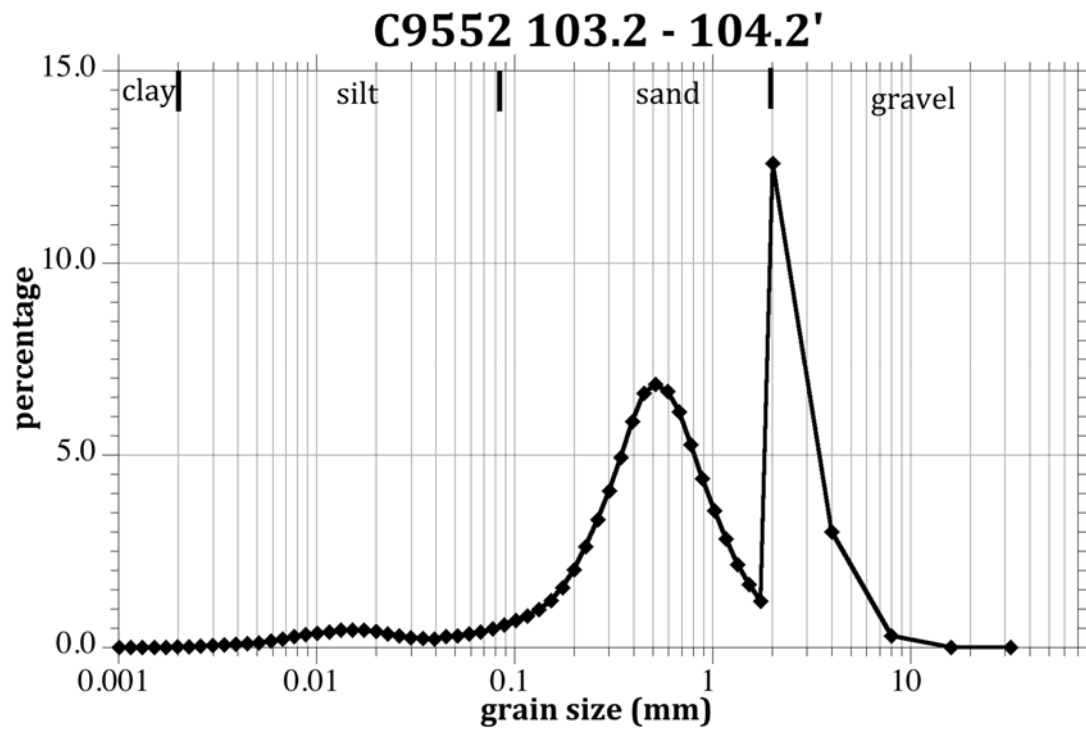
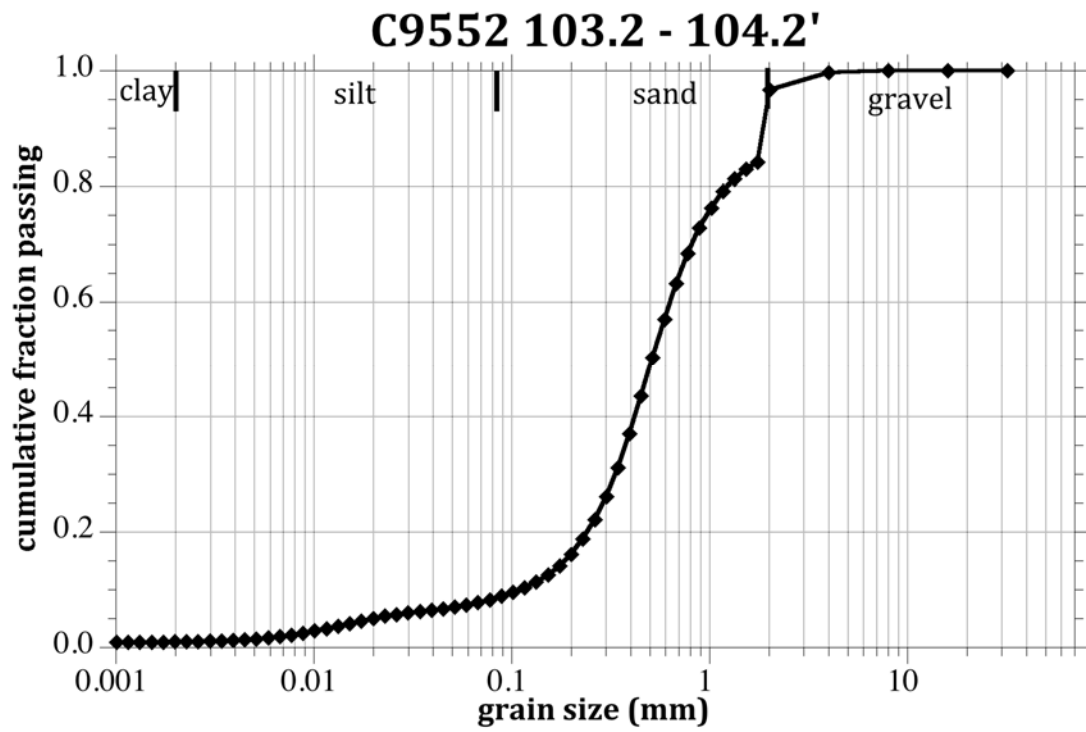
Xue Y, C Murray, G Last, and R Mackley. 2003. *Mineralogical and Bulk-Rock Geochemical Signatures of Ringold and Hanford Formation Sediments*. PNNL-14202, Pacific Northwest National Laboratory, Richland, Washington.

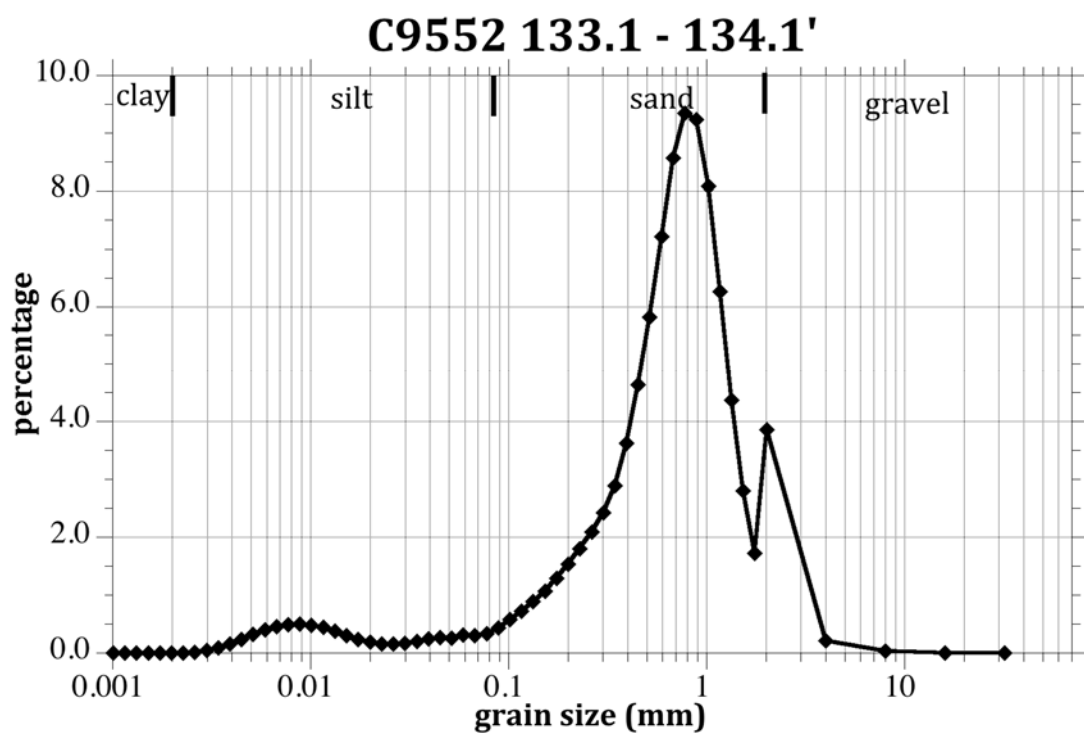
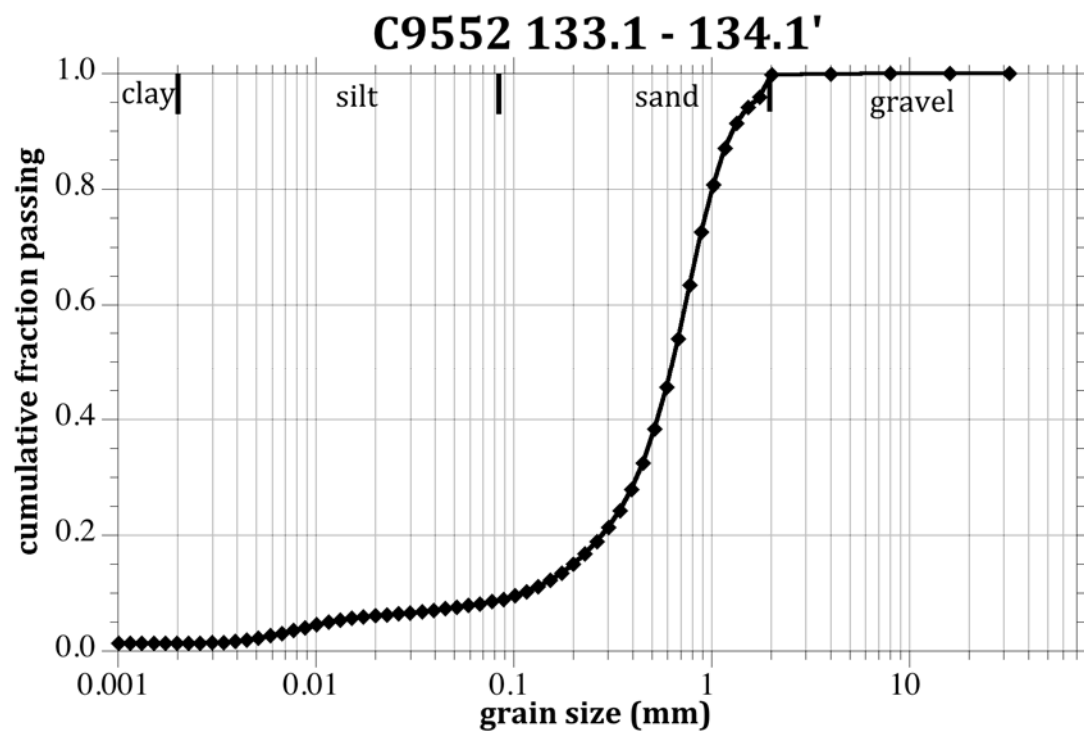
Zachara J, C Liu, C Brown, S Kelly, J Christensen, J McKinley, J Davis, J Serne, E Dresel, and W Um. 2007. *A Site-Wide Perspective on Uranium Geochemistry at the Hanford Site*. PNNL-17031, Pacific Northwest National Laboratory, Richland, Washington.

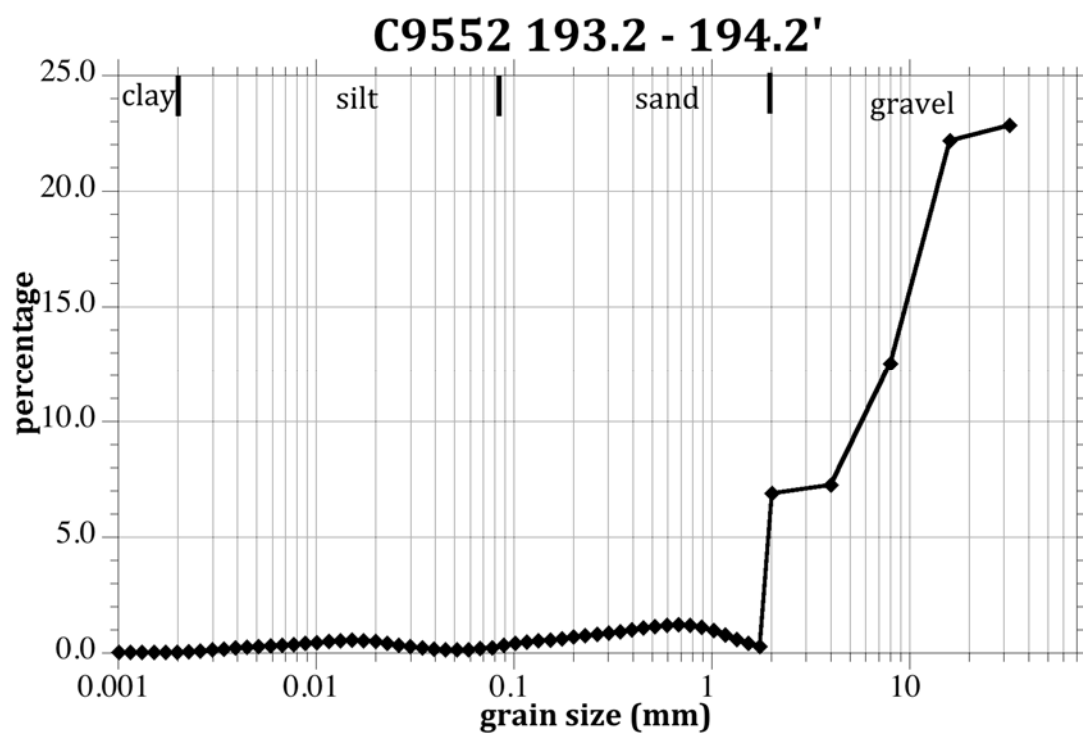
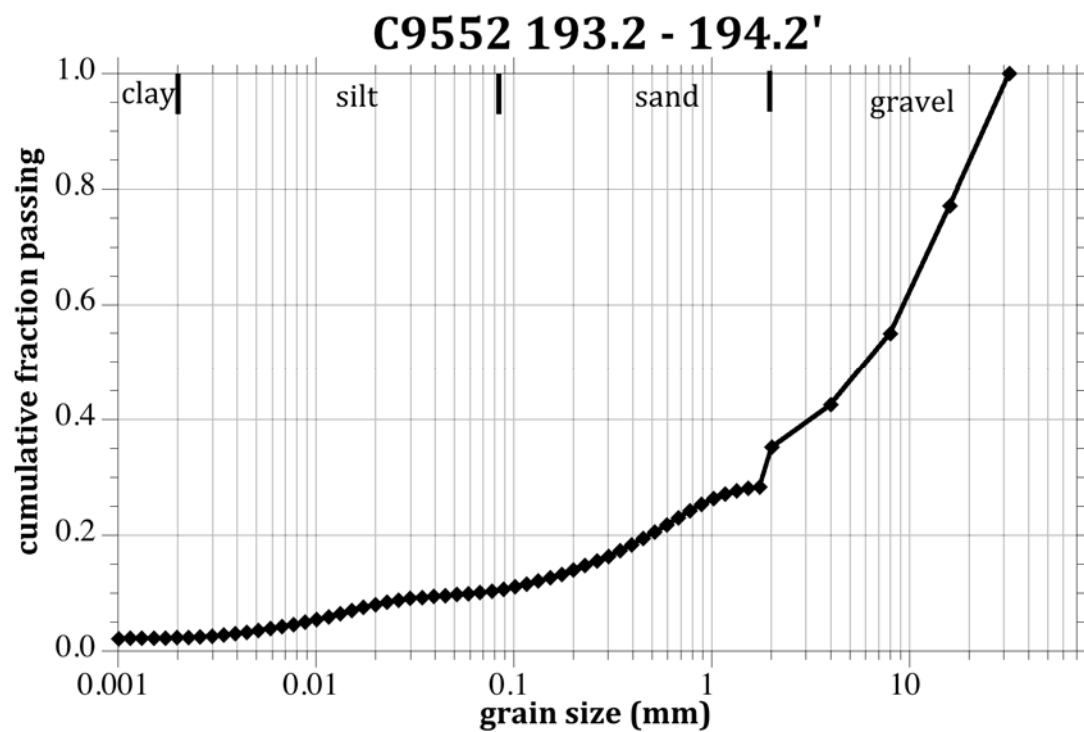
Appendix A

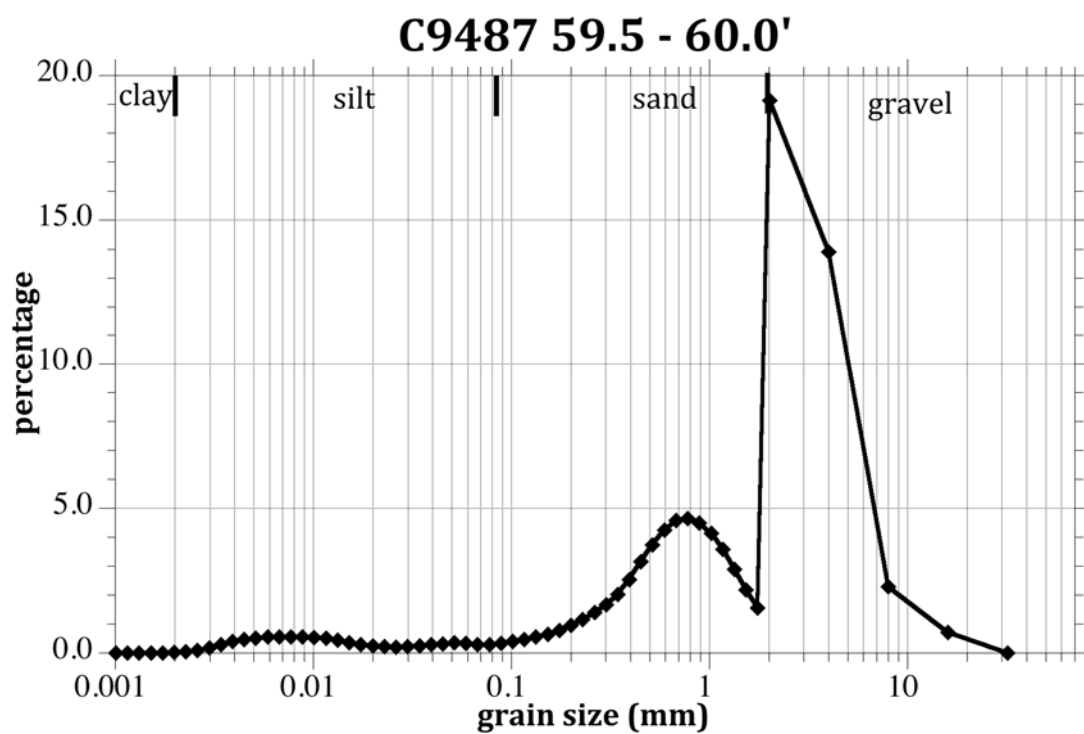
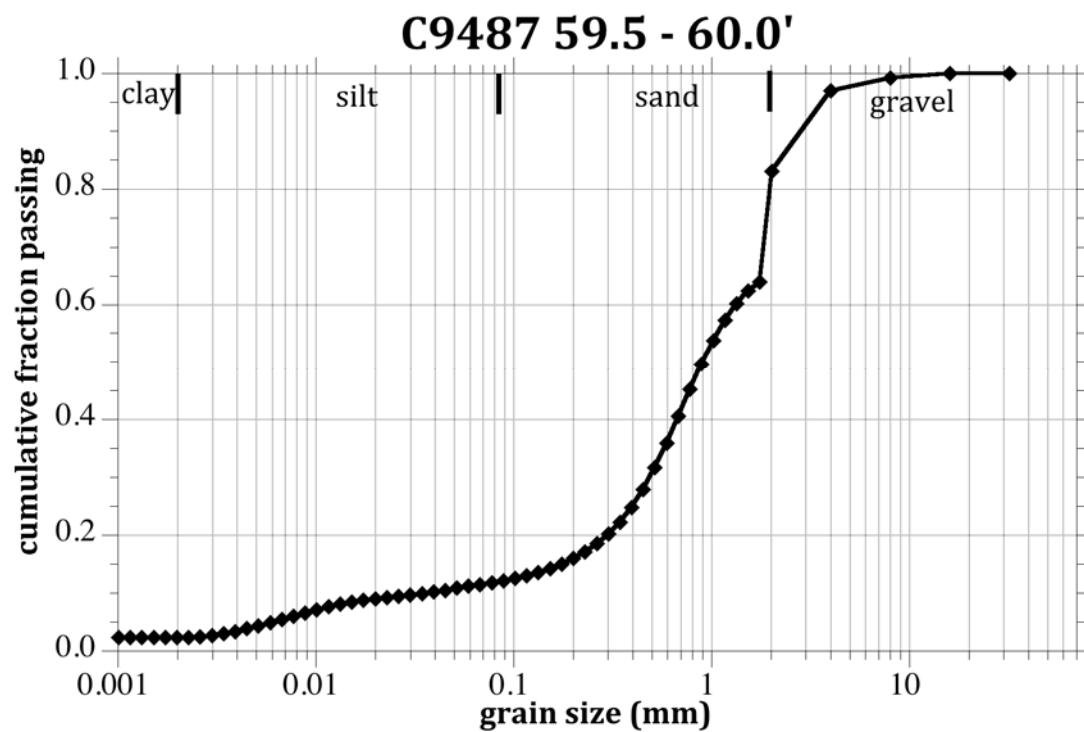
Grain Size Distributions

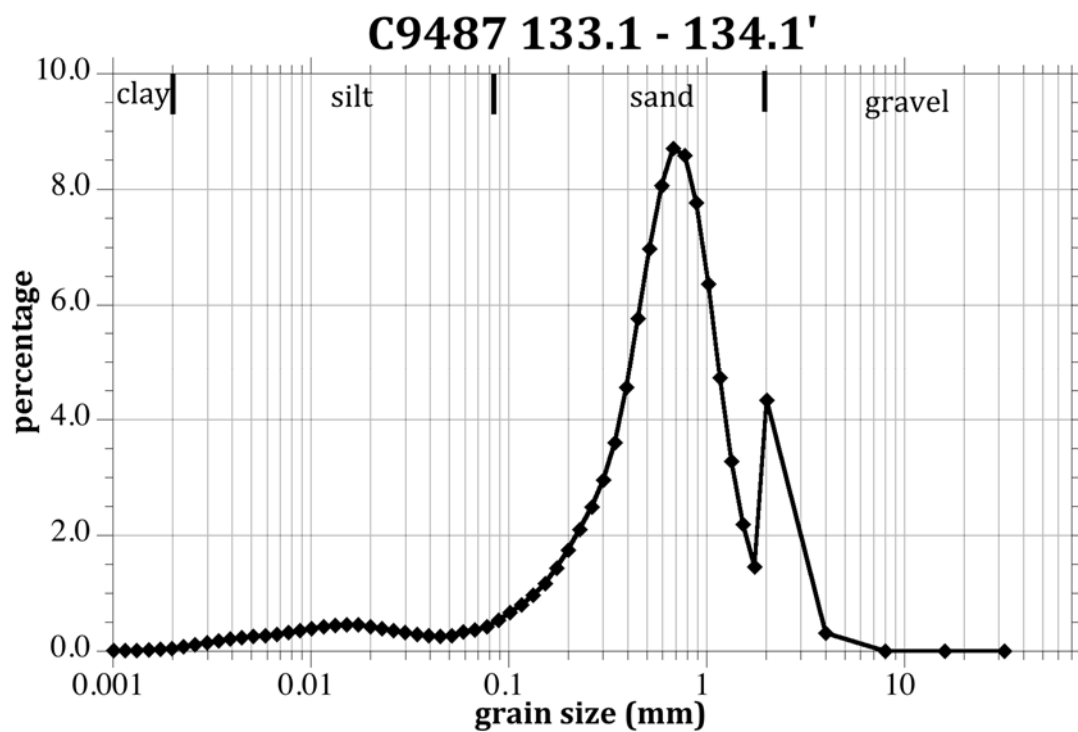
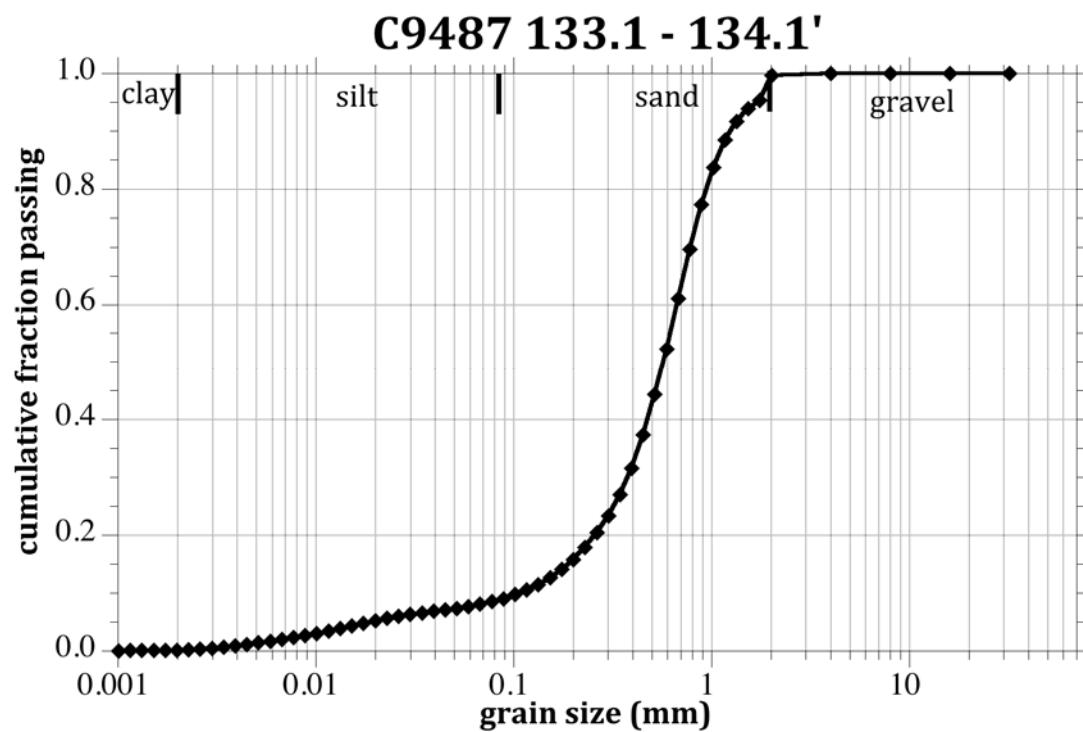
Appendix A - Grain Size Distributions

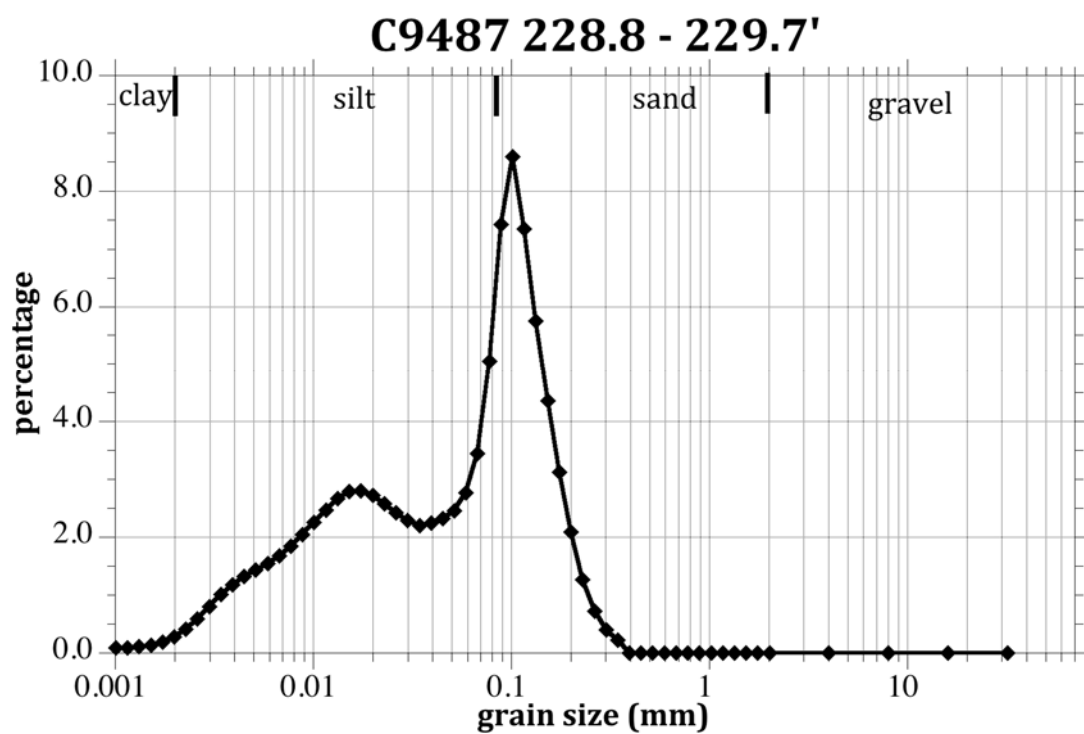
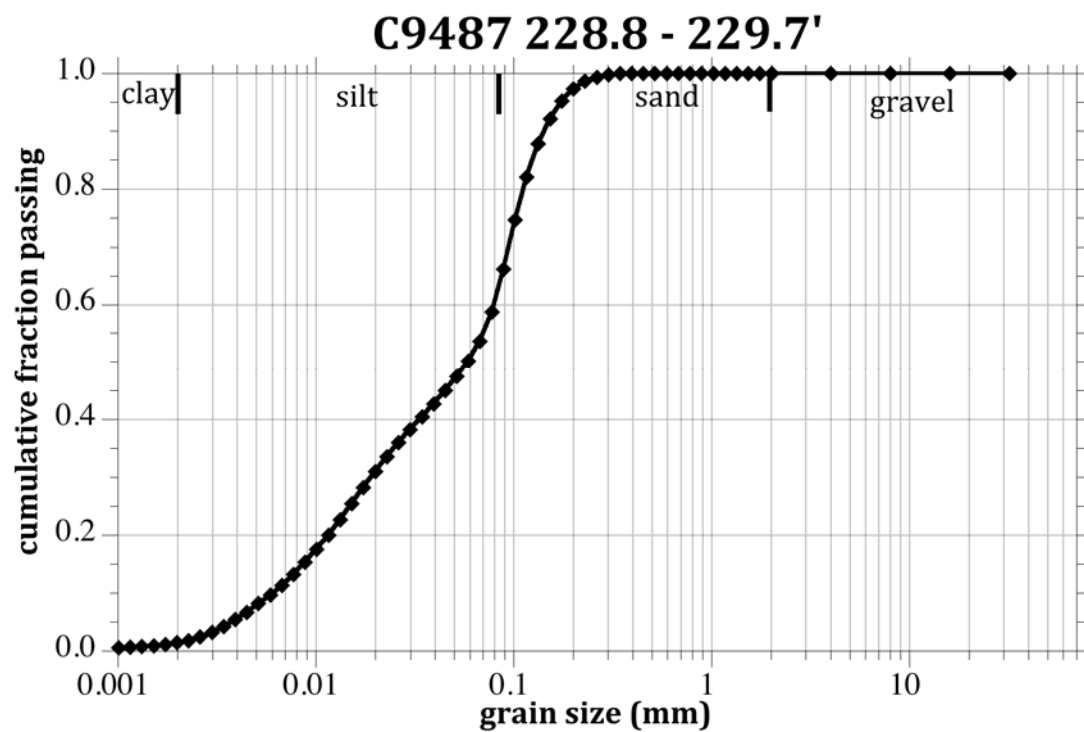


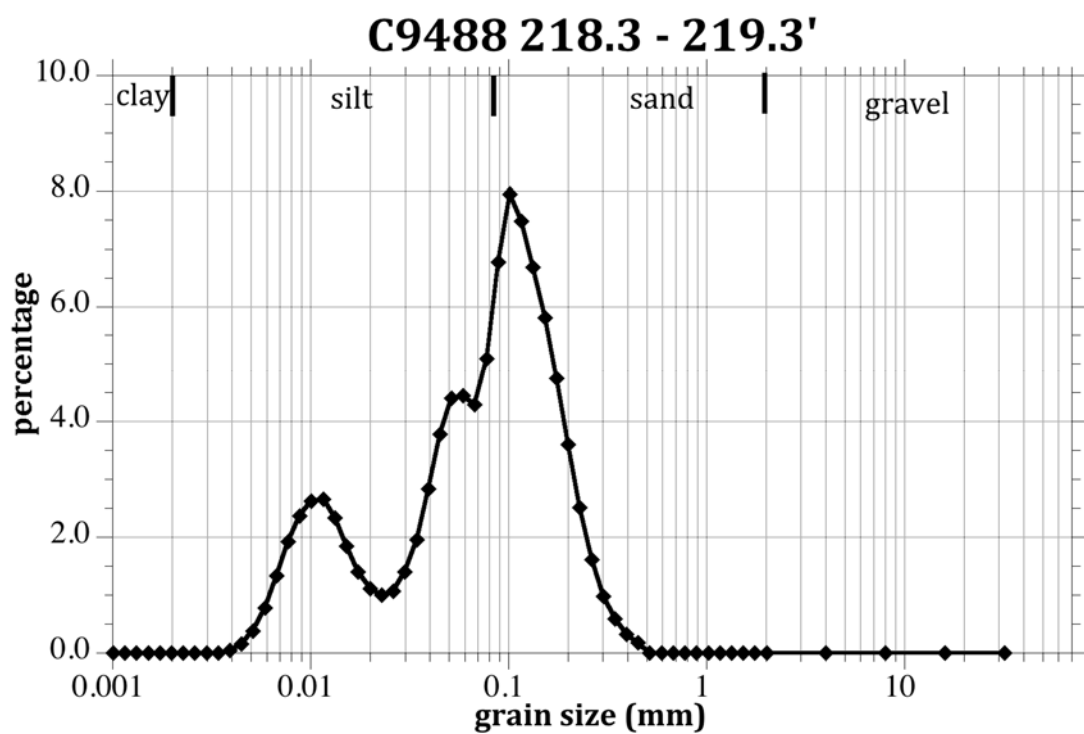
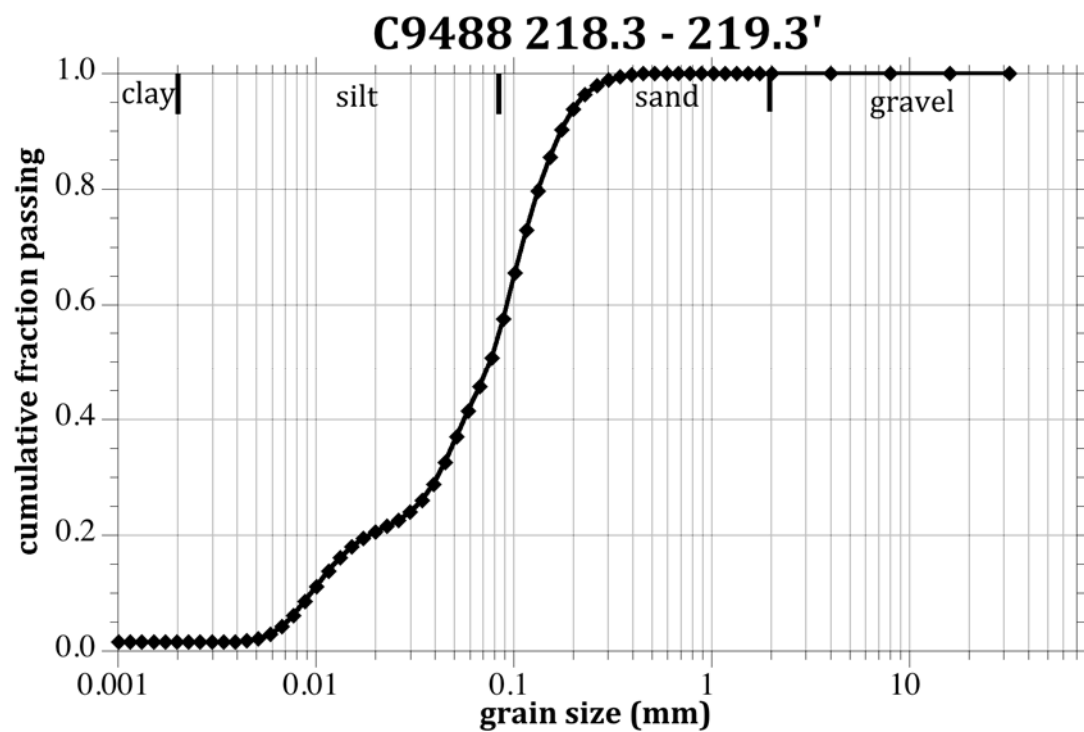












Appendix B

Extractable Contaminants and Ions

Table B.1. Geochemical characterization of sediment pore water by water/sediment (1:1) extraction in mg/L pore water.

Borehole	Depth (ft)	Moisture (g/g)	pH	SpC (mS/cm)	SpC (mS/cm) ^(a)	Ca (mg/L) ^(a)	Mg (mg/L) ^(a)	Na (mg/L) ^(a)	K (mg/L) ^(a)	Fe (mg/L) ^(a)	Cl (mg/L) ^(a)	F (mg/L) ^(a)	SO ₄ (mg/L) ^(a)	NO ₃ (mg/L) ^(a)	NO ₂ (mg/L) ^(a)	PO ₄ (mg/L) ^(a)	CO ₃ (mg/L) ^(a)	TOC (μg/g)
C9552	104.2–105.2	0.0308	7.88	7.28	244	1412	164	36981	252	31	672	ND	29740	114000	ND	ND	1091	4.24
C9552	134.1–135.1	0.0216	8.14	4.66	220	722	316	22130	337	30	685	ND	5231	115700	ND	ND	1450	4.52
C9552	194.2–195.2	0.0317	7.15	3.86	126	6814	1486	2360	305	12	448	ND	1076	71600	ND	ND		
C9487	58.2–59.2	0.0367	9.94	0.64	18.1	ND	ND	1578	390	ND	ND	381	728	1387	ND	ND	1473	
C9487	134.1–135.1	0.0285	10.0	0.201	7.25	ND	ND	754	ND	ND	62	10	152	215	ND	ND	3596	4.56
C9487	230.0–231.0	0.2272	8.68	0.605	3.27	11	5	288	ND	ND	66	31	343	431	22	ND	568	6.05
C9488	219.3–220.3	0.2427	7.93	1.16	5.94	76	41	356	19	ND	109	ND	733	1360	ND	33	934	2.76
ERDF pit	40' uncontam.	0.0102	8.31		15	36.1	9.7	414	46.9	1.1	465	8.6	230	95	ND	ND		

(a) In pore water volume, as originally in pore water and/or solubilized by water extract.

Table B.2. Geochemical characterization of sediment pore water by water/sediment (1:1) extraction in mmol/L pore water.

Borehole	Depth (ft)	Moisture (g/g)	pH	SpC (mS/cm)	SpC (mS/cm) ^(a)	Ca (mmol/L)	Mg (mmol/L)	Na (mmol/L)	K (mmol/L)	Fe (mmol/L)	Cl (mmol/L)	F (mmol/L)	SO ₄ (mmol/L)	NO ₃ (mmol/L)	NO ₂ (mmol/L)	PO ₄ (mmol/L)	CO ₃ (mmol/L)	TOC (μg/g)
C9552	104.2–105.2	0.0308	7.88	7.28	244	35.2	6.74	1174	6.44	2.02E-02	18.9	ND	309	1838	ND	ND	18.2	4.24
C9552	134.1–135.1	0.0216	8.14	4.66	220	18.0	13.0	963	8.62	1.98E-02	19.3	ND	54.4	1867	ND	ND	24.2	4.52
C9552	194.2–195.2	0.0317	7.15	3.86	126	169.	61.1	103	7.80	8.25E-03	12.6	ND	11.2	1155	ND	ND		
C9487	58.2–59.2	0.0367	9.94	0.64	18.1	ND	ND	69	9.96	ND	ND	20.1	7.57	22.4	ND	ND	19.6	4.56
C9487	134.1–135.1	0.0285	10.0	0.201	7.25	ND	ND	33	ND	ND	1.75	0.51	1.58	3.47	ND	ND	59.9	6.05
C9487	230.0–231.0	0.2272	8.68	0.605	3.27	0.281	0.206	13	ND	ND	1.86	1.61	3.57	6.95	0.48	ND	9.47	
C9488	219.3–220.3	0.2427	7.93	1.16	5.94	1.90	1.66	15	0.497	ND	3.06	ND	7.63	21.9	ND	0.35	15.6	2.76

(a) In pore water volume, as originally in pore water and/or solubilized by water extract.

Table B.3. Water and acid extractable concentration of contaminants in sediments.

Borehole	Depth (ft)	U-238 (pCi/g)	U-238 (pCi/g) HNO ₃	Tc-99 (pCi/g)	Tc-99 (pCi/g) HNO ₃	I-127 (µg/kg)	I-127 (µg/kg) HNO ₃	Cr (µg/kg)	Cr (µg/kg) HNO ₃	Cr ^{VI} (µg/kg) alk.	CN- (µg/kg) H ₂ O
		H ₂ O extr.	extr.	H ₂ O extr.	extr.	H ₂ O extr.	extr.	H ₂ O extr.	extr.	extr.	extr.
C9552	104.2 – 105.2	5.05E-04	0.285	78.9	104	2.00	(a)	ND	6430	ND	42
C9552	134.1 – 135.1	2.84E-04	0.222	60.4	79.9	0.931	(a)	ND	6680	ND	36
C9552	194.2 – 195.2	2.61E-04	0.236	29.9	89.1	12.1	(a)	ND	7570	683	ND
C9487	58.2 - 59.2	1.70E-01	3.72	ND	ND	1.64	(a)	ND	4790	ND	ND
C9487	134.1 – 135.1	6.49E-04	0.258	ND	ND	1.36	(a)	ND	8240	1180	ND
C9487	230.0 – 231.0	1.09E-02	0.424	0.80	ND	2.53	(a)	ND	9830	ND	ND
C9488	219.3 – 220.3	1.86E-04	0.405	9.38	ND	3.44	(a)	ND	11200	1280	ND

(a) Aqueous iodine volatilizes as I₂ in acidic matrix, not analyzed.

Distribution

**No. of
Copies**

#	Local Distribution	
	Pacific Northwest National Laboratory	
(6)	Jim Szecsody	P7-59
(2)	Mike Truex	K6-96



Pacific Northwest
NATIONAL LABORATORY

*Proudly Operated by **Battelle** Since 1965*

902 Battelle Boulevard
P.O. Box 999
Richland, WA 99352
1-888-375-PNNL (7665)

U.S. DEPARTMENT OF
ENERGY

www.pnnl.gov